Low Temperature Processing of Baroplastic Core-Shell Nanoparticles and Block Copolymers

by

Juan A. González-León

B.S. Chemical Engineering
National Autonomous University of Mexico (UNAM), 2000

Submitted to the Department of Materials Science and Engineering in Partial Fulfillment of the Requirements for the Degree of

Doctor of Philosophy
in
Polymer Science

At the
Massachusetts Institute of Technology

February 2006

Signature of Author:_____
Department of Materials Science and Engineering
October 3, 2005

Certified by:_____
Anne M. Mayes
Toyota Professor of Materials Science and Engineering
Thesis Supervisor

Accepted by:_____
Gerbrand Ceder
R.P. Simmons Professor of Materials Science and Engineering
Chair, Departmental Committee on Graduate Students

Low Temperature Processing of Baroplastic Core-Shell Nanoparticles and Block Copolymers

by

Juan A. González-León

Submitted to the Department of Materials Science and Engineering
On October 3, 2005 in partial fulfillment of the requirements for the Degree of Doctor of Philosophy in polymer Science

Abstract

Baroplastics are nanophase polymeric materials comprised of two components that can miscibilize under pressure thereby facilitating flow. The possibility of processing these materials at low temperatures was the main focus of this work.

Block copolymer baroplastics comprised of a low T_g and a high T_g component that microphase separate, such as polystyrene-*block*-poly(butyl acrylate) (PS-*b*-PBA) and polystyrene-*b*-poly(2-ethyl hexylacrylate) (PS-*b*-PEHA), were synthesized by ATRP and processed at reduced temperatures by compression molding. The resulting processed specimens were clear and well-defined solid objects. Structural characterization studies on the processed baroplastics showed that the mixing between components during processing is incomplete and distinct hard and soft domains are present even after multiple processing cycles. This suggests that the processing is of a semi-solid nature, where the rigid PS domains are mobilized by the low T_g component. Processing of a control sample exhibiting pressure-induced demixing, polystyrene-*block*-poly(lauryl methacrylate) (PS-*b*-PLMA), yielded incompletely processed objects under the same processing conditions and inferior mechanical properties to its acrylate counterparts.

Low temperature processing of baroplastics and the proposed semi-solid processing mechanism were further demonstrated with the study of core-shell nanoparticles, where the soft homopolymer (PBA or PEHA) formed the core surrounded by a rigid PS shell. These materials could also be processed at reduced temperatures, displaying a wide range of mechanical properties as a function of their composition, going from tough and rigid materials to soft and rubbery ones comparable to commercial thermoplastic elastomers.

Low temperature processing of baroplastics opens a new route to polymer processing, where energy for heating and cooling could be saved, processing times could be reduced and materials with high sensitivity to temperature could be processed.

Thesis Supervisor: Anne M. Mayes
Title: Toyota Professor of Materials Science and Engineering

Index

List of Figures

List of Tables

Acknowledgements

I wish to thank God for giving me the opportunity to be here and meet and collaborate with such wonderful people that made this work possible and worthwhile.

This work would have never been realized without the extraordinary guidance of my advisor Prof. Anne M. Mayes. I want to thank her for all the hard work invested on me, for sharing her vision and enthusiasm, to help me reach goals that seemed impossible. I will always treasure all what I learned from her.

My wife, Yeriley Lopez Jarquin, deserves all my gratitude for always supporting me with her joyous spirit and love. I wish to thank her for all her patience and comprehension. She was always there when things were bad, making them better. She was always there when things were good, making them extraordinary. I love you.

To my parents, Martha Leon Chirinos and Alberto Gonzalez Villaseñor for all their love and support who are always present even though they were far away. I also want to thank my brother, Carlos Gonzalez Leon, who has always shared with me a never-ending desire of learning.

My life and work at MIT wouldn't have been the same without all the great members of the Mayes Group: William Kuhlman, Ikuo Taniguchi, Caitlin Deveraux, Rafal Mikiewicz, Jane Park, Ayse Asatekin, Ariya Akthakul, Ozge Akbulut, Elsa Olivetti, Long Hua Lee, Patrick Trapa, Solar Olugebefola, Nathan Lovell, You-Yeon Won, Stella Park, Sarah Ibrahim and Jong-Hak Kim. I owe them my eternal gratitude for all their help and especially for their friendship. In particular I would like to thank Prof. Metin Acar for the all the block copolymer synthesis work that made this thesis possible, for all his teachings and for being such a good friend. I also want to deeply thank Dr. Sang-Woog Ryu for the development of the emulsion polymerizations and for his sincere and true friendship.

I wish to thank all the "Mexican Mafia" for all their support and for being like a family while we were here: Ulises Martinez (especially for machining one of the molds), Jorge Feuchtwanger, Jorge Carretero, Jorge Vieyra and Raymundo Arroyave.

I would like to thank the UROPs working with me in this project for all their contributions: David Shoen, Jeff Borowitz and Sheldon Hewlett.

I want to thank Peter Morley, from the central machine shop, and Fred Cote, from the Edgerton Center student shop, for all their help in the design and construction of the molds. I especially want to thank the wonderful people from the neutron scattering facilities who are always willing to help: Dr. Boualem Hammouda and Dr. Sushil Satija from NIST, Dr. Pappannan Thiyagarajan and Dennis Wozniak from the IPNS at Argonne National Laboratory and Dr. Rex Helm from LANSCE.

This work was possible thanks to the funding of the Lord Foundation and Corporation, The Seaver Institute and the NSF through our MRSEC IRG-II program DMR-0213282.

Finally, I want to thank my committee members: Prof. Gerbrand Ceder, Prof. Robert Cohen and Prof. Edwin Thomas for their help in the completion of this work.

CHAPTER 1

Background

1.1 Polymer mixtures

Perhaps the simplest approach to design a new material with certain specific properties is to combine other materials that already possess some of the desired properties. Unfortunately, this is not always easy for polymer mixtures, since most combinations phase separate into large scale domains yielding materials with poor and undesired properties. There are only a few known polymer pairs that exhibit total miscibility in the practical range of temperature [1,2]. Immiscibility between polymers results from the inherent chemical incompatibility between the two chemically distinct species and, perhaps the most important factor for polymer incompatibility, the high molecular weight of the polymer chains. Compared to other molecules, polymer chains occupy a large volume, constraining the number of additional configurations available upon mixing components. The effect of the molecular weight on the entropy of mixing can be easily seen in the two first terms of the Flory-Huggins expression for the free energy of mixing per unit volume [3]:

$$\frac{\Delta g_{mix}}{kT} = \frac{\phi_A}{N_A \nu_A} \ln \phi_A + \frac{\phi_B}{N_B \nu_B} \ln \phi_B + \frac{\phi_A \phi_B}{\nu_{AB}} \chi_{AB}^{FH} \qquad [1.1]$$

where ϕ_i is the component volume fraction, N_i is the number of segments or repeat units in the polymer chain (proportional to molecular weight),v_i is the segmental volume of component i, v_{ij} is the average segmental volume and χ_{AB}^{FH} is the interaction parameter between the two components and is inversely proportional to temperature. The number of chain segments, N_i, is in the denominator of both entropic terms, which dramatically reduces the value of the entropy of mixing compared to small molecules (where N equals 1). As can be predicted from the FH equation, polymer mixtures tend to phase separate with decreasing temperature. However, polymer mixing also depends on other factors not considered by FH, such as differences in thermal expansion, compressibility and repeat unit size of the respective homopolymer component, which can drive demixing upon heating [4,5].

1.1.1 Phase behavior of polymer mixtures

As mentioned before, most polymer mixtures present total or partial immiscibility in the useful temperature window. The effect of temperature on the phase behavior of polymer mixtures has been a matter of study for many years. The most common effect of temperature on mixtures is increasing the miscibility of the components. In this kind of behavior, the critical point between the phase-separated and mixed phase, termed the upper critical solution temperature (UCST), is at the maximum of the two-phase boundary region as shown schematically in Figure 1.1. This behavior is due mainly to the increase in entropy of mixing as temperature increases.

Although UCST behavior is the most common behavior encountered in polymer systems, an additional transition may be present called a lower critical solution transition

(LCST)[6]. In LCST systems, an increase in temperature actually results in demixing, as shown schematically in Figure 1.1. LCST behavior can be explained by changes in specific interactions or differences in the volume change on mixing. For systems with specific interactions, such as PEO-water, the probability of forming a hydrogen bond is decreased as temperature is increased. Since these bonds are the main driver in the mixing of the two components, demixing occurs in their absence[7]. In this particular case, a UCST is present after increasing the temperature beyond the LCST, forming an immiscibility loop. Weakly interacting polymer mixtures can also have LCST behavior; this was observed in systems such as polystyrene / poly(vinyl methyl ether) among others[8]. Demixing in this case is due to the differences in thermal expansion between the components[4, 8]. The combination of LCST and UCST may result in phase diagrams of different shapes, as shown in Figure 1.1.

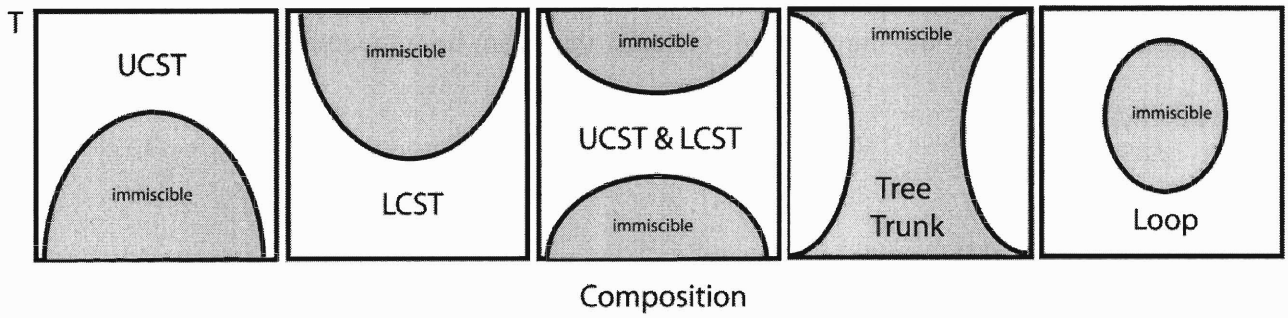

Figure 1.1. Schematic of a UCST and LCST and their possible combinations.

Several polymer blends are widely used in industry, mostly for their low price and processing ease. An example of such a blend is polyvinylchloride/ poly(ethylene-*co*-vinyl acetate) (PVC/EvAc) used in outdoor applications, and sold under the commercial names

Denkovinyl™, Hostalit™ and Vinidur™ among others. [1] Another commercially relevant blend is polypropylene/polyethylene propylene rubber (PP/EPR) with more than 200 applications in the automotive industry, appliances, hardware and plumbing, medical, shoe industry, sports equipment, toys etc. Commercial names for (PP/EPR) are Buna™, Dutral™, Santoprene™, Esprene™, Intolan™, Nordel™ among many others [1].

Strategies to overcome phase separation in polymer systems have been developed. Chemical modification, to create copolymers that interact more strongly with each other (such as the interaction between the CHCl group of PVC and the carboxyl group of poly(methyl methacrylate)) can be performed on some polymer systems to facilitate mixing[1, 9]. In other cases, such as in reactive blends, chemical groups are present that react to form covalent bonds between the components when mixed[1, 10]. An alternate approach to achieve mixed properties is to synthesize random copolymers of the two desired monomer types[11]. Although this yields a material that will not have the problem of phase separation, the number of systems that can be prepared in this way is synthetically limited.

1.2 Phase separated materials

Although mixing polymer components may bring many advantages, having coexisting phase separated domains of finite size of each component may result in different desirable properties that mixed phases do not possess. When a polymer mixture phase separates, chemically similar chains aggregate with each other forming homogenous domains to avoid contacts with the other species. These domains may coalesce and grow until arrested kinetically, forming a macrophase-separated system. The domain size and

interphase region between the two types of domains defines in many cases the resulting material properties[12]. Limited control of the domain sizes in phase-separated materials may be obtained by heavy stirring and mixing of the blend in the melt state, such as the case of the immiscible blends of polyamide/poly(2,6- dimethyl 1.4-phenylene ether) (PA/PPE) where, with the help of compatibilizers, PPE domains are dispersed in the PA matrix[1,13]. Another way to control domain size in blends is to synthesize particles of the desired domain size and mix them in a matrix of a different component, such as in the case of high-impact polystyrene (HIPS), where crosslinked rubber particles are incorporated into the PS[1].

Although these approaches address the problem of domain size, they still suffer from the problem of weak bonding at the interphase between chemically different domains. To improve the interphase between components, an intermediate material can be added between the two domains to improve their miscibility. This is the case of core-shell particle additives where a polymer particle is encased by another polymer that is more miscible with the matrix to improve the interphase between the particles and the matrix. Another approach that follows the idea of surfactants is to add an amphiphilic molecule that migrates to the interphase between two domains and reduces the interfacial tension, yielding smaller and more stable domains. Examples of such emulsifiers are block copolymers, molecules where chemically different homopolymers are linked together by a covalent bond, and each block resides preferentially in one domain, covalently linking the two domains together[10, 14].

1.2.1 Block copolymers

Block copolymers have the advantage in miscibility over blends since the presence of the covalent bond facilitates mixing of the 2 components. However, they can still separate into smaller and more ordered domains than those formed in blends. This microphase separation presents well-defined periodic morphologies as a function of block copolymer chain architecture and composition. The size and structure of the phase domains dictate the overall properties of the material.

These structures can go from spheres to cylinders to gyroids to lamellae. The different structures, as a function of the number of repeat units, N, the interaction parameter, χ, and block fraction, f, can be mapped in a χN vs. f phase diagram as shown in Figure 1.2.[15]

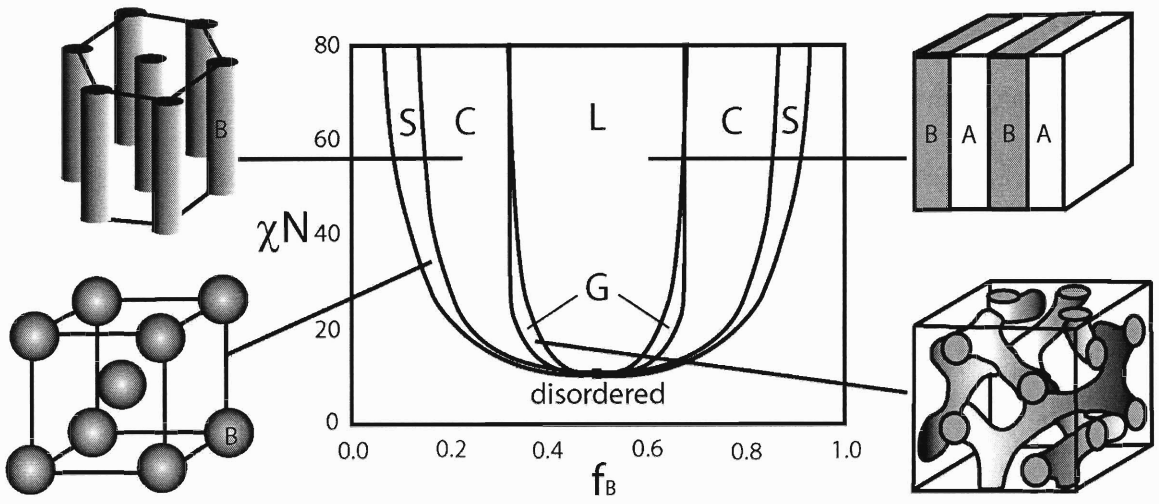

Figure 1.2. Calculated phase diagram of a diblock copolymer as a function of one block component fraction, f. Lamellae (L), gyroid (G), cylinder (C) and sphere (S) morphologies are predicted for defined values of f and χN[16].

For block copolymers disorder-to-order transitions occur in a similar manner as in the demixing of blends, and are thus called upper disorder-order transitions, UDOTs, and lower disorder-order transitions, LDOTs[17]. The microphase separation of block copolymers results in properties that simple polymer blends do not possess, allowing them to be potentially used as thermoplastic elastomers[18, 19], non-ionic surfactants[20,21] and self-organized templates for other organic or inorganic materials microfabrication[22, 23].

Thermoplastic elastomers, or TPE's, are a particular class of block copolymers very relevant to this work. TPE's are block copolymers (either di- or triblock) comprised of a soft and a hard component. These materials present elasticity comparable to crosslinked rubbers, since the hard component domains function as physical crosslinks that anchor the soft component, allowing it to stretch but not to flow. Commercial trade names of such TPEs include Stereon (Firestone), Kraton D (Kraton) and Septon (Kuraray) among others; These materials are based on polystyrene-*block*-polybutadiene-*block*-polystyrene (SBS) or polystyrene-*block*-poly(ethylene-*co*-butylene)-*block*-polystyrene (SEBS) block copolymers. Though not as heat and solvent resistant as chemically crosslinked rubbers, the market for these materials has steadily increased over the past years, in applications such as footwear, wire insulation, hot melt adhesives and sealants, reaching $1.8B in 2002[19, 24].

1.2.2 Core-shell polymer particles

Polymer particles with a core-shell structure have been used for a variety of applications in the past due to the advantage of having in the same particle properties inherent to two

different materials. Cross-linked core-shell particles have been widely incorporated into commercial thermoplastics as impact strength enhancers, allowing the introduction of a rubbery core by the presence of a more compatible shell[25, 26]. Such is the case of toughened polystyrene, where rubbery particles absorb the stress, giving the overall material higher toughness than the matrix alone[27].

A common application for single component polymer particles is in coatings. Coatings are formed by the sintering of polymer particles from emulsion[28, 29]. This process is normally carried out by drying and annealing of the latex, allowing the polymer to coalesce into a cohesive film.[30] This latex process is widely used in many common applications such as gloves and coatings. Latexes with a core and a shell have been used to add a different chemistry to the coating. For example, Ha et al. created a fluorinated shell over a polystyrene core to form highly hydrophobic particles[31]. Core-shell particles with low T_g crosslinked elastic cores and high T_g glassy shells have been also used for coatings, resulting in films with good mechanical properties[28,29].

Uncross-linked core-shell particles have been used mostly as coatings, not as a bulk material[30]. The main concern is processing, since either solvent or melt processing would cause the components to macrophase separate[32]. Recently there has been an increased interest in polymer/polymer and inorganic/polymer core-shell particles because of their potential application in photonic crystals, biocatalysis and drug delivery[33-35].

1.3 Polymer processing

Polymer processing can be carried out by a wide variety of methods that turn the raw material obtained from polymerization into a useful object. For this processing to occur,

it is required that the polymer behave as a fluid, such as in a solution or melt, so it can be reshaped. Once in the new form, the polymer must return to its solid state, by solvent evaporation or cooling, in order to hold the new shape. Melt processing is the most widely used polymer processing approach. In this case, the polymer is heated above its glass transition temperature, T_g, and melting temperature, T_m, (if crystalline) and made to flow through a die into a mold that is then cooled down to solidify the object before being removed.

The most widely used techniques for melt processing are extrusion and injection molding. Extrusion is based on a rotary screw that pumps melted polymer through a die of a defined shape, as shown in Figure 1.3 [36].

In extrusion, the polymer is fed as small pellets (~0.5 cm) through a feeding hopper. These polymer pellets are melted in the first section of the extruder and the screw conveys the polymer into a further section of the machine. Once the polymer is completely melted, it is pressurized and conveyed by the rotating screw until it exits through an orifice of defined shape called a die. After the polymer has left the die it is further aligned and cooled to keep the shape obtained by passing through the die. Extrusion is used to obtain a continuous shape such as bars and tubes; it is also used to melt polymers for other subsequent processing techniques such as injection molding.

Injection molding is a variation of extrusion where once the molten polymer pass through the screw section it is accumulated in the melt state that is then forced by a ram to flow into a closed mold. The mold is cooled, and the solid polymer object is released. Injection molding allows the formation of 3D objects with great detail.

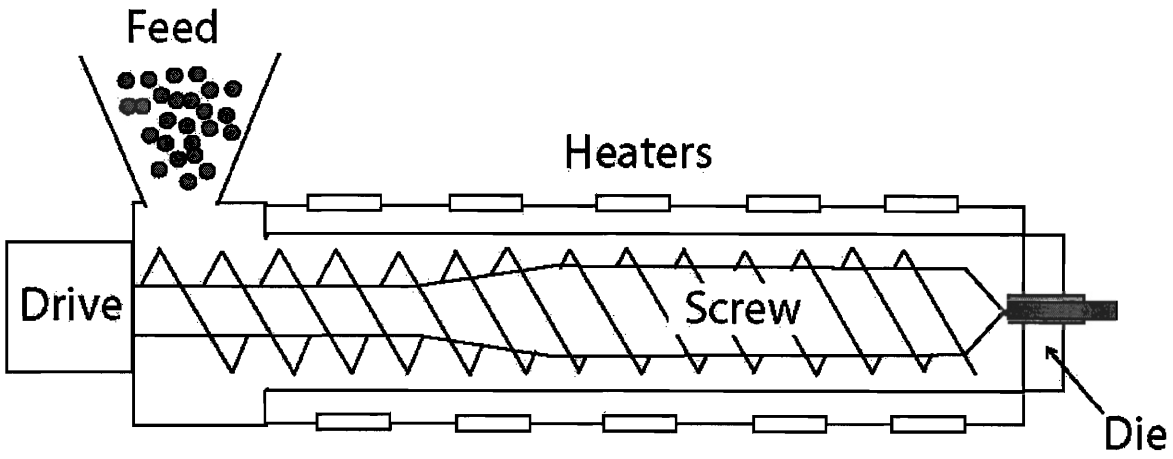

Figure 1.3. Schematic illustration of an extruder.

Polymer blends and block copolymers can be processed by melt extrusion and injection molding. Processing also allows polymer compounding with inorganics and other additives, a practice that is very common in industry.

Thermoplastic elastomers can be processed as regular thermoplastics by extrusion and injection molding, which is one of their greatest advantages over thermoset rubbers [18]. Their ability to become partially fluid when heated beyond their T_g and UDOT allows them to be processed as any thermoplastic polymer and, although not in practice currently, to be recycled [19].

Polymer core-shell particles may be processed by extrusion at higher temperature if their structure is held together by heavy crosslinking. Silverstein and Narkis were able to process crosslinked core-shell particles by extrusion where the overall particle shape was conserved.[37, 38] In the case where no crosslinks are present in the core-shell particle, the

structure will be lost in the melting process and the components will mix or macrophase separate as with any polymer blend[32].

Another industrially important processing method that is relevant to this thesis is compression molding. A schematic illustration of the compression molding setup is shown in Figure 1.4.[36] In this case, the raw polymer, or an extruded or injected preform, is placed between a two-part mold. This mold is then heated and closed by compression to deform the polymer into the mold shape; the mold is finally cooled and opened to release the object. Although all polymers could potentially be processed by this technique, it is used mostly to process layered composites and large objects that cannot be made by injection molding.

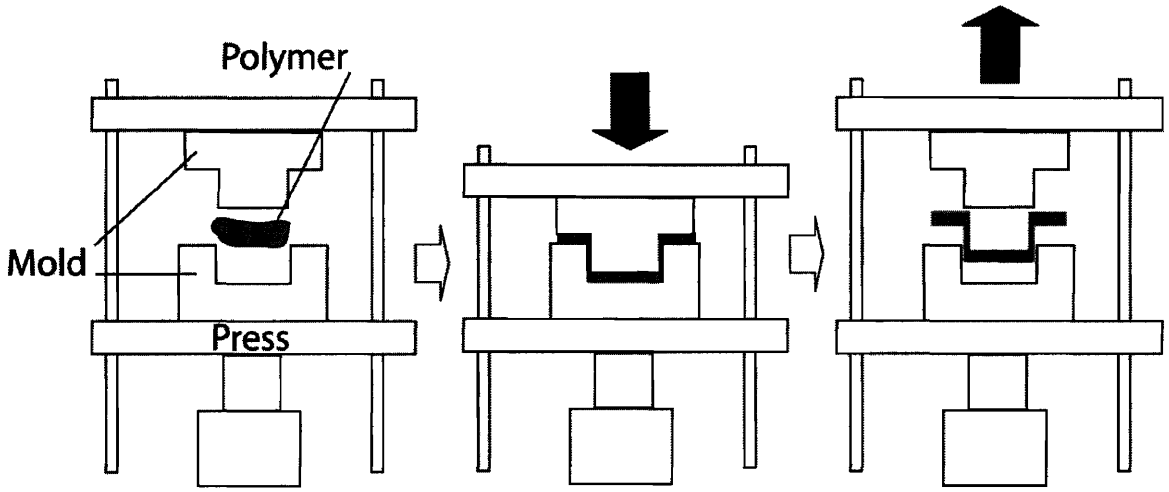

Figure 1.4. Schematic illustration of the compression molding sequence.

Some advances have been made recently in a novel area of polymer processing called solid phase processing[39]. In this processing technique, polymers are extruded or melt

spun at temperatures very near or just below their melting point. Solid phase processing also includes composites and hard to process polymers such as polyaramids. By these techniques a high degree of alignment of the unmelted portion can be obtained, which makes this technique particularly attractive to obtain high modulus fibers.

Solid state processing still requires temperatures well above the T_g of the processed polymer or some other processing agent such as solvents. However, there are some things in common to the work presented in this thesis, such as the presence of a rigid component throughout the processing operation.

1.4 Pressure effects on polymer phase behavior

Although applying pressure to the molten polymer to achieve flow is a common practice, little has been studied about the effect of pressure on polymers and polymer mixtures. Pressure can affect the mobility of polymer chains, which confined in a smaller volume, have less space to move and flow. This effect is observed as an increase in the T_g of polymers at elevated pressures[40]. The effect of pressure during processing has been also the subject of several studies where the viscosity varies at different pressures. This effect also results from the non-zero polymer compressibility under pressure[41-43].

Effects of pressure on phase behavior have been studied for several block copolymer systems, including polystyrene-*block*-poly(butyl acrylate) (PS-*b*-PBA), polybutadiene-*block*-polyisoprene (PB-*b*-PI),[44] polystyrene-*block*-poly(methylphenylsiloxane) (PS-*b*-PMPS)[45], poly(ethylene propylene)-*block*-poly(ethyl ethylene) (PEP-*b*-PEE)[46] and PEP-*block*-poly(dimethyl siloxane) (PEP-*b*-PDMS)[47]. Pressure effects have also been studied for polymer blends such as PVDF/PEMA[6] and certain polyolefins blends[48]. Pressure can

either increase or decrease the miscibility of polymer pairs. For example, in the PS-*b*-PI[49] and poly(dimethylsiloxane)/ poly(hexylmethylsiloxane) systems,[50] demixing with pressure has been observed. In systems such as polyethylbutylene/polymethylbutylene[51], poly(ethylene oxide)/ poly(ethylene oxide -*block*- poly(dimethylsiloxane)[52] and PS-*b*-PBMA[53] pressure induced miscibility has been observed. In some cases, such as PEP-*b*-PDMS, opposite effects are observed at different pressures, where mixing occurs at lower applied pressures and demixing occurs at higher pressures[47].

The volume change on mixing, ΔV_{mix}, is related to the free energy change of mixing, ΔG_{mix}, by:

$$\frac{\partial \Delta G_{mix}}{\partial P} = \Delta V_{mix} \qquad [1.1]$$

ΔV_{mix} is highly correlated with the effect of pressure on miscibility. A positive ΔV_{mix} implies that the components occupy more volume when mixed than separated. When subject to occupy less volume, as when pressure is applied, they prefer to demix. On the other hand, if the volume change on mixing is negative, as is always found with LCST systems, the components will mix with the application of pressure[48]. The origin of finite ΔV_{mix} values can be traced to differences in thermal expansion, compressibility and ultimately the components' chemistry and structure (packing).

The effect of pressure has been observed experimentally as a shift in the phase boundary in temperature vs. composition phase diagrams[45, 48]. The shift in the boundary with pressure, quantified through the pressure coefficient, dT_{ODT}/dP, can be simply represented by the Clausius-Clapeyron equation:[49, 55]

$$\frac{dT_{ODT}}{dP} = \frac{T\Delta V_{mix}}{\Delta H_{mix}} \qquad [1.2]$$

where ΔH_{mix} is the enthalpy of mixing. Equation 2 makes clear that the sign of ΔV_{mix} will determine the effect of pressure on the miscibility, as ΔH_{mix} is typically positive.

Experimentally, and relevant to the systems studied in this work, a series of PS/n-alkyl methacrylate block copolymers were studied by Ruzette et al. showing several phase behaviors and pressure dependences[55]. For n-alkyl methacrylates with n ranging from 2 to 6, pressure induced miscibility was found, with pressure coefficients on the order of 150°C/kbar. For systems with n=1 and n>8, demixing with pressure was found. Recently the pressure behavior of the poly(pentyl methacrylate)/ polystyrene block copolymer system was studied and an immiscibility loop in the phase behavior was reported with a pressure coefficient of 725 °C/kbar[56].

Phase separating block copolymers that present pressure induced miscibility were coined "baroplastics" after the Greek *baros* (meaning pressure) and *plastikos* (meaning moldable)[57], since the disordering of the block copolymers creates a state that can flow.

1.5 Baroplastics

After the observed phenomenon of the dramatic effect of pressure on miscibility in certain block copolymer systems, a question was raised: Can this pressure-induced transition be useful for processing baroplastic systems at reduced temperatures?

If a phase separated block copolymer system comprised of a soft, low T_g component and a hard, high T_g component disorders, it will behave as a viscous liquid, potentially allowing it to flow and be processed. In baroplastics, the mixing would happen with the application of pressure, and after reshaping the material, as pressure is released, the block copolymer would phase separate again, restoring the original solid-like behavior. Figure 1.5 shows a schematic of the pressure-induced shift of the order-disorder transition, indicating the expected rheological changes during this transition.

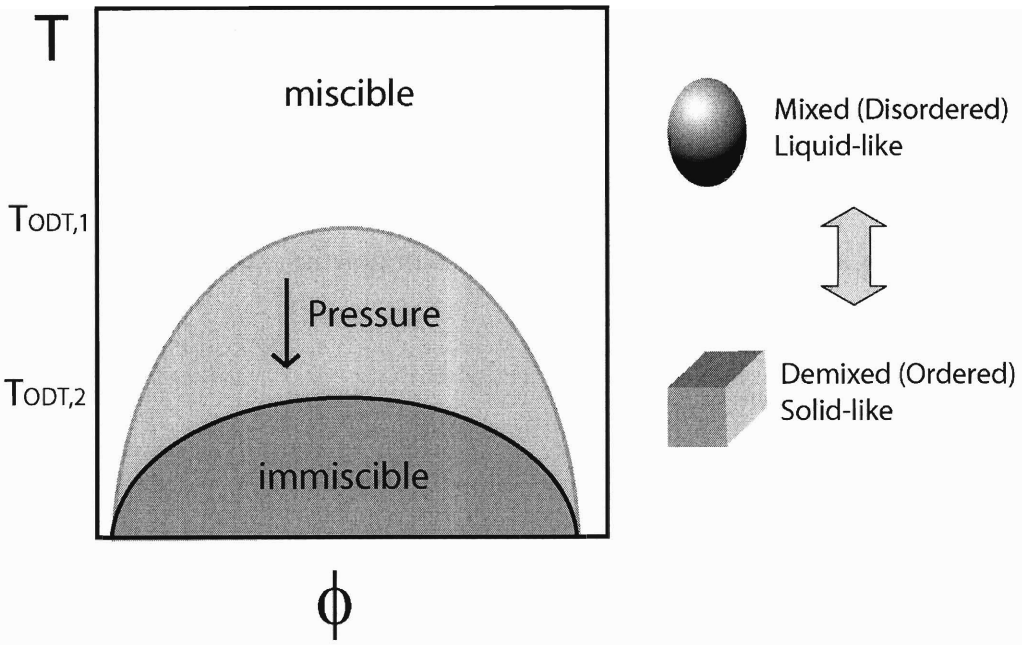

Figure 1.5. Schematic illustration of the pressure-induced shift of the order-disorder transition temperature.

If this pressure-induced transition can occur at temperatures below the T_g of the rigid component, low temperature molding could be possible. A high pressure coefficient, such as in the case of poly(n-butyl methacrylate)-*block*-polystyrene or poly(pentyl

methacrylate)-*block*-polystyrene, would be required to achieve such processing at temperatures as low as room temperature.

Small angle neutron scattering (SANS) measurements for a poly(n-butyl acrylate)-*block*-polystyrene, PBA-*b*-PS, (53 wt% PS and molecular weight of 64,000 g/mol) showed a T_{ODT} ~100°C with a dT_{ODT}/dP of ~100 °C/kbar.[58] If a pressure of 0.75 kbar is applied to this system (~10,000psi), which is at the higher end of conventional polymer processing operations, the T_{ODT} would be shifted down to 25°C. For this PS/PBA composition, the mixed T_g is ~0°C, which would allow flow at a processing temperature of 25°C. This is a very rough calculation for the proposed low temperature processing of baroplastics, but demonstrates, at least thermodynamically, that low temperature processing of baroplastics is possible. It is to be noted that polymer chain kinetics will play a significant role in this process in practice, constraining the pressure-induced mixing process.

The advantages of low temperature processing would be many, potentially including energy savings, since melting and cooling are eliminated. Another advantage would be that since pressure can be applied and released practically instantaneously, processing cycles would become shorter. In addition, a material that is not heated during processing would, in principle, avoid thermal degradation. One of the problems with plastics recycling, among many others such as sorting and compatibilization, is that thermal degradation limits the recycle life of the material to a very few processing cycles.[59] Baroplastics could yield materials with longer recycling life by avoiding thermal degradation.

The main goal of the work presented in this thesis was to demonstrate the feasibility of low temperature processing of baroplastics. After demonstrating that low temperature processing is possible, the focus of the work became the characterization of the molded samples in order to understand the underlying processing mechanism. In addition, an analysis of the design of baroplastic systems suitable for low temperature processing, as well as the synthesis, processing and characterization of a novel core-shell baroplastic are included in this work.

The experimental methods used for the synthesis, processing and characterization of block copolymer and core-shell baroplastics are described in Chapter 2.

Chapter 3 includes a discussion about the selection of the components for pressure-induced miscible systems. The need for a simple model to predict the phase behavior of polymer systems is discussed and predictions obtained using the compressible regular solution (CRS) model are shown. Evidence of the pressure-induced miscibility in the polymer systems studied in this work is shown and guidelines for the design of other low temperature processable baroplastics are presented.

Block copolymer baroplastics are discussed in Chapter 4. Results from their atom transfer radical polymerization (ATRP) and proof of their low temperature processing are shown. Certain factors that affect their processing, such as composition and structure, are discussed. Structural characterization of their processing is also presented in this chapter, showing that only partial mixing between the components was obtained during

processing. In addition, the role of pressure-induced miscibility is studied through examination of a non-pressure induced miscible control system.

Chapters 5 and 6 discuss the synthesis, processing and characterization of core-shell baroplastics. Core-shell particle synthesis, structure and low temperature processing are the main focus of Chapter 5. In this chapter, evidence that supports the proposed processing mechanism in Chapter 4 is presented. Chapter 6 describes different processing techniques for core-shell baroplastics and mechanical properties of the processed specimens are compared with comparable commercial thermoplastic elastomers. Effects on the mechanical properties of particle composition and size, as well as processing conditions such as temperature, are also discussed in this chapter.

The last chapter summarizes the work presented in this thesis and proposes future directions of work and study on these novel materials.

CHAPTER 2

Experimental Methods

2.1 Block copolymer synthesis

Block copolymers can be synthesized by a diverse number of methods such as ionic, condensation and free radical polymerizations. Each polymerization procedure has its advantages and disadvantages, and not every block copolymer can be obtained by every method. Regular free radical polymerizations, although very simple to do, lead to high polydispersity polymers with poor control over molecular weight and architecture. Only a few block copolymers are possible through this route, which requires a large difference in reactivity to form blocks, such as in poly(vinylcarbazole) and poly(oxetane) [60, 61]. Ionic polymerization can yield block copolymers with very low polydispersity and well-controlled structure; the polymerization is, however, difficult to realize and very sensitive to impurities and reaction conditions. During recent years a number of what have been called "living" free radical synthesis methods have been developed for the synthesis of well-defined and controlled block copolymer architectures[62]. These controlled methods are free radical polymerizations where, by the use of a co-catalyst that slows down the polymerization rate, polymer chains can propagate homogenously (controlled by the co-catalyst) yielding a "living" polymerization. In addition, free radical living polymerizations are less sensitive to impurities than ionic synthesis and in general offer a

more robust reaction. Among such methods, atom transfer radical polymerization, ATRP, is simple to carry out and works well for the polymerization of styrenes and acrylates[63,64].

Figure 2.1 shows a scheme of the ATRP process. In ATRP, a metal catalyst (usually copper) is used in combination with a multifunctional ligand to form a complex that is able to sequester the terminal halogen from the reacting chain forming a free radical. This free radical is then able to react with a monomer unit, increasing the chain length. This process is highly reversible, stopping the reaction by recapping the reacting chain with a halogen atom; this recapping is the key process in the control and "life" of the polymerization.

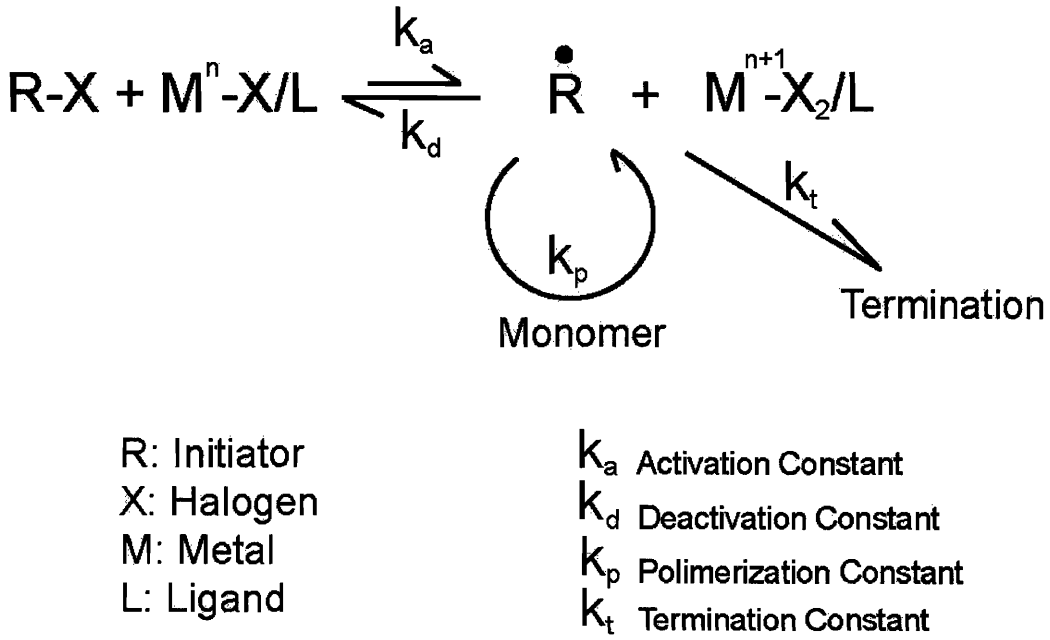

Figure 2.1. Scheme of ATRP.

For this work, block copolymers of several acrylates and styrene were carried out by Prof. Metin Acar, Sheldon Hewlett and the author via ATRP. This polymerization method was chosen because of its relative simplicity compared to other methods, its adequacy for the polymerization of acrylates and styrenes (which covers the materials studied in this work) and because of the potential for scale up of such syntheses to industrial scale for commercial use.

ATRP allows diblock and triblock copolymer synthesis by sequential steps (1 pot) [65] or by separated steps (2 pots), where one component is polymerized first in a simple batch, and then continued with the second monomer in a secondary batch after several purification steps[66]. A typical procedure for sequential addition was carried out as follows: The polystyrene block was polymerized using methyl-2-bromo-propionate (MBP) as initiator and CuCl/N,N,N′,N′,N"-pentamethyldiethylene triamine as catalyst complex in concentrated toluene solution at 110 °C. Once the styrene polymerization reached completion, the acrylate monomer was added to obtain the second block. The resulting polymer solution was then passed through an alumina column to remove the catalyst and precipitated in methanol. The recovered block copolymers were purified by repeated dissolution in dichloromethane followed by precipitation in methanol. A more detailed description of the procedure and materials is provided in Appendix A. Triblock copolymers were obtained by the same procedure by replacing the MBP initiator for the bifunctional 2,6 –dibromoheptanedioate. [67, 68]

The obtained materials' molecular weights were characterized by gel permeation chromatography (GPC) at 30 °C on a Viscotek GPCmax instrument equipped with a

refractive index detector to obtain the molecular weight relative to polystyrene standards. THF was the eluent at a flow rate of 1.0 mL/min. Composition was determined by ^1H nuclear magnetic resonance (NMR) spectra on a Bruker DPX (300 MHz) in $CDCl_3$.

2.2 Core-shell particles

Spherical polymer particles may be obtained by several polymerization methods, such as emulsion, dispersion and suspension. These methods, although very similar, differ in the size of particles obtained. Emulsion polymerizations yield particles with sizes on the order of 0.1-0.5μm, dispersion between 1 and 50 μm and suspension larger than 100 μm. The core-shell nanoparticles used in this thesis were obtained by two-step emulsion polymerization.

In emulsion polymerization non-polar monomers are emulsified in a polar dispersing medium (usually water) with the help of a surfactant. Although the mechanism for the nucleation of polymer particles is not totally understood, it has been observed that the polymer particles grow from "empty" surfactant micelles rather than from the large monomer droplets. The polymerization has been understood to occur in three stages: In the first stage, initiator molecules enter the surfactant micelles along with a few monomer units that migrate from the larger monomer droplets. In the second stage, more monomer migrates into the reacting micelles continuing the polymerization. Fresh free radicals are initiated in the dispersion phase and enter into the micelles to react with the monomer. In the last stage, all the monomer droplets disappear and all the monomer in the micelles, which have now become polymer particles, reacts to completion[69]. Figure 2.2 shows a schematic of the three stages.

Although emulsion polymerization of one component is a straightforward procedure, the synthesis of more complex structures such as core-shell particles brings new considerations during reaction. It is well known that two-stage emulsion polymerization can lead to several particle morphologies, from a perfect core-shell to a core with dispersed domains of the shell component to a totally inverted "shell-core" particle. Factors such as immiscibility of the monomer and polymer components, reaction temperature and addition times dictate the final structure[70-72].

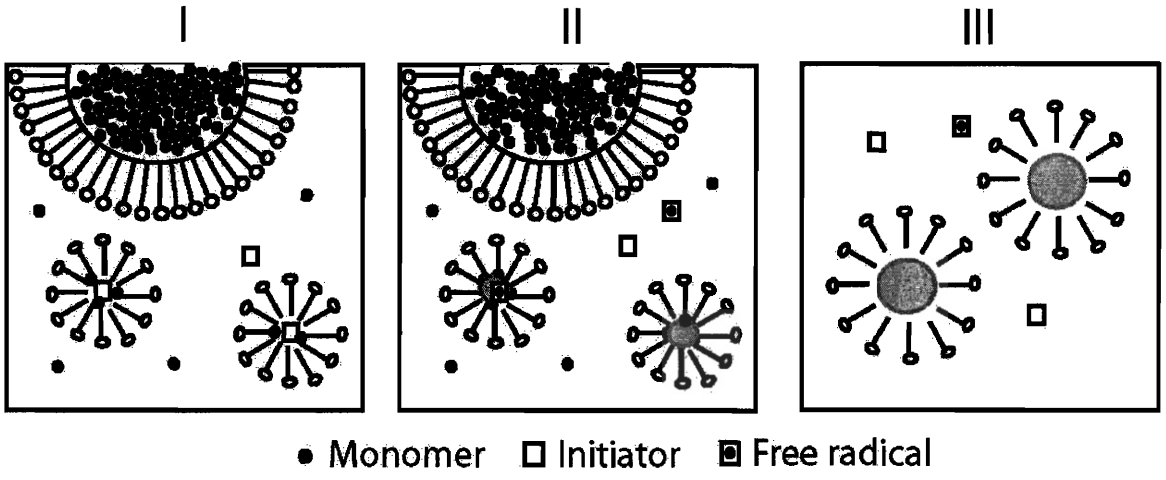

Figure 2.2. Stages of emulsion polymerization.

For this work, core-shell nanoparticles with a poly(butyl acrylate) or poly(2-ethyl hexyl acrylate) core and polystyrene shell were synthesized by Dr. Sang-Woog Ryu or the author via a two-stage emulsion polymerization technique as reported by Ha et al.[31] In a typical procedure, the emulsifier trimethyl(tetra-decyl) ammonium bromide (TTAB) is added to de-ionized water and stirred vigorously until fully dissolved. The monomer that will form the core is then added and stirred for 30 min to form the monomer droplets. The

reaction flask is then introduced in an oil bath at 60°C. The water soluble initiator, 2,2' azobis (2 methyl propion-amide) dihydrochloride (V50), is finally added and the reaction is run for approximately 12 h. After the initial reaction period, an emulsion of the second monomer in water is added drop wise and the reaction is continued for another 12 h. The resulting core-shell particle emulsion is precipitated in methanol and washed several times in a 50/50 wt% water/methanol mixture to remove the emulsifier. Finally the resulting material is dried in a vacuum oven at room temperature for 2 days. A more detailed explanation of the technique and methods used is contained in Appendix A.

Molecular weights of the core and shell were obtained by GPC with polystyrene standards using IR and UV detectors. UV detection at 254 nm was used to identify PS peaks from the refractive index (RI) signal that incorporates the sum of the two components. Individual molecular weight distributions were fit from the collected data. Composition was characterized by NMR as for the block copolymers. The particle size distribution was determined at 25 °C in deionized water using a ZetaPALS particle sizer (Brookhaven Instruments Co.) fitted with a 676 nm laser source located in Prof. Langer's (ChE) and Prof. Irvine's (DMSE) laboratories.

2.3 Processing

Processing of the block copolymers and core-shell nanoparticles was carried out in a commercial hydraulic press using custom made molds. For compression molding, a Grimco press with temperature control was utilized. Material in the powder form was introduced into the mold (about 1g), which then was closed carefully, placed in the center

region of the press and pressed at a given pressure for a specified time. The pressure reported as applied is the reading from the hydraulic gauge of this press. This pressure is related to the press hydraulic piston cylinder area. For most of the samples, a 5 minute period under pressure was used. When processing was carried out at a temperature other than 25°C, a 10 minute thermal equilibration period was adopted before the application of pressure. The simplest molds utilized were two flat aluminum plates that have a ~1mm gap when closed as shown in Figure 2.3a. These molds were used to obtain films of a specific thickness. This kind of mold was also used to obtain other shapes, such as the one shown in Figure 2.3b.

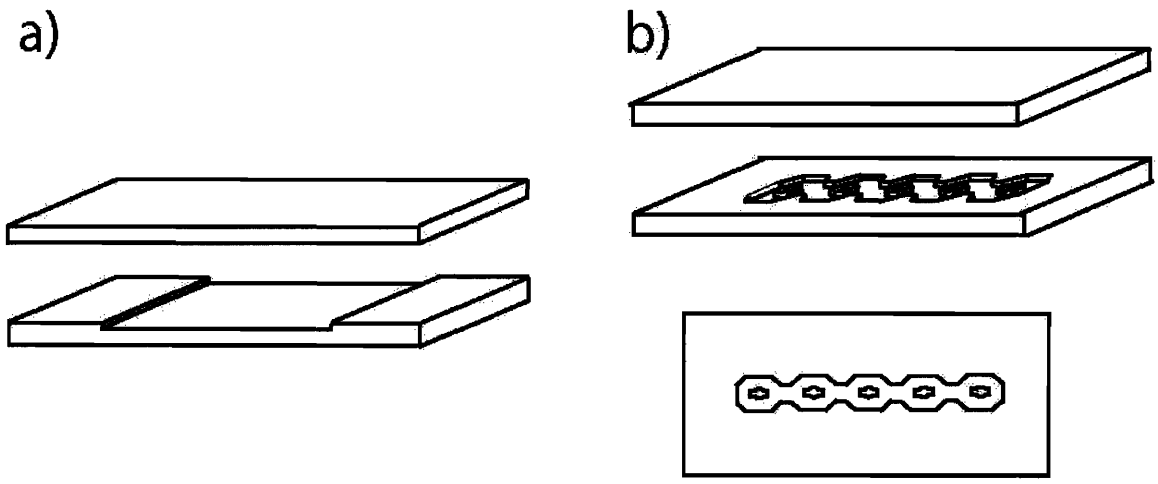

Figure 2.3. Aluminum plate molds for a) films and b) a custom shape.

More elaborate molds were designed to shape other 3D objects, which were machined in stainless steel and are separable to facilitate the release of the product. On certain occasions opening of the molds became difficult; in this case, two screwdrivers were used to pry the mold open. A sketch for this kind of mold is shown in Figure 2.4.

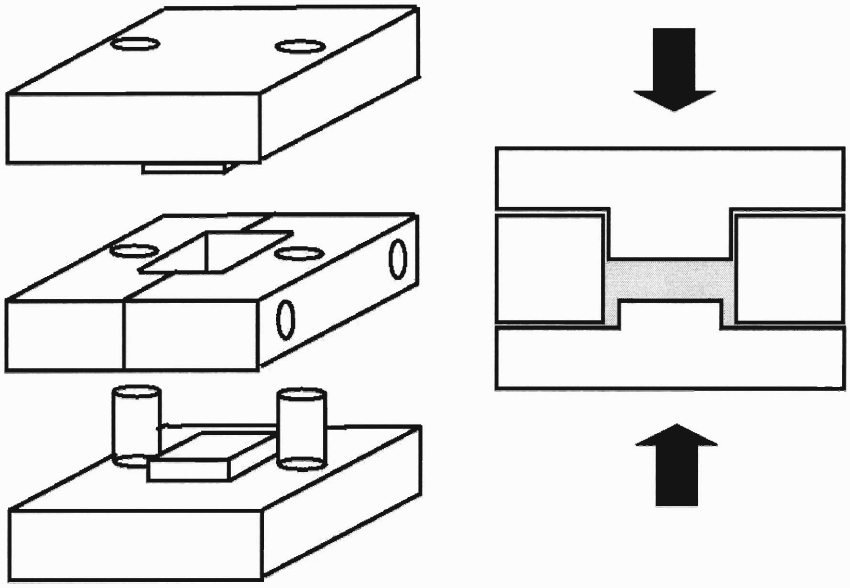

Figure 2.4. Stainless steel mold for a box lid.

A standard processing operation in a stainless steel mold to form a rectangular sheet is shown in Figure 2.5.

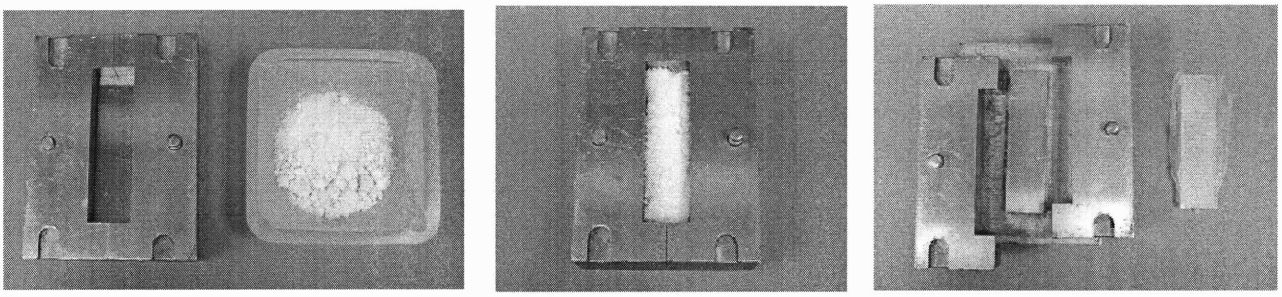

Figure 2.5. Pictures of filling mold, closing mold and mold open with processed object.

For polymer reprocessing, a processed object was cut into smaller pieces (~0.5cm) with a razor blade or scissors. The cut pieces were then placed in the mold and pressed as described above.

A simple extrusion device was designed to extrude material using a hydraulic press. This custom made "extrusion piston" consisted of a piston and a chamber with a small orifice (0.5 mm diameter) on one side from which the polymer could flow when subjected to pressure from the piston. A sketch of the piston mold is shown in Figure 2.6.

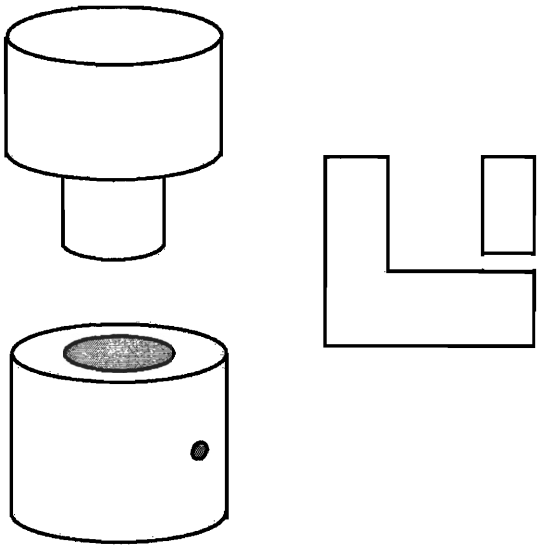

Figure 2.6. Schematic of stainless steel piston mold.

This simple geometry enable the calculation of the true pressure applied to the material to allow an estimate of the material viscosity. As in compression molding, powder was loaded into the chamber (~0.8g) and the piston inserted before being placed in the press as shown in Figure 2.7. For the extrusion experiments a Carver Inc. hydraulic press with a load control unit was utilized. Pressure in this case can be calculated using the area of the piston and the force displayed by the machine. As for compression molding, reprocessing was carried out by cutting the extruded object and reintroducing the cut pieces into the mold to be pressed again.

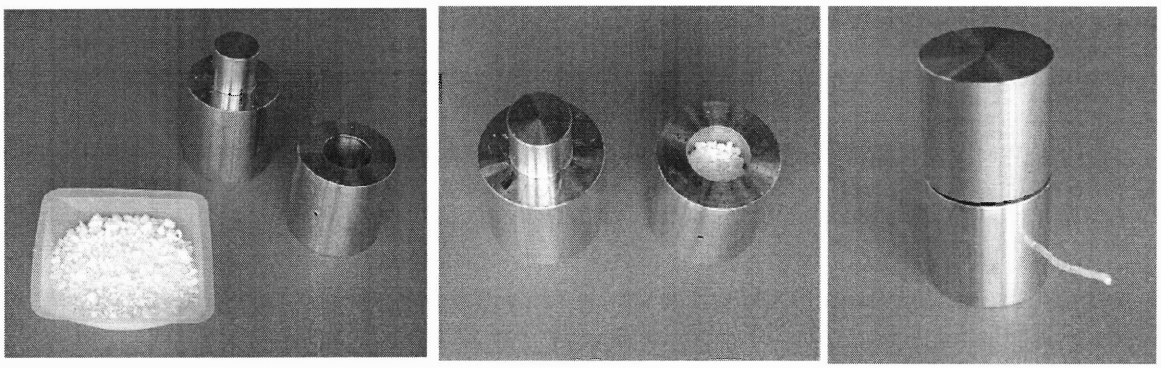

Figure 2.7. Piston mold procedure of a core-shell sample.

2.4 Material characterization

2.4.1 SANS and SAXS

Small angle neutron and X-ray scattering (SANS and SAXS) experiments can provide information about the microphase structure of materials. In the case of microphase separated polymers, a scattering peak can be observed in an intensity vs. wavevector, q, plot. The peak is formed by the constructive interference of scattered neutrons or x-rays due to the periodicity of the defined microphase-separated domains.[73] The peaks will have a maximum at a specific wave vector, that can be related to real dimensions, d, by:

$$d \approx \frac{2\Pi}{q} \qquad [2.1]$$

This dimension represents a complete period of the repeating domains. In the case of block copolymers this dimension, d, corresponds to the size of a block copolymer bilayer. For core-shell particles d is roughly the particle size. The intensity of the peak is related to the sharpness of the interphase between the phases (degree of phase separation) and the contrast between the domain components. In the case of X-rays the contrast corresponds to differences in electron density. Small angle X-ray scattering was performed with a

Molecular Metrology (Northampton, MA) instrument located at the Institute for Soldier Nanotechnologies (ISN), consisting of a Cu Kα x-ray source (λ=1.542 Å), 3-pinhole-collimated beam of diameter ~0.6μm, and a 2D gas-proportional, multi-wire Gabriel detector at 1.465m from the sample.

For small angle neutron scattering (SANS), contrast between the components depends on the neutron scattering length density. Neutron scattering is particularly useful for polymers, since contrast can be increased by deuteration of one of the components.[73]

In addition, neutrons are more penetrating than X-rays and environmental chambers for measurements, such as the pressure cell used in this thesis, are easier to construct. SANS was performed at the Manuel Lujan Jr. Neutron Scattering Center at Los Alamos National Laboratory on the Low-Q Diffractometer, LQD, with the following instrument configuration: wavelength = 1.5 - 15 Å at 20 Hz, scattering angle = 6-60 mrad on a 59 cm diameter detector, resulting in a q range of 0.003 to 0.5 $Å^{-1}$. SANS was also measured at the Intense Pulsed Neutron Source, IPNS, at the Argonne National Laboratory on the Small Angle Neutron Difractometer, SAND, with the following instrument configuration: wavelength = 1 - 14 Å at 30 Hz, with a sample to area detector distance of 2 m, on a 40 x 40 cm diameter detector area, resulting in a q range of 0.0035 to 0.6 $Å^{-1}$. A stainless steel pressure cell with mounted sapphire windows was used for the in-situ pressure experiments. Helium gas was used as the compression fluid. Samples were ~1 cm diameter disks of variable thickness. Scattered intensities were corrected for background and thickness in the standard manner.

2.4.2 DSC and MDSC

Differential scanning calorimetry, DSC, consists of measuring the actual amount of power (rate of heat flow) involved with the change in temperature, evolution or absorption of heat by the sample during a specific material thermal event, such as the latent heat required for melting[74]. The amount of heat flow is quantified as the difference between a reference empty cell and the material of interest. This technique has become very useful for studying polymers since it allows the measuring of glass transition temperatures in amorphous materials and melting points in crystalline polymers. It has also become an important tool to understand the structure of phase-separated materials since the presence of two defined T_gs, belonging to the individual components, confirm phase separation. If only one T_g is identified, between the T_g of the components, this will be proof of a mixed material[78, 79].

Modulated differential scanning calorimetry, MDSC, is a recent technique that applies a sinusoidal modulation of the temperature to specimens and tracks its lag with respect to the reference analogous to dynamic rheology.[75, 76] MDSC allows a better identification and more quantitative measurement of heat capacities, T_g and T_m.[75, 76] It can also separate the reversible and the irreversible components of the heat flow curve, making easier the identification of thermal history effects or other non-reversible events on the measurement of thermal transitions. DSC and MDSC were carried out in a TA instruments Q100 at a heating rate of 20°C/min in sealed aluminum pans. MDSC was done with a modulation of +/- 1.5°C every 60 seconds. Samples were run from –150°C to 150°C with a ramp rate of 3°C/min.

2.4.3 TEM

Since the features we want to observe are on a length scale much smaller than the limit of an optical microscope, transmission electron microscopy was used to observe the microphase-separated structure of polymers.[77] Due to the low penetration of the electron beam, microtomed samples are required for proper observation by TEM. Samples were cryomicrotomed on a MT-X ultramicrotome and a Leica ultracut UCT machine. Samples were microtomed at –85°C to avoid any deformation of the low T_g component. Once the microtomed section was cut, a metal ring was dipped in a concentrated sucrose solution to form a film that was used to adsorb the section and place it on a Cu mesh grid. The Cu mesh grid was then rinsed overnight in DI water to dissolve the sucrose before staining with RuO_4. A carbon coating was deposited at the top of each sample to increase conductivity and avoid damage to the sample. Transmission electron microscopy was carried out on a JEOL 200CX TEM, operated at 160 kV.

2.4.4 Mechanical Tests

To characterize and quantify the effects of processing on the materials in this work, different mechanical tests on processed objects were carried out.

i) Tensile Tests

Tensile tests consist of pulling a strip of material at a constant rate while recording the force needed to continue pulling. The strip, as shown in Figure 2.5 is usually cut into a "dogbone" shape to ensure that breakage occurs in the middle region, rather that at concentrated stress points at the top and bottom caused by the grips.

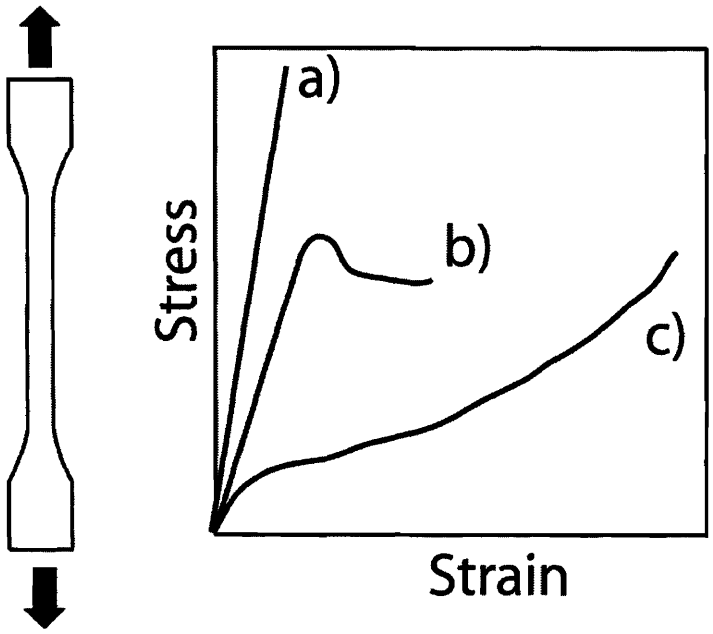

Figure 2.8. Dogbone specimen for tensile test. Stress vs. strain curves for typical polymer mechanical behaviors.

Several material properties can be obtained with this test, perhaps the most important being the elastic modulus. The engineering modulus utilized in this work corresponds to the slope of the initial linear region of the stress vs strain curve. Higher modulus corresponds to stronger materials. Curve a) in the stress vs strain curve in Figure 2.8 shows the behavior commonly encountered for strong and rigid polymers, which, although having a high modulus, cannot undergo much deformation before breaking. Curve b) shows another common behavior for tougher plastics, where a certain amount of strain occurs before breakage. Another feature common in polymers is that after a certain stress, non-reversible deformation or yielding occurs, shown as a maximum on the stress vs strain curve. Curve c) shows the behavior of a soft but very stretchable polymer. This behavior is common for elastomers and rubbers where a small force is required for

deformation but large strains are possible before breaking. Tensile test procedures are described in more detail in ASTM D412-98a.[78]

Tensile tests were carried out on an Instron 4501 at a strain rate of 30 mm/min under ambient conditions. Dogbone shaped samples were cut from films obtained by either extrusion from a custom made piston-mold or by compression molding between two plates employing a ~0.5 mm thick spacer. At least 2 samples of each system were measured. Engineering stress is reported in every case.

ii) Tensile Set

Although the tensile test is the most common mechanical test for materials, it doesn't provide all the information about a polymer's mechanical properties. Another test, which is very similar to the tensile test, is tensile set. Tensile set experiments are done on the same specimens as the tensile test, except that a 100% extension is held for 10 min and then the sample is allowed to recover for another 10 min. The sample size before and after stretching is measured and reported as a percentage of change called the tensile set. This test is very common for rubbers and elastomers since it is a measure of elasticity.[79] Tensile set procedures are also described in ATSM D412-98a. For this work, identical specimens as for the tensile test were cut from processed films and tested.

iii) Tear Strength

The tear strength test is done to measure the susceptibility of a material to propagate a crack or tear. As shown in Figure 2.9, one way to perform the tear strength test is with

samples cut into a "trouser shape", where the "legs" are pulled at a constant rate while recording the force required to continue pulling.[80] The typical obtained plot is also sketched in Figure 2.9. The tear strength is simply defined as the ratio between the maximum force (or mean value of force) and the median thickness of each specimen. For this work, samples were cut by hand into the trouser shape sample as described in ATSM D624-00.[81] Measurements were done on the Instron 4501 at a rate of 300mm/min until the sample broke or reached the machine force limit.

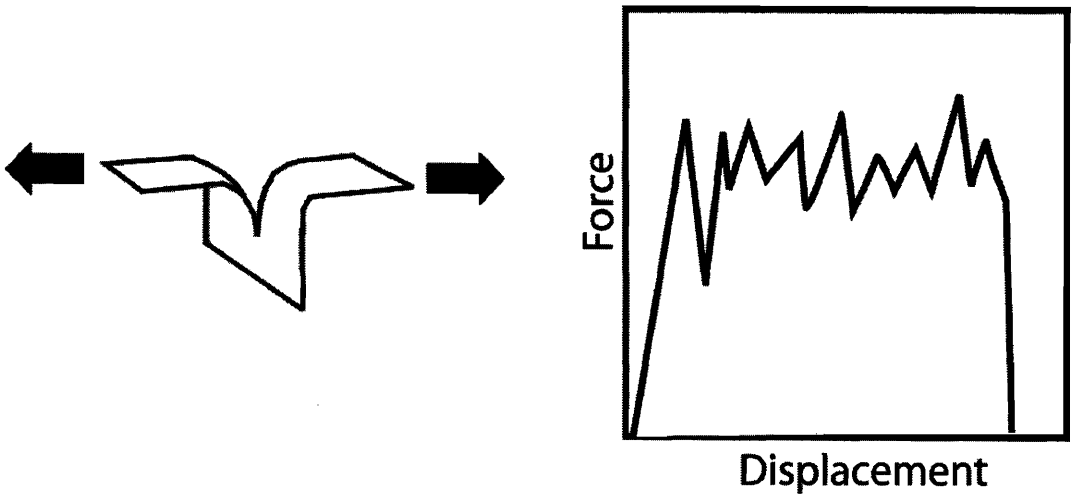

Figure 2.9. Tear strength test specimen. Typical force vs. displacement plot.

CHAPTER 3

Selection of Baroplastic Components

In this chapter, the criteria for the selection of pressure induced miscible systems suitable for low temperature processing is discussed. Baroplastic systems are selected based on their components' individual properties, previous experimental data and phase behavior calculations using the compressible regular solution (CRS) model. Other parameters, such as synthetic feasibility, availability and cost are also considered in the design. The pressure-induced miscibility of the selected systems for low temperature processing is also demonstrated.

Although the pressure behavior for a number of polymer systems have been studied, no fully predictive model for pressure-induced mixing systems has been developed. Ruzette identified that a key parameter affecting the phase behavior of polymer pairs is their density and how it changes with temperature (thermal expansion) and pressure (compressibility).[57] As described in the first chapter, simple polymer mixture thermodynamics can be described by the Flory-Huggins (FH) equation[3]. This model captures the main features of upper critical solution temperature (UCST) phase separation but is unable to predict lower critical solution temperature (LCST) behavior, which is a direct outcome of compressibility in polymer mixtures. In the FH model compressibility effects are neglected by using a fixed cell volume and filling all lattice sites, so LCST behavior and pressure dependence cannot be captured.

Numerous models for the free energy of polymer mixtures have been developed that are based on an equation of state and therefore compressibility can be taken into account. In so-called cell models, compressibility and thermal expansion are taken into account by allowing change in the cell volume, in contrast to FH theory where it is fixed. In addition, the interaction between components is calculated using a Lennard-Jones type potential. Examples of such models are the Flory, Orwoll, Vrij (FOV) model and the Prigonine "square-well" cell model (CM). [82] A different kind of model was developed by Sanchez and Lacombe called the lattice fluid (LF) model, in which compressibility is accounted for by the addition of vacant sites into the lattice, which represent the free volume present in the mixture and are assumed to mix randomly with the polymer. In this model the lattice sites are fixed and changes in the free volume are accounted for by the addition/removal of vacancies in the lattice. The LF model is successful in describing LCST behavior and has been widely used to analyze phase behavior data.[83, 84]

Simha and Somcynsky combined the two approaches described above in their hole theory.[85] In their approach, the cell can change in volume and the interactions are accounted for by a potential, but the free volume is also accounted for by the addition/removal of vacancies in the lattice. This model is successful in capturing the miscibility of polymer mixtures as well as in describing other effects, such as pressure effects, on phase behavior.[85,86] Freed and coworkers developed the lattice cluster model (LC) in which connectivity of the repeat units is taken into account by allowing a single monomer unit to occupy more than one neighboring cell in the lattice. This molecular representation has been useful in capturing the effect of monomer size, shape and structure, as well as chain architecture on the thermodynamic properties of the blend. The

LC theory has been able to model not only LCST behavior but also the effect of pressure on the phase behavior of polymer blends by inclusion of compressibility effects with the addition of empty lattice sites.[87, 88]

Models based on perturbation theory, in which the interactions are divided into repulsive and attractive parts, have also been able to capture the different phase behaviors present in polymer mixtures. The perturbed-chain statistical model (PC-SAFT) is an example of such models, in which the molecules are assumed to be chains of freely jointed spherical segments that interact among each other.[89] The perturbed hard-sphere chain equation of state (PHSC) is a similar model wherein the effective hard-sphere diameter and attractive energy parameters are theoretically based functions of temperature.[90] The Cho and Sanchez equation of state (CS) is also based on perturbed chain theory, where the reference free energy of hard chains is composed of an ideal Gaussian chain contribution with no volume exclusion and an excess free energy which incorporates a finite excluded volume contribution[91, 92].

Despite the fact that the above models can capture compressibility effects in polymer systems, yielding to the calculation UCST as well as LCST behavior, they still need experimental information about the specific polymer pair under study. In particular they all require an experimental value (or correction factor) for their interaction parameter expressions, losing generality and therefore their use as practical predictive tools.

To address the need for a predictive model for the phase behavior of compressible polymer mixtures, Ruzette and Mayes developed the compressible regular solution (CRS)

model.[93] This model was shown to capture, at least qualitatively, the phase behavior of polymer binary[93] and ternary[94] systems, using only pure component properties. The model is a regular solution model that accounts for the reduced probability of interactions between polymer segments because of thermal expansion. The free energy per unit volume is expressed as:

$$\Delta g_{mix} = kT\left[\frac{\phi_A\tilde{\rho}_A}{N_A v_A}\ln\phi_A + \frac{\phi_B\tilde{\rho}_B}{N_B v_B}\ln\phi_B\right] + \phi_A\phi_B\tilde{\rho}_A\tilde{\rho}_B\left(\delta_{A,0}-\delta_{B,0}\right)^2 + \phi_A\phi_B\left(\tilde{\rho}_A-\tilde{\rho}_B\right)\left(\delta_A^2-\delta_B^2\right) \quad [3.1]$$

where $\tilde{\rho}_i$ is the reduced density (density/hard core density), v_i is the hard core molar volume, $\delta_{i,0}$ and δ_i are the solubility parameters at 0 K and temperature T, respectively, N_i is the number of repeat units per chain and ϕ_i is the volume fraction of component i. The standard Berthelot mixing rule is invoked in this model, such that the solubility parameter of the mixed state is a geometric average of the component values. The first term of equation [3.1] accounts for the translational entropy of mixing in a similar way to the Flory-Huggins formalism. The second term can be related directly to the Flory-Huggins interaction parameter approximation:

$$\chi^{FH} = \frac{\sqrt{v_A v_B}}{kT}\left(\delta_{A,0}-\delta_{B,0}\right)^2 \quad [3.2]$$

Note that this term is always positive, destabilizing the mixture. The third term of the model, which arises solely from the compressibility of the components, can be either positive or negative, enabling the model to predict USCT and/or LCST behavior. The

term becomes zero in the incompressible limit ($\tilde{\rho}_A = \tilde{\rho}_B = 1$), yielding the classic FH expression for the free energy of mixing.

The density and its dependence on temperature, $\rho_i(T)$, was assumed to follow the form:

$$\rho_i(T) = \rho_i^* e^{-\alpha_i T} \qquad [3.3]$$

where α_i is the coefficient of thermal expansion for component *i*, obtained from exponential fits to previously reported P-V-T data,[82,95] either as the empirical Tait equation or from the Sanchez-Lacombe lattice fluid equation of state.[96] The hard core density, ρ_i^*, is taken to be the extrapolation of this fit to 0 K. From this value, one can obtain $\tilde{\rho}_i$ and $v_i = M_i / N_{Av}\rho_i^*$, where M_i is the molecular weight of the repeat unit or molecule and N_{Av} is Avogadro's number. To obtain solubility parameter values for a given temperature T, the solubility parameter at 298 K was first calculated by group contribution methods[97,98] and then extrapolated to the required temperature using the following expression:[93]

$$\delta_i^2(T) = \delta_i^2(298)\left(\frac{\tilde{\rho}_i(T)}{\tilde{\rho}_i(298)}\right) \qquad [3.4]$$

Figure 3.1 shows the calculated phase diagram of the PS/PBA and poly(styrene)/ poly(2-ethyl hexyl acrylate) (PS/PEHA) blend systems (*N*=5000 for all components). The parameters used in these calculations are shown in Table 3.1. It can be observed from Figure 3.1 that UCST and LCST behavior is predicted for both systems, although the LCST is outside the experimental window for PEHA/PS. PEHA/PS also presents a lower

UCST than PBA/PS for comparable number of repeat units, *N*, suggesting a higher miscibility between the PEHA and PS components.

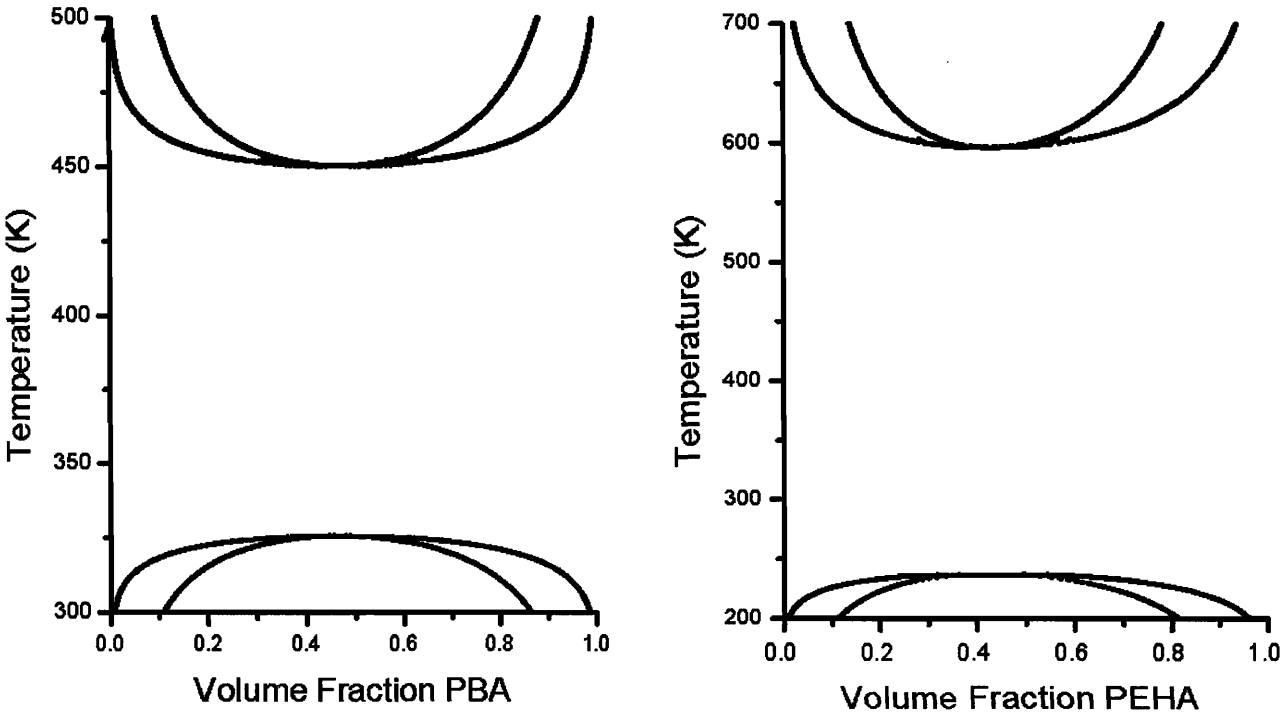

Figure 3.1. Calculated phase diagrams of PS/PBA and PS/PEHA. N=5000 for all components.

The CRS model was utilized to predict the phase behavior of certain polymer pairs, and to obtain some insight about the pressure dependence of their miscibility. For the proposed low temperature processing of baroplastic systems, phase separation between the components is desired at room temperature and atmospheric pressure. Nevertheless, the mixed state boundary should be close enough to be able to be displaced below room temperature by pressure during the processing. Knowledge, at least qualitative, of the phase diagram for baroplastic candidate materials becomes then a necessity.

Table 3.1 CRS model homopolymer parameters

	ρ* [a] (g/cm^3)	α ($10^{-4}K^{-1}$)	δ_{298} ($J^{1/2}/cm^{3/2}$)	$N_{av}v$ (cm^3/mol)	T_g (°C)
(PS)Polystyrene	1.24	5.13	18.19	83.87	100
(α-MPS) Poly(α-methyl styrene)	1.33	5.76	18.50	88.72	173
(PMMA) Poly(methyl methacrylate)	1.42	5.48	19.65	70.42	100
(PEMA) Poly(ethyl methacrylate)	1.42	7.47	19.00	80.28	65
(PBMA) Poly(butyl methacrylate)	1.29	6.89	18.45	110.1	20
(PiBMA) Poly(isobutyl methacrylate)	1.31	6.15	18.10	108.4	55
(PtBMA) Poly(tertbutyl methacrylate)	1.44	7.00	17.69	98.61	120
(PCHMA) poly(cyclohexyl methacrylate)	1.36	6.24	18.70	168	80
(POMA) Poly(octyl methacrylate)	1.15	5.80	17.45	172.2	-20
(PLMA) Poly(lauryl methacrylate)	1.14	6.80	16.94	222.8	-50
(PMA) Poly(methyl acrylate)	1.55	8.82	20.43	55.48	10
(PEA) Poly(ethyl acrylate)	1.39	7.24	19.56	71.94	-25
(PBA) Poly(butyl acrylate)	1.22	6.18	18.64	106.7	-55
(PiBA) Poly(isobutyl acrylate)	1.23	4.75	18.38	97.56	-25
(PtBA) Poly(tertbutyl acrylate)	1.35	5.81	17.20	88.89	40
(PHA) Poly(hexyl acrylate)	1.17	5.53	18.75	133.3	-60
(PCHA) Poly(cyclo hexyl acrylate)	1.27	5.54	18.07	121.26	20
(PEHA) Poly(2-ethyl hexyl acrylate)	1.25	4.78	18.05	151.2	-70
(PC) Polycarbonate	1.51	6.33	19.07	168.2	145
(PI) Polyisoprene	1.09	6.51	16.40	62.62	-50
(PMB) Poly(methylbutylene)	0.91	5.94	16.19	76.94	-
(PEB) Poly(ethylbutylene)	0.88	6.09	16.34	98.97	-

a. obtained from density fits to $\rho_i = \rho_i^* e^{-\alpha_i T}$

Knowing the temperature vs composition phase diagram is not enough information to identify a polymer pair as a baroplastic material suitable for low temperature processing. Although the CRS model is not a complete equation of state model, its parameters and in particular its third term can provide some guidelines regarding pressure effects on a given polymer pair. It was observed that pressure-induced miscibility occurs in systems having components of similar densities. A range in densities was determined by observation of the n-alkyl methacrylate/polystyrene systems where pressure induced miscibility occurs. It was determined that the two components densities, ρ_A and ρ_B, should be close enough such that $0.94\ \rho_A < \rho_B < 1.06\ \rho_A$ at 25°C.[58]

The CRS third term is a result of the differences in thermal expansion between components. It was observed that its numerical value as temperature was extrapolated to 0K, which represents a reduction in the free volume in a similar fashion as increasing pressure, differs between systems exhibiting pressure-induced mixing and pressure-induced demixing.[99] Figure 3.2 shows plots of the third term as it approaches 0K for different polymer systems. It can be observed that for the pressure-induced mixing system poly(methylbutylene)/poly(ethylbutylene) (PMB/PEB)[51] (Figure 3.2a) the values are negative and have a negative slope. Similar behavior is observed for the PS/PBA system (Figure 3.2b). In contrast, positive values and positive slopes are observed for pressure-induced demixing systems such as PS/PI and PS/PLMA (Figure 3.2c and 3.2d respectively).

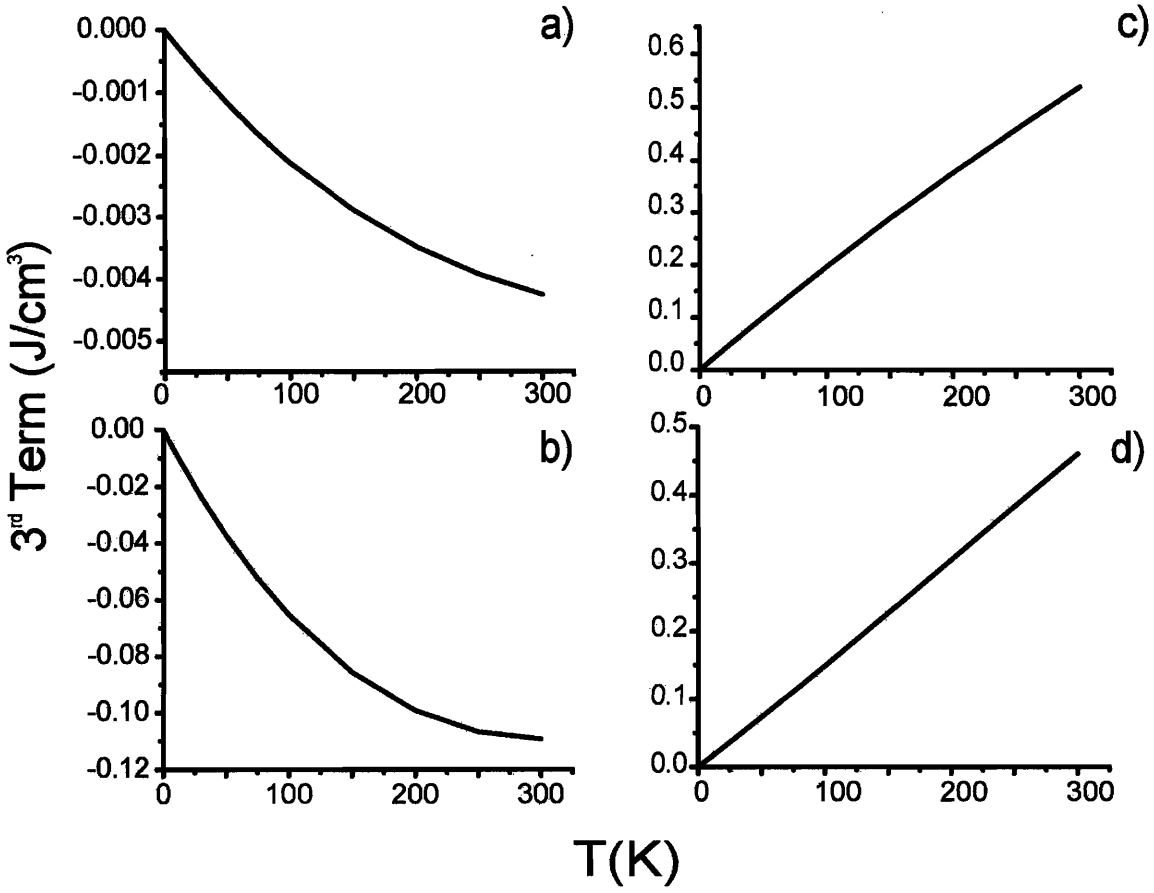

Figure 3.2. CRS model third term values as function of temperature of a) PMB/PEB, b) PS/PBA, c) PS/PI and d) PS/PLMA.

Other systems for which the third term approaches zero at 0 Kelvin from negative values, and whose ambient-state densities nearly match[54], have been found to exhibit pressure-induced miscibility, including PS/PBMA[53], PS/poly(hexyl methacrylate)[53,57], PS/poly(pentyl methacrylate)[100], polybutadiene (PB) /PI[44] and poly(ethylene propylene)-*block*-poly(ethyl ethylene) (PEP-*b*-PEE)[46]. By contrast, these conditions are not met also for PS/PB, a commercially important block copolymer system that has been found to exhibit reduced miscibility with applied pressure.[49, 101]

For comparison, Figure 3.3 shows how the first and second terms of the CRS model change as temperature approaches 0K for a PBA/PS system. Figure 3.3a shows the translational entropy contribution to the CRS model as a function of increasing number of repeat units, *N*. It can be observed that the magnitude of this term is substantially reduced at higher molecular weights. The 2nd term of the CRS model, proportional to the incompressible interaction energy term, as a function of temperature is shown in Figure 3.3b. At 0K, a positive numerical valued is obtained, as would be obtained by the use of an incompressible χ^{FH} interaction parameter. The 2nd term value decreases with increasing temperature due to the volume expansion of the polymer components. It can also be observed that the numerical values of the 3rd term (Figure 3.2b) are comparable in magnitude to the values of the 2nd term. Table 3.2 shows examples of the values for the three terms of the CRS model for pressure induced mixing and demixing systems at 300K. It can be seen that in every case the third term has a significant contribution to the total interaction energy value.

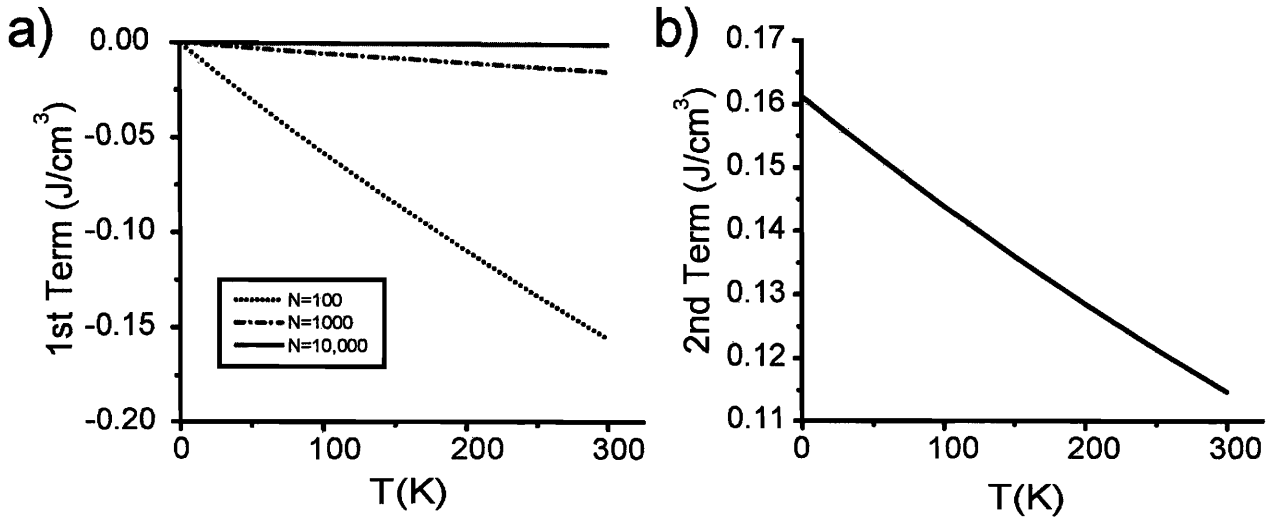

Figure 3.3. CRS model a) first and b) second terms as function of temperature for PS/PBA.

Table 3.2 CRS model terms

System	1st term (J/cm^3)	2nd term (J/cm^3)	3rd term (J/cm^3)	Δg_{mix} (J/cm^3)
PMB/PEB	-0.083	0.007	-0.004	-0.080
PS/PBA	-0.077	0.114	-0.109	-0.072
PS/PI	-0.100	0.431	0.538	0.869
PS/PLMA	-0.060	0.122	0.460	0.538

N=200 and T=300k.

An important parameter for the selection of baroplastic systems to be studied for low temperature processing is the glass transition temperature, T_g, of its components. It is desired that the T_g of the hard component is high (higher than 25°C) to provide rigidity to the system at room temperature. The soft component T_g is desired to be as low as possible to provide fluidity to the system when mixed. The mechanical and rheological properties at a given temperature for a disordered block copolymer depend on the glass transition temperature of the mixed state, $T_{g,mix}$. A disordered block copolymer will behave as a liquid at a temperature above its $T_{g,mix}$. Since room temperature processing was one of the main objectives of this work, the polymers comprising the baroplastic systems and their relative amounts were chosen such that their $T_{g,mix}$, is below 25°C. Composition was targeted using a simple combination rule to obtain $T_{g,mix}$: [102]

$$\frac{1}{T_{g,mix}} = \frac{w_A}{T_{g,A}} + \frac{w_B}{T_{g,B}} \qquad [3.5]$$

where w_i is the weight fraction and $T_{g,i}$ is the glass transition (in Kelvin) of component i.

Components and their relative amounts may be changed if the desired working temperature is to be different, as long as one component's T_g is below the working temperature and the other above. As will be discussed in more detail in the following chapters, composition plays an important role in the processing and final mechanical properties of baroplastic materials.

Along with the simple guidelines describe above, other practical design criteria must be considered, such as availability and price of the monomer as well as synthesis feasibility and ease. Styrene and acrylate chemistries are ideal for baroplastic systems. They are commercially available monomers and can be synthesized into block copolymers by atom transfer radical polymerization (ATRP), which has great potential for industrial scale up, or into polymer particles by emulsion polymerization.

This work focused on the study of two systems, namely PS/PBA and PS/PEHA, but the possible spectrum of baroplastic systems is very large. Table 3.3 shows combinations of polystyrenes, poly(methacrylates) and poly(acrylates) that comply with the criteria described above. Other systems with different chemistries such as polycarbonate were also considered and a possible baroplastic candidate is predicted with PMA.

Pressure induced miscibility for the PS/PBA system was demonstrated by Ruzette.[58] Figure 3.4 shows the SANS intensity plot of a 100k g/mol PS-*b*-PBA block copolymer at 180°C as a function of pressure.

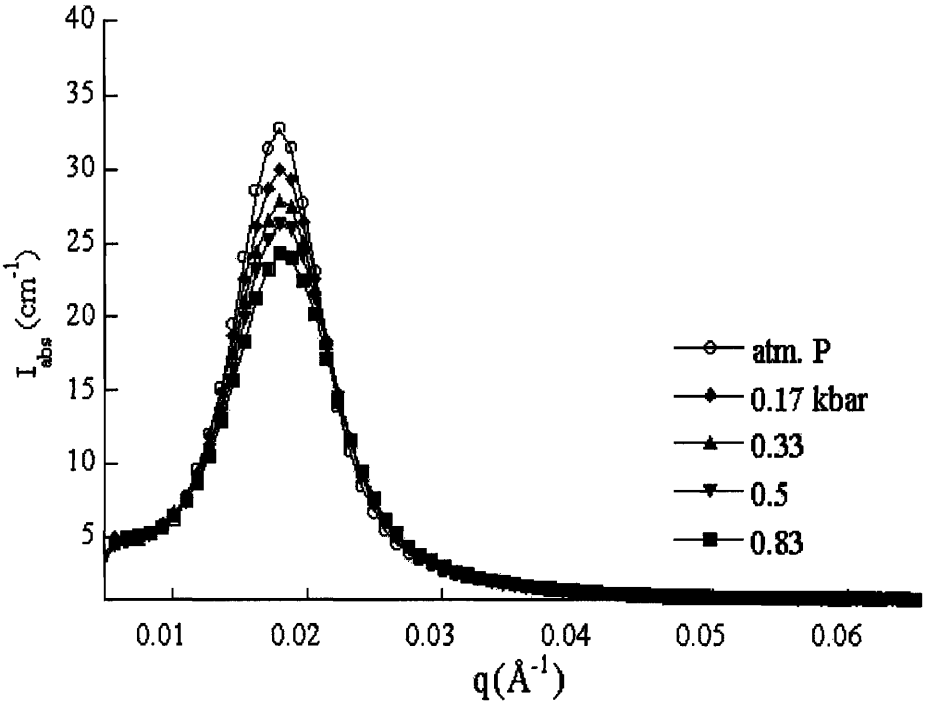

Figure 3.4. SANS Intensity (*I*) vs wavevector (*q*) plot for a 100k g/mol PS-*b*-PBA block copolymer at 180°C.

The intensity of the scattering peak decreases with increasing pressure, as a result of increased mixing between the block copolymer phase-separated domains. Since it was demonstrated that PS-*b*-PBA becomes more miscible under the application of pressure, it was an ideal system to test the potential room temperature processing of baroplastic materials.

To demonstrate the pressure induced miscibility of the PEHA/PS system, SANS measurements were performed on a 76k g/mol (d8)PS-*b*-PEHA. In this case, the measurements were carried out at 30°C after the sample was previously annealed to

obtained a sharp phase separation peak. Figure 3.5 presents the resulting intensity plot as function of increasing pressure.

Table 3.3 Baroplastic candidates

Polymer A	**Polymer B**	ρ_A/ρ_B	$T_{g,mix}$ (°C)[a]
PBMA	PHA	1.06	-25
	PBA	1.04	-20
	PiBA	0.98	-4
PtBA	PEA	1.01	6
PiBMA	PEA	0.97	10
	PiBA	1.02	10
PEMA	PMA	0.95	35
PCHMA	PEA	1.01	20
	PiBA	1.06	20
	PMA	0.95	40
PMMA	PMA	1.01	50
PtBMA	PEA	1.04	30
	PMA	0.98	50
PS	PEA	0.95	25
	PBMA	1.01	50
α-MPS	PEHA	1.03	5
	PiBA	1.05	45
	PEA	0.99	45
	PMA	0.94	70
	PCHA	1.04	80
PC	PMA	1.06	65

[a] assuming 50:50 composition

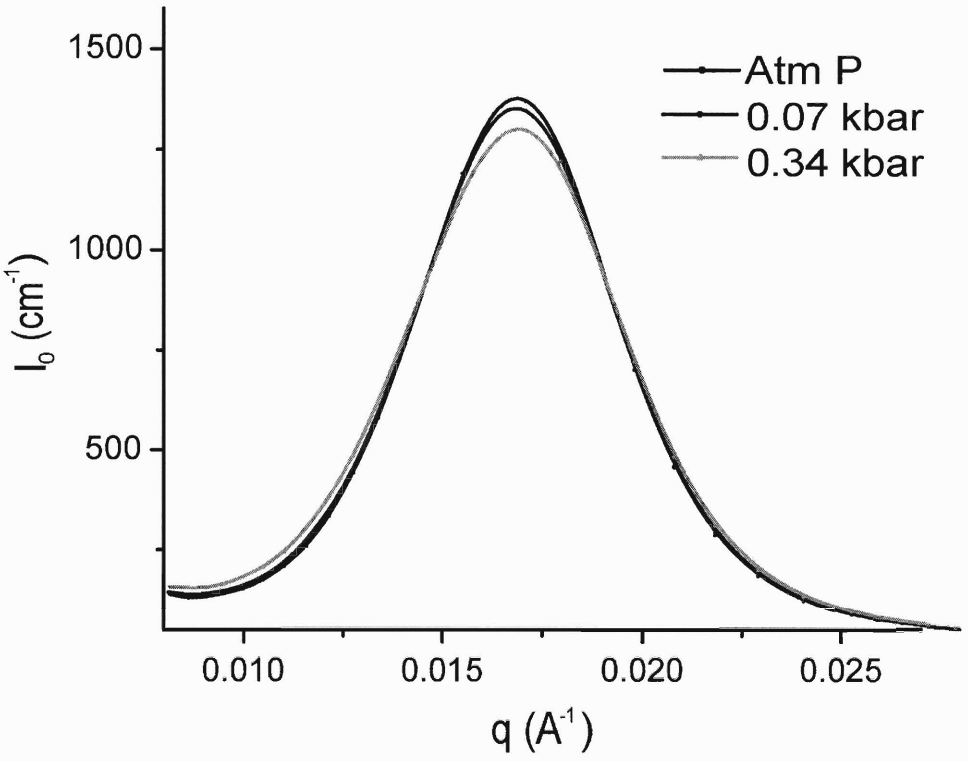

Figure 3.5. SANS scattering intensity profiles for the (d8)-PS-b-PEHA (SbE2) system at room temperature and different applied pressures.

From Figure 3.5 it can be observed that there is a small decrease of the peak intensity as pressure increases at room temperature, demonstrating that the PEHA/PS systems present pressure induced miscibility. Unfortunately decompression measurements couldn't be carried out to check for reversibility.

It can be also observed that the intensity decrease is small and the peak is still sharp at 5000 psi, indicating that a microphase-separated structure is still present during the pressurization. Complete mixing is most probably hindered by the slow polymer chain kinetics at this temperature. This experiment demonstrated that partial mixing at low temperatures is possible. However, as discussed in more detail in the following

chapters, the low temperature processing of baroplastics results not only from the pressure-driven mixing of their components.

CHAPTER 4

Block Copolymer Baroplastics

In this chapter, the characteristics of the obtained block copolymers from atom transfer radical polymerization (ATRP) are described. The processing of these materials at low temperatures is demonstrated and a processing mechanism is proposed. The effect of composition and structure on mechanical properties and processability of block copolymer baroplastics is also discussed. In addition, the role of pressure-induced miscibility is studied by the use of a copolymer control that exhibits pressure induced demixing.

4.1 Block copolymer synthesis and characterization

The characteristics of the block copolymers used in this work are shown in Table 4.1. Block copolymer polymerizations were traced by GPC to monitor the chain growth within the block and to confirm the continuation of the second block. This could be observed as a shift of the peak to lower elution time (higher molecular weights). The obtained polydispersities were on the order of 1.4 - 1.7, which are typical in ATRP. In some cases a residual portion of unreacted homopolymer was detected as a shoulder to the block copolymer peak. If a substantial quantity of unreacted homopolymer was present, it macrophase separated from the block copolymer leading to an opaque final product. Techniques to separate homopolymer from the final mixed product have been reported[60], although it was found difficult to perform in our materials.

Table 4.1. Block copolymer characteristics.

Block Copolymer	Synthesis method	Wt% PS	M_n (g/mol) (M_w/M_n)
PS-*b*-PBA (SbB1)	1 pot	40	57k (1.6)
PBA-*b*-PS (SbB2)	2 pots	53	82k (1.42)
PS-*b*-PBA (SbB3)	1 pot	67	59k (1.7)
PS-*b*-PBA (SbB5)	1 pot	55	38k (1.2)
PS-*b*-PBA-*b*-PS (SbBbS)	2 pots	29	105k (1.6)
PS-*b*-PEHA (SbE1)	1 pot	49	35k (1.7)
(d8)PS-*b*-PEHA (SbE2)	1 pot	50 (target)	76k (1.6)
PS-*b*-PEHA-*b*-PS (SbEbS)	1 pot	41	30.6k (1.6)
PS-*b*-PLMA (AV PLMA) (SbL1)	2 pots*	47	115k (1.3)

* Prepared by A-V. Ruzette.

Composition was determined as calculated from the integral ratio of characteristic resonances for PS at 6.3 – 7.2 ppm (styrene aromatic) and the acrylate polymer at 3.9 – 4.1 ppm (-OCH_2- of BA, EHA or LMA) from ^{1}H NMR measurement.

Evidence of microphase separation was obtained through differential scanning calorimetry (DSC), small angle neutron and X-ray scattering (SANS and SAXS), and atomic force microscopy (AFM). From DSC measurements, a low T_g and a high T_g corresponding to the acrylate and PS, respectively, could be observed. In some cases the measured T_g values do not correspond exactly to the pure homopolymer values. This is most probably due to a certain degree of intermixing between the components that shifted the T_gs to intermediate values, a phenomenon commonly observed in block copolymers.

Shifts in T_g observed for blocks polymerized in the second step of the reaction can also be attributed to the presence of residual monomer from the first step during the formation of the second block, leading to a mixed block between the first and second monomers. This occurs particularly for the single pot ATRP syntheses[65]. This problem can be avoided by conducting the polymerization in separate batches for the first and second monomers (2 pots), with a purification step of the first monomer in between. Nevertheless, this method has the potential risk of blocking the reactivity of the first block chain end halogen, necessary for the ATRP of the second block[68].

Phase separation was also demonstrated for the 35k g/mol PS-*b*-PEHA (SbE1) sample by AFM. Figure 4.1 shows the AFM image in tapping mode of (SbE1) as cast from a dilute tetrahydrofuran (THF) solution on mica. The observed region was near the edge of the cast droplet, where the film thickness allows for the phase separation to occur perpendicular to the substrate surface[103]. It can be observed that a lamellar morphology is formed with defined regions of PEHA and PS.

SANS further demonstrated the presence of microphase separation in the block copolymers. Figure 4.2 shows the intensity vs. wave vector plot for the (d8)PS-*b*-PEHA as a function of temperature.

From Figure 4.2 it can be observed that the initial state at 25°C, which corresponds to the material as obtained from the precipitation, is phase separated, as indicated by the presence of an intensity peak. The peak is broad, suggesting a highly defected morphology.

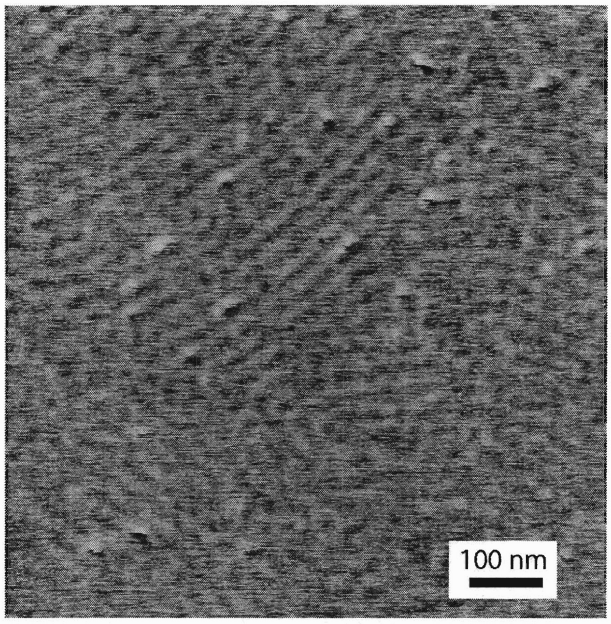

Figure 4.1. AFM image of PS-*b*-PEHA (SbE1) as cast on mica.

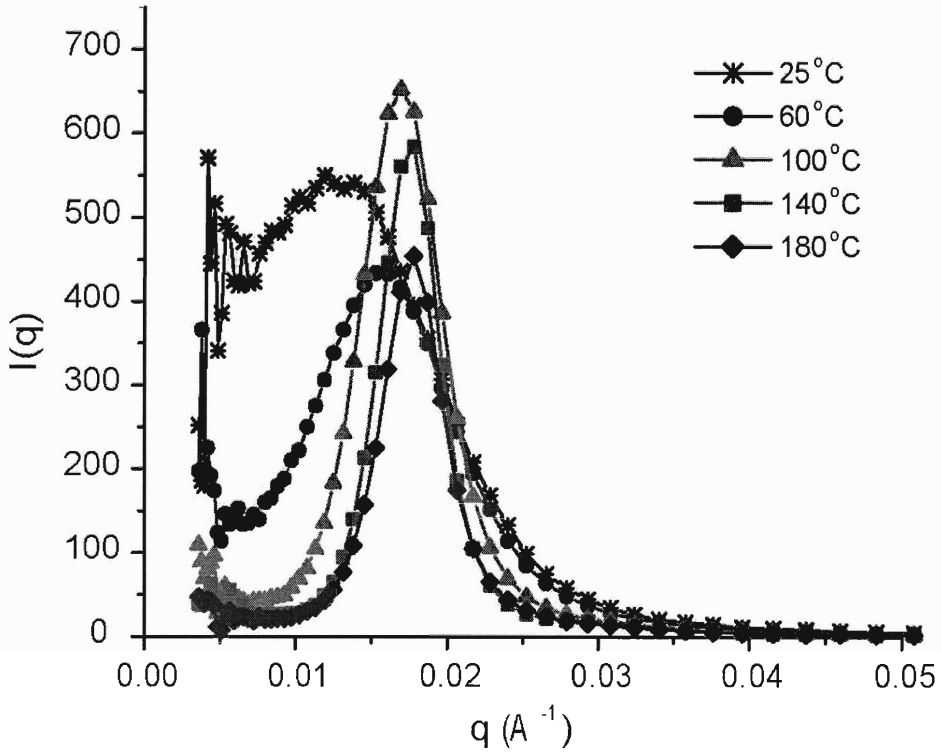

Figure 4.2 Scattering intensity profile for a 76k g/mol (d8)-PS-*b*-PEHA (SbE2) as function of increasing temperature.

It can also be observed that the peak becomes more defined as temperature is increased, enabling rearrangement to a more ordered structure. As temperature is increased above 100°C, the peak decreases, indicating that the (d8)PS-*b*-PEHA system presents UDOT type behavior as predicted by the CRS model. From the intensity curve at 140°C, a domain spacing of 35 nm can be extracted. In addition, a secondary peak at q ~ 0.03Å (a factor of $\sqrt{3}$ relative to the main peak) could be observed, which corresponds to a hexagonally packed cylinder structure[15].

4.2 Processing of block copolymers

Baroplastic block copolymers were processed by compression molding as described in the experimental methods section. Figure 4.3 shows processed objects of PS-*b*-PBA (SbB5) at 25°C with an applied pressure of 34.5 MPa (5000psi) for 5 minutes next to the material as obtained from the polymerization. The processed lid was flexible and copied the mold with enough accuracy to fit the original box from where the lid was copied to make the mold[103].

This simple compression molding experiment demonstrated that room temperature processing of baroplastic block copolymers is possible.

The PS-*b*-PEHA system can also be processed at reduced temperatures by simple compression molding experiments. Figure 4.4b shows a PS-*b*-PEHA (SbE1) object processed at 30°C with an applied pressure of 34.5 MPa for 5 minutes, next to the polymer as obtained from polymerization (Figure 4.4a).

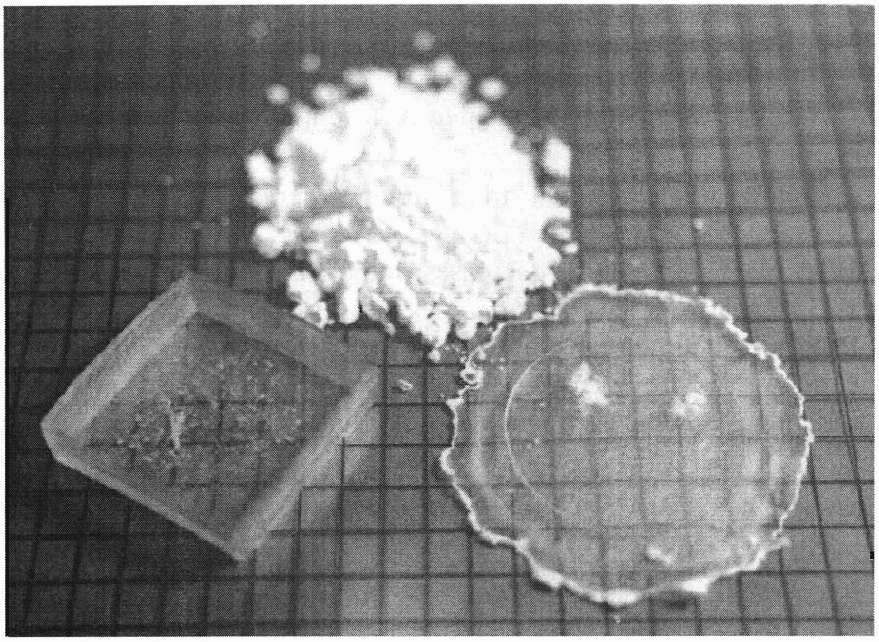

Figure 4.3. Baroplastic sample of 38k g/mol PS-*b*-PBA (SbB5) as obtained from freeze-drying and after processing by compression molding at 25 °C using a pressure of 34.5 MPa (5000 psi).

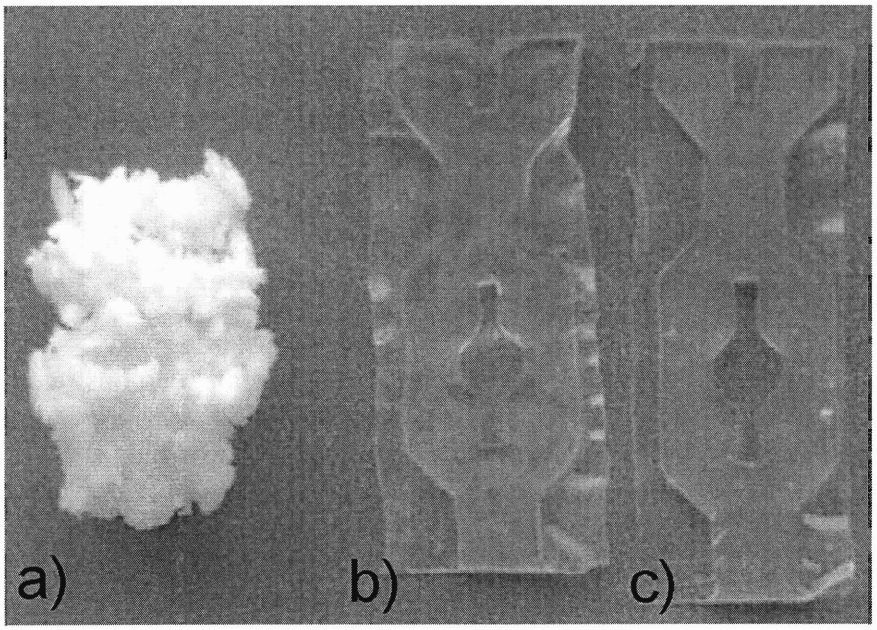

Figure 4.4. 35k g/mol PS-*b*-PEHA (SbE1) as a) obtained from polymerization and processed b) 1 time and c) 10 times at 30°C with an applied pressure of 34.5 MPa for 5 minutes.

In this case, a transparent object, which copied the employed aluminum mold, was also obtained. In an attempt to demonstrate the potential of baroplastics to be recycled at low temperatures, this sample was reprocessed 9 additional times, each time cutting the obtained object into ~4 mm pieces and subjecting them again to the pressurization process. Figure 4.4c shows the resulting object after 10 processing cycles at 30°C with an applied pressure of 34.5 MPa for 5 minutes each[99].

4.3 Processing Mechanism

SANS measurements were performed on similar systems as the ones described above before and after low temperature processing. Figure 4.5a shows the intensity plot for the PS-*b*-PEHA (SbE1) system, processed, annealed and processed after annealing[99]. It can be observed that the peak becomes sharper after annealing the processed sample at 25°C as expected (Figure 4.2). After processing the annealed sample, the peak decreases in intensity and widens, consistent again with pressure-induced miscibility. Figure 4.5b shows the same system as obtained from polymerization, processed 1 and 10 times. It was found that the intensity of the peak decreased with increasing processing cycles. This decrease in intensity can also be related to an increase in miscibility between the two components as the sample is subjected for longer times to the processing pressure.

DSC measurements from the same PS-*b*-PEHA (SbE1) system (Figure 4.6) show that the low T_g transition remains almost unchanged, the high T_g becomes more resolved at a slightly higher temperature and a mixed T_g appears around 60°C, whose signal seems to

become stronger with more cycling processes, supporting pressure induced mixing during processing

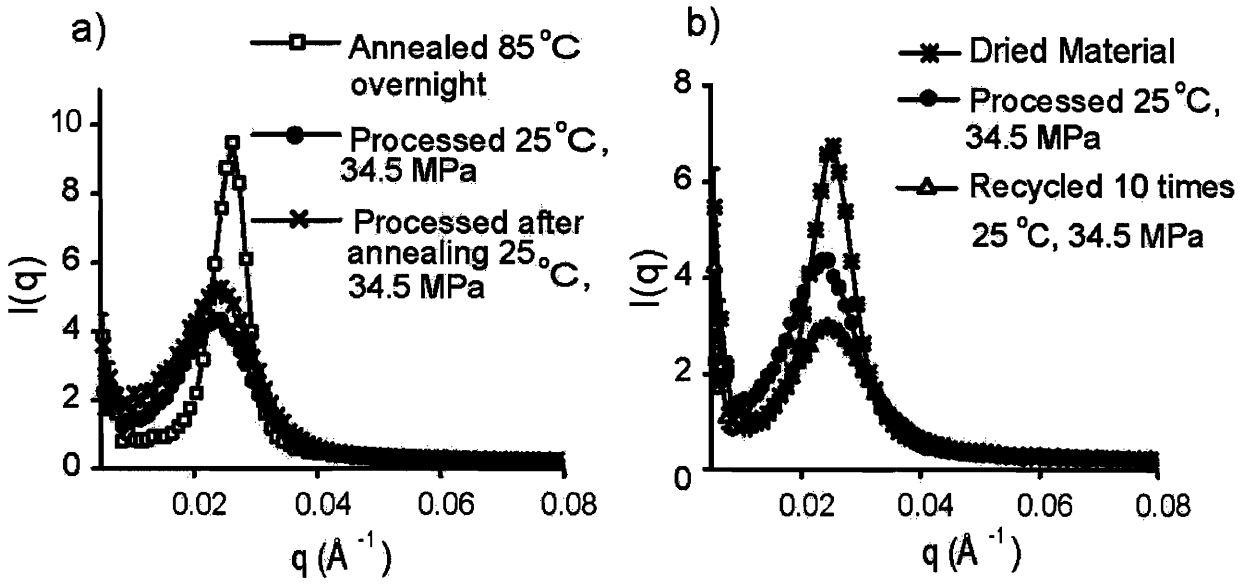

Figure 4.5. SANS scattering intensity profile for PS-*b*-PEHA (SbE1) a) processed after annealing and b) processed for 1 and 10 times at the indicated temperature and pressure conditions.

From these experiments two important features about the low temperature processing of baroplastics become clear. First, that mixing is actually occurring during processing by the application of pressure, at least at the interphase level. Second that the mixing is not complete during pressurization, and distinct domains are always present even after several processing cycles.

These results suggest that the system is able to flow even though the rigid domains are not totally mixed with the low T_g component. The low T_g acrylate domains serve as a

mobile layer and binder to the rigid PS domains, allowing flow and molding into a new shape

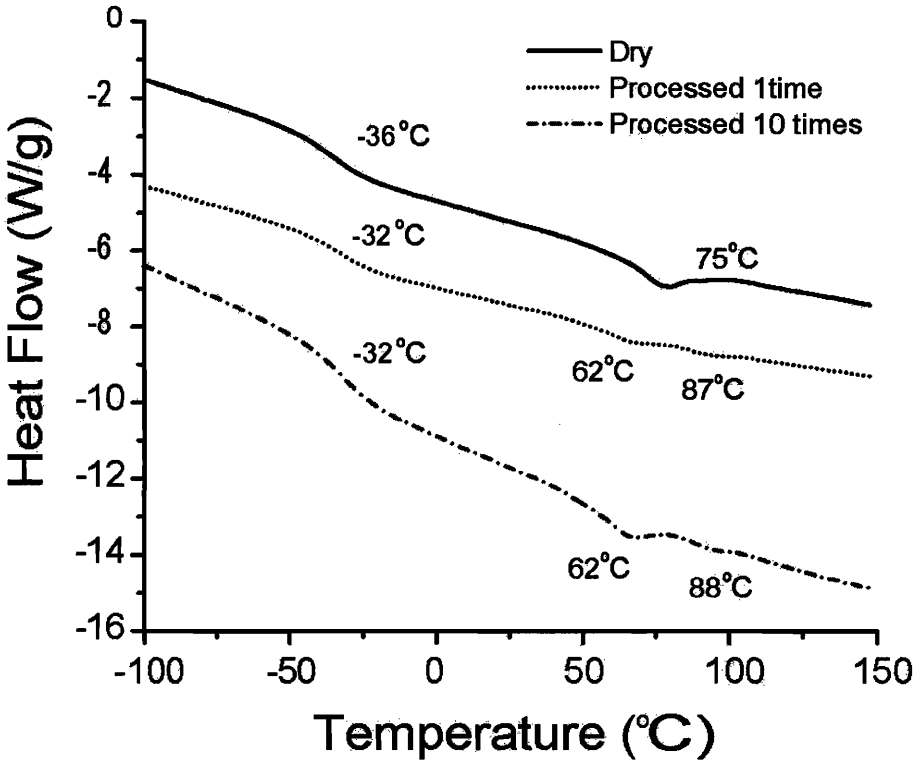

Figure 4.6. Heat flow curves for PS-*b*-PEHA (SbE1) as obtained from the polymerization (dry) and processed 1 and 10 times at 25°C with a pressure of 34.5 MPa.

Similar processing mechanisms have been reported for the processing of other non-polymeric systems comprised of a soft, liquid-like component and a hard component, such as in the cold extrusion of chocolate wherein well-defined extrudates were obtained ~10 degrees below the melting point. The soft, cocoa butter component apparently mobilizes the unmelted sugar crystals (which comprise about 45% of the mixture) and other solid components under sufficient applied pressure.[104] Another example of such processing is the rheocasting of semi-solid metal alloys.[105]

A key question, then, is what role does pressure-induced miscibility play on the low temperature processing of baroplastics? To address this issue, a control sample of 115k g/mol PLMA-*b*-PS (SbL1), a non pressure-induced miscible system, was subjected to the same processing conditions as the 82k g/mol PS-*b*-PBA (SbB2) sample. Figure 4.7 shows the two compression-molded samples processed at 25°C for 5 min under an applied pressure of 5000psi. As can be observed, SbL1 (Figure 4.7a) resulted in a mixture of processed and unprocessed regions, in contrast to SbB2 (Figure 4.7b) where complete molding was achieved. The amount of unprocessed portions of the PLMA-*b*-PS (SbL1) was reduced by further pressurization; however, a complete processed sample was almost impossible to achieve at room temperature. This suggests that although low temperature processing can be carried out in pressure-induced demixing systems, it is more difficult to carry out than in baroplastic systems.

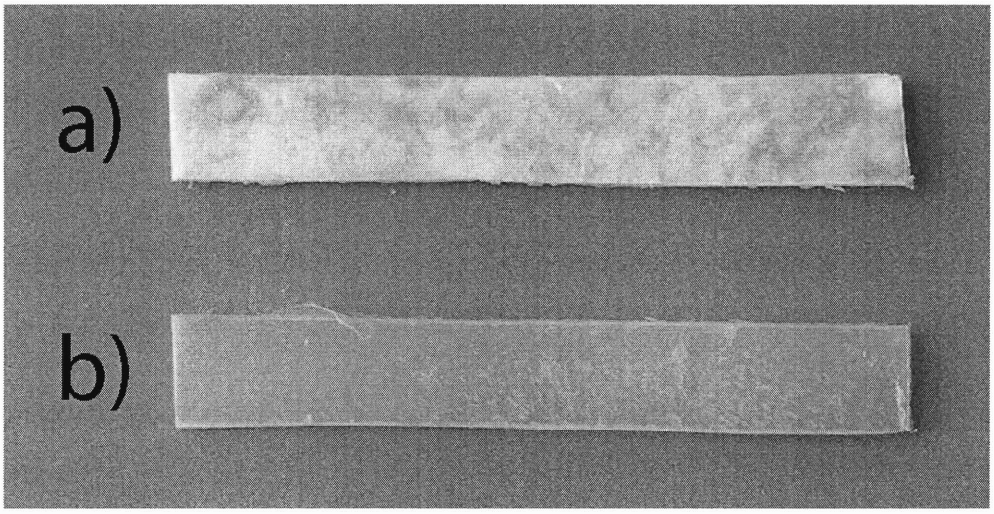

Figure 4.7. Compression molded samples of a) PLMA-*b*-PS (SbL1) and b) PS-b-PBA (SbB2) at 25°C with an applied pressure of 5000psi for 5 minutes.

Mechanical tests were measured on PLMA-*b*-PS (SbL1) samples that were processed at 25°C for 5 min under an applied pressure of 5000psi twice. The resulting tensile properties weren't very different to those of comparably processed PS-b-PBA (SbB2). However, tear strength measurements showed a significant difference between the two systems. Figure 4.8 shows the curves for the corresponding tears forces per sample thickness. It can be observed that SbB2 requires a higher force to propagate the tear and needs a substantially larger energy to break the sample (0.065 J for SbB2 compared to 0.014 J for SbL1). Although these differences could be partially attributed to the presence of unprocessed regions in SbL1, they are consistent with tear strength experiments performed on core-shell particles described in Chapter 6.

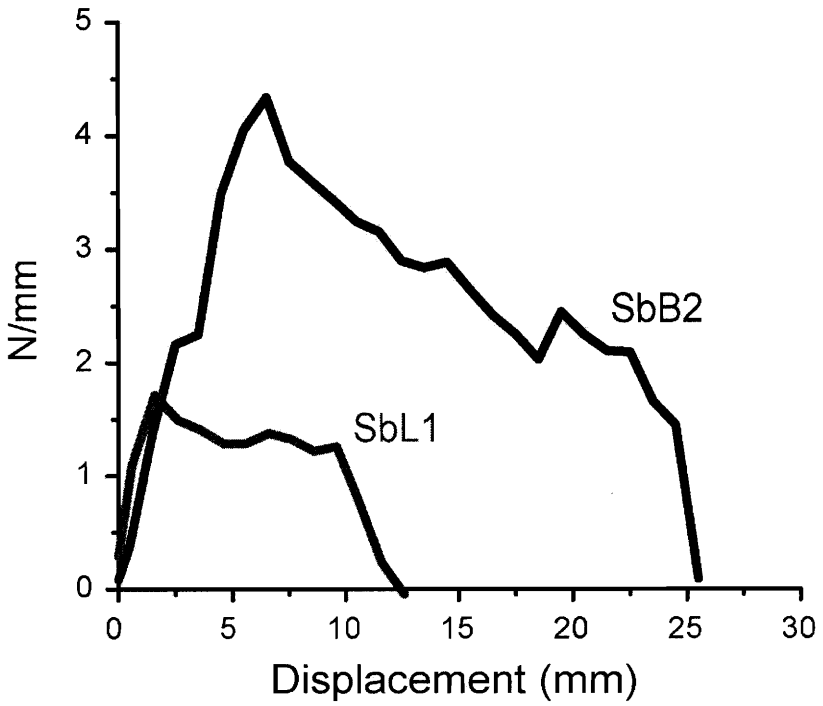

Figure 4.8. Force per sample thickness vs. displacement plot from tear strength test for PLMA-*b*-PS (SbL1) and PS-*b*-PBA (SbB2).

The ability to at least partially process a pressure induced demixing system at room temperature clearly suggest that pressure-induced miscibility is not required, although it facilitates the low temperature processing and yields cohesive objects with better mechanical properties. Low temperature processing seems to be also a function of the polymers present (low and high T_gs), their composition, molecular weight, as well as their structure. The generality of baroplastic processing will be discussed in the following chapters with the processing of core-shell baroplastic nanoparticles.

Baroplastic block copolymers of different compositions were also tested for processability under the same conditions as mention before. 57k g/mol PS-*b*-PBA (SbB1) has a lower PS content (40 wt % PS), which resulted in a soft and tacky material. Although the material is phase separated (as confirmed by DSC) and it is easily deformed by the application of pressure, it lacks strength and cohesion to form a useful solid object. It was difficult to release from the mold due to adhesiveness and has poor mechanical properties. In this case, the soft domain appears to control the mechanical properties, deforming and breaking with a minimum stress.

Samples with higher PS content were also tested for processability. PS-*b*-PBA (SbB3), with 67 wt% PS, was compression molded under 25°C with an applied pressure of 34.5 MPa for 5 minutes and resulted in an opaque object, resembling more a compacted powder object rather than a cohesive and processed specimen. For this composition PS lacks the mobility that the soft component provides. The mobile low T_g phase also seems to be necessary as a "binder" between the rigid domains to hold and form a cohesive object.

These results suggest that there is a defined window in composition where the low temperature processing of block copolymers is possible and results in cohesive objects with good mechanical properties.

4.4 Mechanical properties

Tensile tests as described in the experimental methods section were carried out on the processed block copolymer samples. Table 4.2 shows the elastic modulus, yield strength, strain to break and ultimate strengths for the measured samples.

The obtained mechanical properties, for example the elastic modulus of PS-*b*-PBA (SbB2) processed at 25°C with an applied pressure of 34.5 MPa for 5 minutes (200MPa), were substantially inferior to pure PS (E~2000 MPa) but comparable with thermoplastic elastomers of high hardness (E~23-230 MPa)[106].

Mechanical property measurements of PS-*b*-PBA (SbB2) were carried out also on samples processed at 90°C, to compare the low temperature processing with "regular" melt processing. For the case of higher temperature, a substantially higher modulus (450 MPa) was obtained. However, strain to break and ultimate strength were not significantly affected by the increase in temperature. These results suggest that although low temperature processing forms cohesive objects, the final product morphology is not equivalent to that of high T processed samples.

Tensile tests were also performed on the 35k g/mol PS-*b*-PEHA (SbE1) system. Figure 4.9 shows the stress vs. strain plot for samples processed 1 and 10 times at 25°C with an applied pressure of 34.5 MPa for 5 minutes. Comparing the mechanical properties of PS-*b*-PEHA (SbE1) processed 1 time to those from PS-*b*-PBA (SbB2) it can be observed that the modulus is substantially lower (E= 12 MPa) than for PS-*b*-PBA, as well as the yield strength and ultimate strength, while a much larger strain to break is measured on the PEHA system. These differences are most likely the result of differences in composition (SbE1 system has 49 wt% PS), molecular weight and the lower T_g of PEHA (–70°C).

Table 4.2. Block copolymer mechanical properties

Block copolymer	**Young Modulus (MPa)**	**Yield Strength (MPa)***	**Strain to Break (%)**	**Strength at break (MPa)**
PBA-*b*-PS (SbB2)	201 ± 10	---	9.8 ± 2	4.2 ± 0.3
PBA-*b*-PS (SbB2) @ 90°C	448 ± 22	10.6 ± 0.9	5.5 ± 1.8	8.9 ± 0.9
PS-*b*-PEHA (SbE1) 1 time processed	12 ± 0.5	---	114 ± 15	0.7 ± 0.2
PS-*b*-PEHA(SbE1) 10 times processed	16.6 ± 1.6	---	122 ± 15	0.6 ± 0.1
PS-*b*-PBA-*b*-PS (SbBbS) @90°C	8 ± 0.7	---	180 ± 24	2.4 ± 0.2
PS-*b*-PLMA (SbL1)	198	---	7	4.9

All Mechanical properties are on samples processed at 25°C unless noted otherwise.

* Reported only where a clear yielding point was observed

Figure 4.9 also shows the stress vs. strain plot for a recycled specimen of the same PS-*b*-PEHA (SbE1) system. Although a small increase in modulus is seen, no significant changes in ultimate strength or strain to break were found. Changes in molecular structure as the cause of mechanical property differences are unlikely, since molecular weights of the two specimens measured by GPC showed no significant differences after 10 processing cycles. Changes in the mechanical behavior are more likely due to the effect of pressure during the processing cycles on domain phase separation, as explained before.

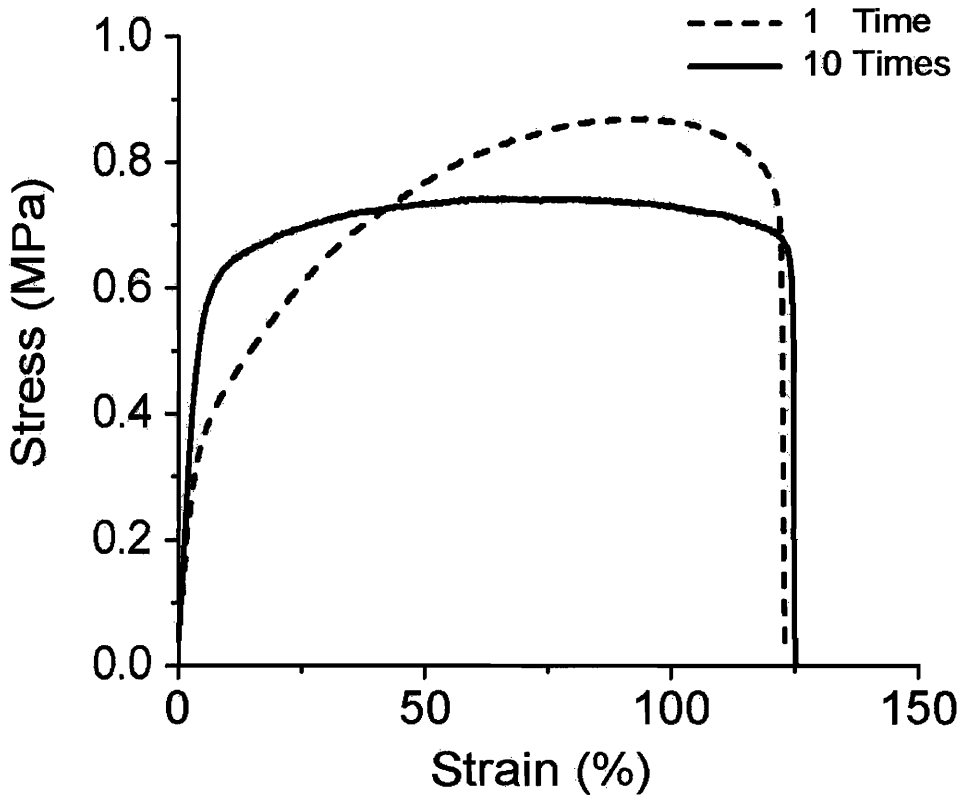

Figure 4.9. Stress vs. strain curves for PS-*b*-PEHA (SbE1) processed 1 time (---) and 10 times (—) at 25°C with an applied pressure of 34.5 MPa for 5 minutes.

In an attempt to improve the mechanical properties of the processed block copolymers, and to become more comparable to commercial thermoplastic elastomers (TPE) such as PS-*b*-polyisoprene-*b*-PS or PS-*b*-EBR-*b*-PS, triblock versions of the PS/PBA and PEHA/PS systems were synthesized. The PS-*b*-PEHA-*b*-PS (SbEbS) sample was unable to flow at room temperature, yielding a compacted powder specimen, very similar to diblock samples with high PS wt% content. A PS-*b*-PBA-*b*-PS (SbBbS) sample, with 29 wt% PS, when compression molded at 25°C under the same conditions as the diblock copolymer, yielded a highly deformed sample. The sample was unable to be processed at temperatures below 70°C. This further indicated that complete mixing does not take place during the processing and implies that the mobility present in the diblock copolymer, where one end of the soft block is free, is required to achieve the necessary mobility for low temperature processing.

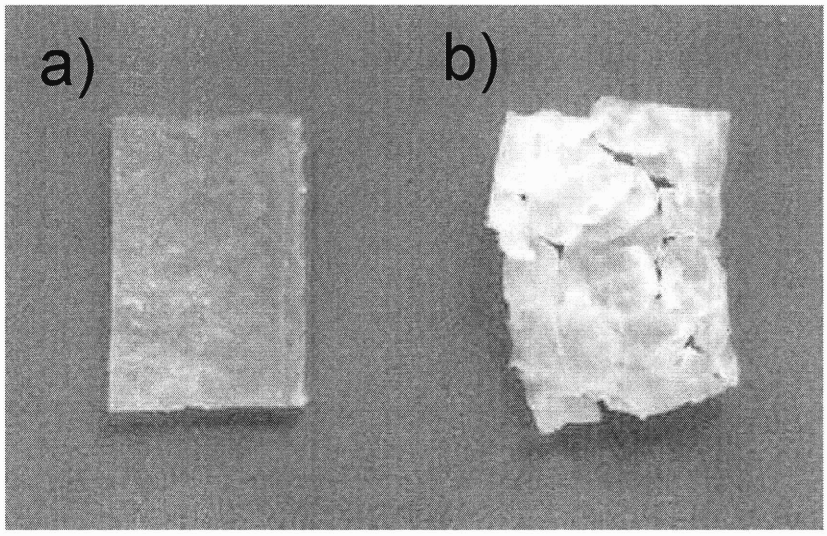

Figure 4.10. Compression molded samples of a) 105k g/mol PS-*b*-PBA-*b*-PS (SbBbS) and b) 140k g/mol PS-*b*-PB-*b*-PS (30 wt% PS) at 70°C with an applied pressure of 5000 psi for 5 minutes.

However, the 105k g/mol PS-*b*-PBA-*b*-PS (SbBbS) triblock with 29 wt% PS sample could still be molded into a defined shape at temperatures below the T_g of polystyrene by the application of pressure. A control sample of 140k g/mol PS-*b*-polybutadiene-*b*-PS, with 30 wt% PS which is a pressure demixing system, was subjected to the same conditions where processing was achieved for the PS/PBA system (70°C, 5000psi 5min). As shown in Figure 4.10, the PS/PB system couldn't form a cohesive object and the original pellets were only bound at a few points. This result supports the conclusions from the PLMA/PS control experiments that pressure induced miscibility facilitates processing.

CHAPTER 5

Core-Shell Baroplastics

As discussed in the previous chapter, block copolymer baroplastics are able to flow and process at reduced temperatures. It was observed that complete mixing doesn't occur during the pressure processing, and distinct domains are preserved after processing. Based on these results, a different approach to design low-temperature processable baroplastics using structured homopolymer blends was attempted. Core-shell nanoparticles with the mobile, low T_g material in the core and the hard, high T_g polymer in the shell were synthesized. This structure allows the two chemically different homopolymers to be in intimate contact at the nanometer scale in a well-defined and controlled structure. In addition, synthesis by emulsion polymerization is relatively simple and a wide spectrum of polymeric materials can be synthesized by this method. This chapter presents results from the synthesis, characterization and processing of core-shell baroplastics.

5.1 Synthesis and characterization

Core-shell polymer particles were synthesized as described in the experimental methods section (Chapter 2) by emulsion polymerization. Table 5.1 shows the characteristics of the core-shell nanoparticles studied in this work.

Compositions of the resulting particles ranged from 38-67 wt% PS, as calculated from the integral ratio of characteristic resonances for PS at 6.3 – 7.2 ppm (styrene aromatic)

Table 5.1. Size and composition of core-shell nanoparticles

Core/shell	Composition[a] (PS wt%)	Particle size (nm)[b] core/core-shell	M_w/M_n (g/mol) core	M_w/M_n (g/mol) shell
BS1 PBA_{43}/PS_{57}	57	163/201	561k/190k	48k/4k
BS2 PBA_{37}/PS_{63}	63	49/62	480k/156k	256k/112k
BS3 PBA_{34}/d8-PS_{67}	67 (calc)	59/82	707k/64k	654k/71k
BS4 PBA_{47}/PS_{53}	53	65 (shell)	2×10^6 [d]/1.53×10^6	1.2×10^6/153k
BS5 PBA_{56}/PS_{44}	44	55/58	167k/68k	1.0×10^6/400k
BS6 PBA_{59}/PS_{41}	41	55/60	991k/346k	133k/10k
BS7 PBA_{42}/PS_{58}	58	43/53	736k/129k	56k/7k
BS8 PBA_{37}/PS_{63}	63	61/78	994k/324k	27k/3k
BS9 PBA_{36}/PS_{64}	64	102/154	852k/230k	99k/9k
BS10 PBA_{49}/PS_{51}	51	58/72	622k/141k	190k/45k
BS11 PBA_{51}/PS_{49}	49	50/60	657k/35k	18k/4k
BS12 PBA_{45}/PS_{55} (sw50)	55	48/56		
ES1 $PEHA_{51}/PS_{49}$	49	61/74	1.1×10^6/495k	910k/303k
ES2 $PEHA_{42}/PS_{58}$	58	60/75	1.28×10^6/443k	1.1×10^6/473k
ES3 $PEHA_{62}/PS_{38}$	38	64/70	1.18×10^6/149k	84k/8.5k
ES4 $PEHA_{61}/PS_{39}$	39	58/72	469k/76k	1.1×10^6/890k
ES5 $PEHA_{53}/PS_{47}$	47	54/67	-	-
LS1 PLMA/PS	54	59/61	1.1×10^6 /518k	222k/127k

a Calculated by ^{1}H NMR.
b Measured by dynamic light scattering.
c Calculated from ^{1}H NMR and equation 1.
d Outside GPC calibration limit.

and the core polymer at 3.9 – 4.1 ppm (-OCH_2- of BA or EHA) from ^1H NMR measurement.

^{13}C NMR measurements were also performed to check for branching or crosslinking of the acrylate components as has been reported in the literature for poly(butyl acrylate) emulsion polymerization.[108] No branching was observed to within the instrument resolution. However, high molecular weights for the acrylates and methacrylates were obtained. The molecular weights were poorly controlled and GPC traces show that the core and the shell polymers both exhibit very large polydispersities (PDI range ~2-10, Table 5.1). Higher molecular weights were usually obtained for the core acrylate and methacrylate polymers while the PS synthesis usually yielded a much lower molecular weight due to the addition of chain transfer agent (2-dodecanethiol) during the 2nd stage of polymerization. Figure 5.1 shows a typical GPC trace of the core and shell polymers, where the high molecular weight (shorter elusion volume) corresponds to PBA and the lower molecular weight (large elusion volume) corresponds to PS. It should be noted that in some cases a high molecular weight PS was also obtained.

The high molecular weights and large polydispersities obtained in core-shell particles are characteristic of the emulsion polymerization. These high molecular weights affect the phase behavior of the two components, increasing their phase separation boundary. The UCST, as calculated by the CRS model, for the PBA/PS system with molecular weights of 50,000 g/mol is increased by about 100°C when the molecular weights are changed to 1M g/mol. Polymer chain mobility would also be affected by higher molecular weights

and slower kinetics would be expected. However, as explained in the following sections, core-shell nanoparticles could be processed at low temperature and their high molecular weights provide processed objects with excellent mechanical properties.

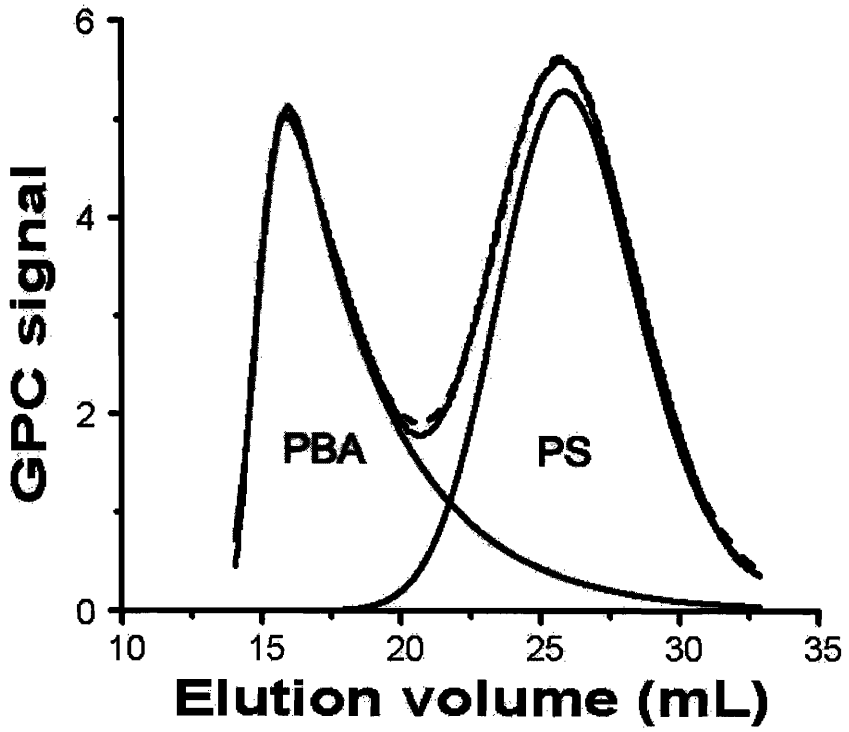

Figure 5.1. GPC traces for PBA_{51}/PS_{49} (BS11). Fitted molecular weight distributions for PBA and PS shown.

The sizes of the obtained polymer particles by dynamic light scattering (DLS) were in the range of 50 to 200nm. Figure 5.2 shows representative particle size distribution histograms of the parent PEHA core and final $PEHA_{51}/PS_{49}$ (ES1) core-shell particles. Both histograms indicate very narrow particle size distributions [109].

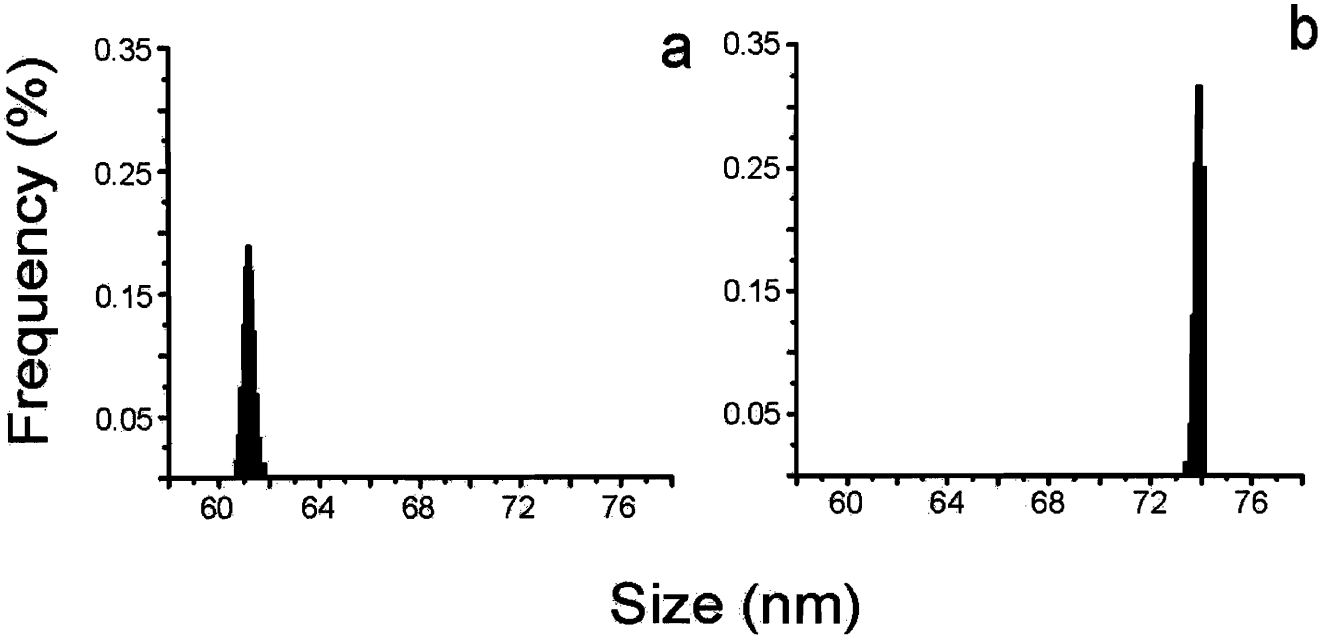

Figure 5.2. Particle size distribution histograms of (a) PEHA core (b) $PEHA_{51}/PS_{49}$ (ES1) core-shell.

Results of kinetics studies on a PEHA/PS system (Figure 5.3) show that the average particle size increased monotonically in the first 3 hours of stage one and then remained almost constant for 11 hours, indicating that the EHA was effectively consumed. Particle size increased with the addition of styrene and reached 80 nm with no evidence of residual core particles, although the rate of particle growth in the second stage was slightly lower. An incremental increase in diameter after the addition of the second monomer supports the formation of a core- shell structure, but is not sufficient evidence of a core-shell particle.[74] Other structures, such as an inverse core-shell or a swollen core with embedded PS domains would also show this change in dimension by the addition of a second component. [73]

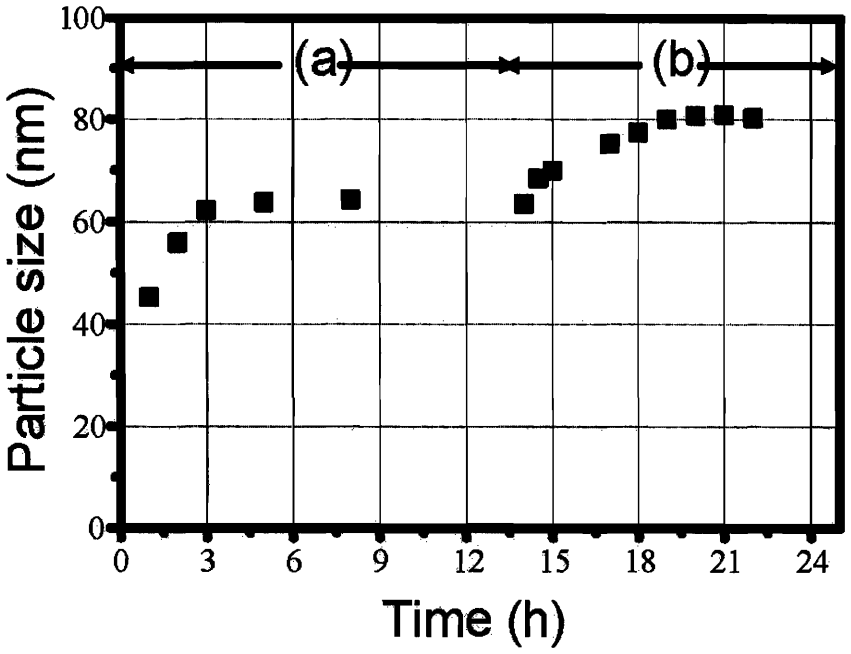

Figure 5.3. Particle size evolution of (a) first and (b) second stage as a function of polymerization time for a PEHA/PS (ES1) system at 65°C.

As discussed by Stubbs and Sundberg [74], at least 2 methods should be used to identify the structure of a particle obtained by emulsion polymerization. One of those methods should include an imaging technique such as atomic force microscopy (AFM) or transmission electron microscopy (TEM). Direct observation provides unique information about the structure of the polymer particles. AFM imaging confirmed the formation of spherical particles by emulsion polymerization. A very dilute emulsion (~1:100) of the core-shell particles, as obtained from the polymerization, was cast onto a Si wafer and measured on a Digital Instruments (Santa Barbara, CA) Nanoscope IIIa scanning probe microscope. Figure 5.4 shows the AFM image of PBA_{45}/PS_{55} (BS12) where spherical particles are clearly observed.

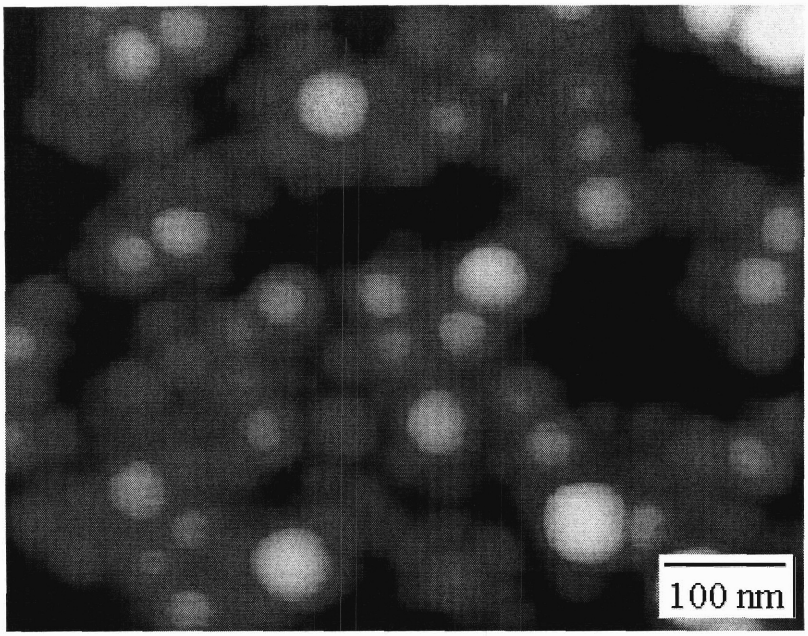

Figure 5.4. AFM of core-shell PBA_{45}/PS_{55} (BS12) particles casted on Si wafer.

Figure 5.5 shows a TEM image for processed 200 nm core-shell particles (BS1) where the core-shell structure can be clearly observed. The darker regions correspond to PS, selectively stained by RuO_4[27]. Interestingly, the observed particles are not spherical but ellipsoidal and directionally oriented. These structural features are likely due to uniaxial deformation occurring during sample preparation, since the AFM image (Figure 5.4) of the particles dried from the emulsion state revealed them to be spherical in shape.

Further analysis of the nanoparticle structure was conducted by modulated differential scanning calorimetry (MDSC). Figure 5.6 shows a typical MDSC heat flow curve for a core-shell nanoparticle system just after drying (BS6). MSDC is able to separate the measured heat flow into its reversible and non-reversible components, which are also shown in Figure 5.6. Two distinct glass transitions are observed as expected in a microphase-separated structure. In addition, a mixed glass transition, $T_{g,mix}$, is observed

around 60°C, which is attributed to the interphase of the two components. This $T_{g,mix}$ is a contribution of the non-reversible component of the heat flow curve, indicating that it corresponds to a mixed state at the interphase and not to the presence of a random copolymer.

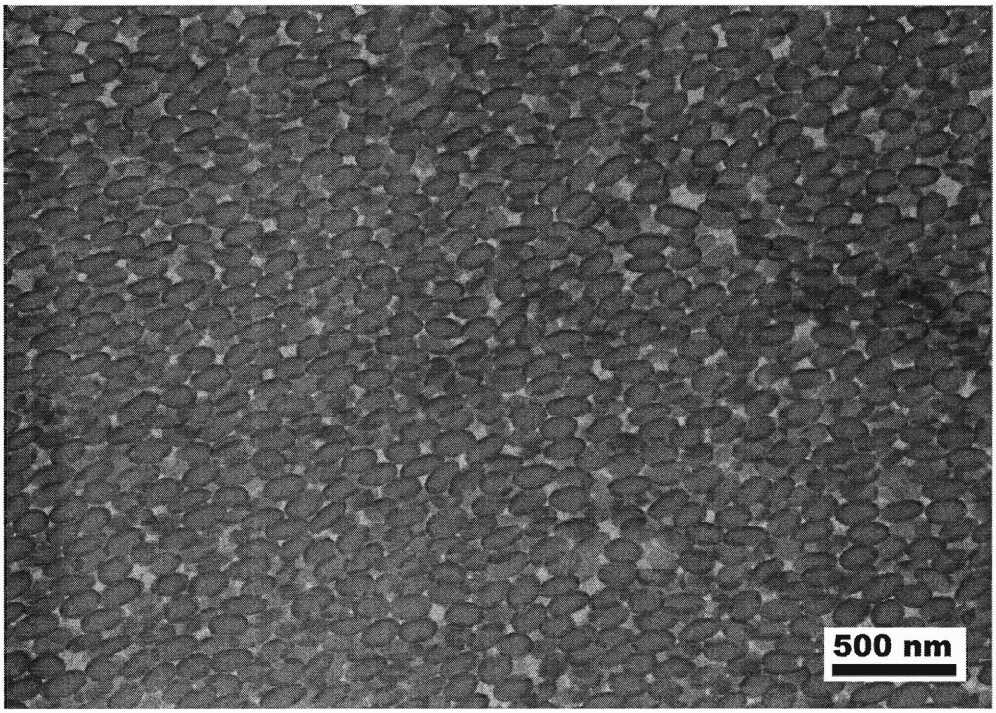

Figure 5.5 TEM image from PBA_{43}/PS_{57} (BS1) processed at 25°C under 34.5 MPa for 5 min.

A change in the specific heat (C_p) of a polymer occurs across its glass transition temperature where frozen chain segments are unfrozen and become more mobile. This change in specific heat, ΔC_p, is proportional to composition. Through careful measurement of the ΔC_p at each component's glass transition, it is possible to quantify

the amount of each component present at the interphase[73, 74, 78]. Following Hourston et al.[79] the fraction of each component present at the interphase, δ_i, can be calculated as:

$$\delta_i = w_{i0} - \frac{\Delta C_{p,i}}{\Delta C_{p,i0}} \qquad [5.1]$$

where $w_{i,0}$ is the total weight percent (from ^{1}H NMR), $\Delta C_{p,i0}$ and $\Delta C_{p,i}$ are the specific heats of the pure homopolymer i and for the polymer in the core-shell particle. The partial fraction of core component, c_c, and shell component, c_s, at the interphase can then be calculated as:

$$c_s = \left(1 - \frac{\delta_c}{(\delta_c + \delta_s)}\right) \quad \text{and} \quad c_c = \left(\frac{\delta_c}{(\delta_c + \delta_s)}\right) \qquad [5.2]$$

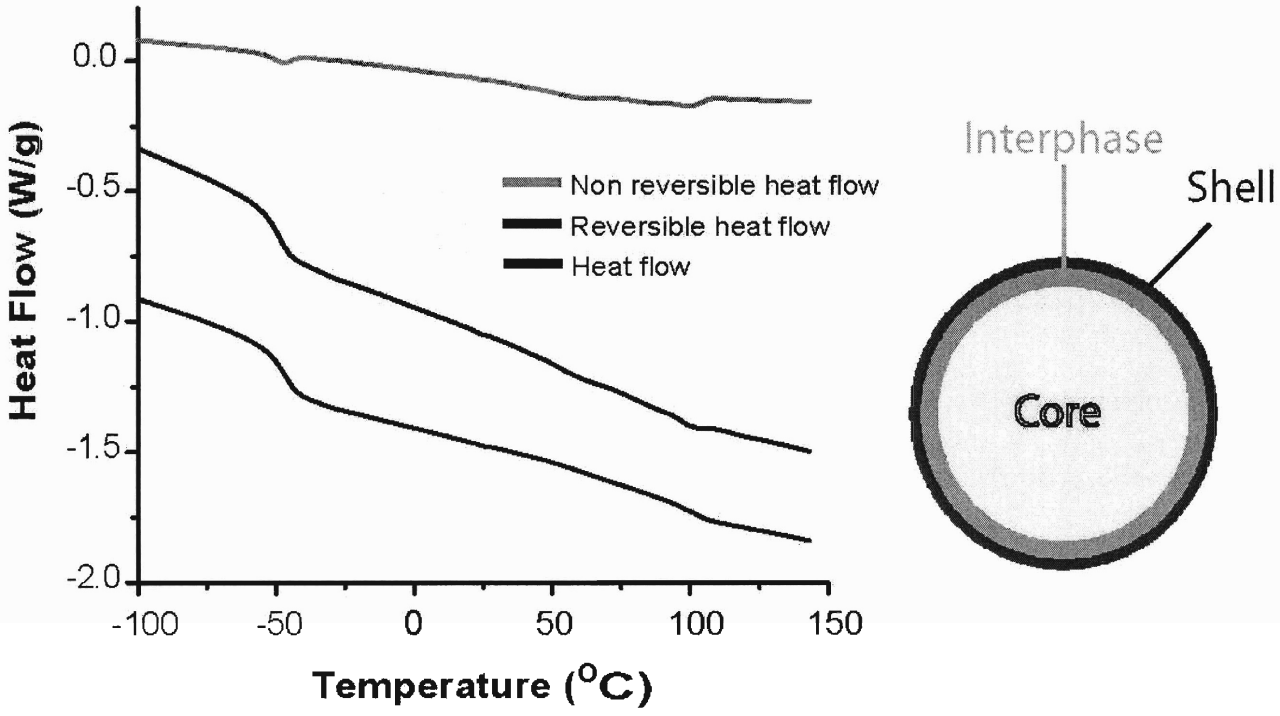

Figure 5.6 MDSC of BS6 PBA_{59}/PS_{41} core-shell and schematic of a core-shell particle from the MDSC analysis.

To estimate the size of the interphase layer, the total volume, V_{Total}, and mass, M_{Total}, for the particle, the volume, $V_{Interphase}$, and mass, $M_{Interphase}$, for the interphase and the volume, V_{Core}, and mass, M_{core}, for the core were calculated as:

$$M_{Total} = V_{Total}\left(w_{c0}\rho_c + w_{s0}\rho_s\right); \qquad V_{Total} = \frac{4}{3}\pi\left(\frac{D_{Total}}{2}\right)^3 \qquad [5.3]$$

$$M_{Interphase} = M_{Total}\left(\delta_c + \delta_s\right); \quad V_{Interphase} = \frac{M_{Interphase}}{(c_c\rho_c + c_s\rho_s)} \qquad [5.4]$$

$$M_{Core} = (w_{c0} - \delta_{c0})M_{Total}; \qquad V_{Core} = \frac{M_{Core}}{\rho_c} \qquad [5.5]$$

where D_{Total} is the particle size by dynamic light scattering (DLS) and ρ_c and ρ_s are the densities for the core and shell polymers, respectively. The interphase thickness, $T_{Interphase}$, was calculated using $V_{Interphase}$ and V_{Core} as:

$$T_{Interphase} = \left(\frac{\left(V_{Interphase} + V_{Core}\right)}{\left(\frac{4}{3}\pi\right)}\right)^{1/3} - \left(\frac{\left(V_{Core}\right)}{\left(\frac{4}{3}\pi\right)}\right)^{1/3} \qquad [5.6]$$

The obtained results for some selected core-shell particles are shown in Table 5.2. A PBA_{59}/PS_{41} (BS6) core-shell particle drawn to proportion calculated as described above is shown in Figure 5.6.

As can be observed from Table 5.2, several of the studied particles yielded that about half of the polystyrene homopolymer is mixed with core homopolymer (as can also be observed for the particle drawing on Figure 5.6), which results in interphases on the order of 3 to 5 nm thick, with average compositions in the range of 70-90 wt% PS.

Composition values were also calculated using the measured $T_{g,mix}$ from MDSC through the Fox equation, giving comparable results. In some cases, the interphase size nearly matches the calculated PS shell thickness, consistent with TEM micrographs of the corresponding samples, where only a thin PS shell was observed.

Table 5.2. Calculated interphase characteristics of core-shell particles

	Interphase Thickness (nm)	PS Shell Thickness (nm)	ΔC_p method calculated interphase composition (wt% PS)	MDSC $T_{g,mix}$ (°C)	Fox eq. calculated interphase composition (wt% PS)
PBA_{59}/PS_{41} (BS6)	3.5	2.2	81	53	78
PBA_{51}/PS_{49} (BS11)	6.7	1.7	71	57	80
$PEHA_{42}/PS_{58}$ (ES2)	5.5	4	93	57	85
PBA_{59}/PS_{41} (BS6)	4.4	1.5	84	52	78
PBA_{43}/PS_{57} (BS1)	5	20	92	60	82
PLMA/PS (LS1)	5	2.2	93	50	77

Coverage of the poly(acrylate) core by the polystyrene shell appears complete for higher PS content samples (above 50 wt% PS), for which a powdery product is obtained upon precipitation. For lower PS contents, the obtained samples were not as powdery, which might indicate incomplete coverage of the core by the glassy shell component.

5.2 Processing of core-shell particles

Core-shell baroplastics were able to flow and be processed at temperatures as low as room temperature, similar to their block copolymer counterparts[103]. Figure 5.7 shows compression molded lids of PBA_{37}/PS_{63} (BS2) processed at an applied pressure of 34.5

MPa (5000 psi), for 1 min at 25 °C along with the dry raw material as obtained from the polymerization. It can be observed that clear and cohesive objects can be obtained with core-shell baroplastics in relatively short processing times.

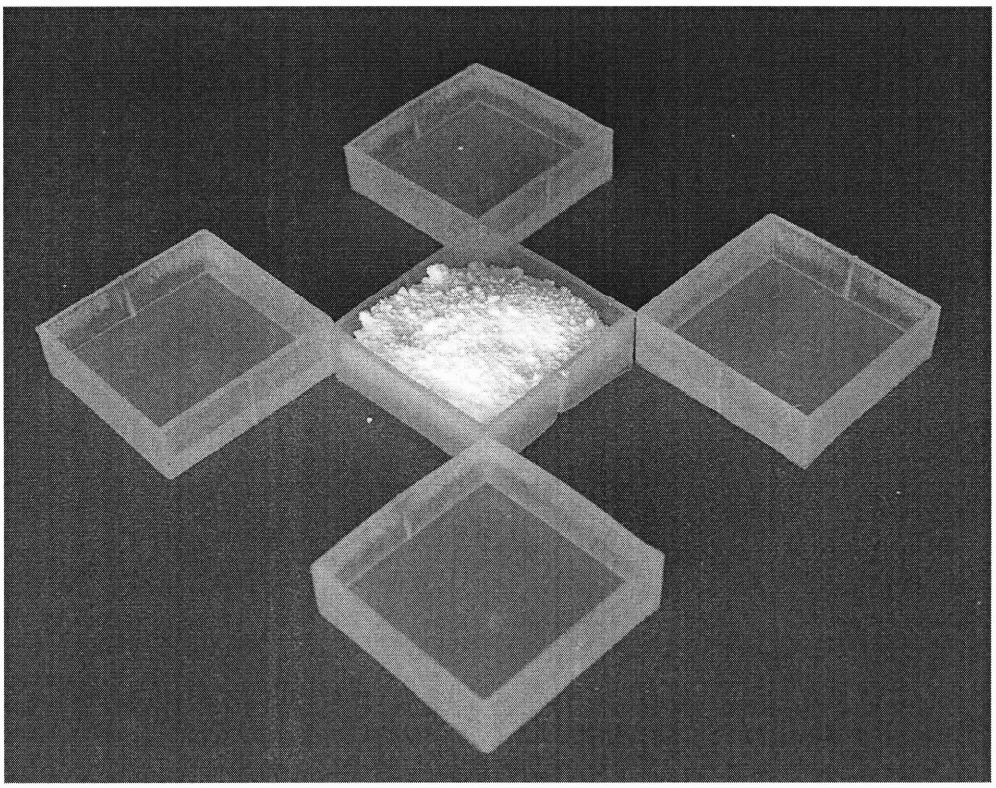

Figure 5.7. Processed samples of PBA_{37}/PS_{63} (BS2) at 25°C under 34.5 MPa for 1 min. middle box contains original dry powder as obtained from polymerization.

Similar to the PS-*b*-PEHA block copolymer, reprocessing of core-shell baroplastics was also possible as shown in Figure 5.8, depicting a compression molded specimen processed at 34.5 MPa for 5 min at 25 °C from the dried state and one reprocessed 10 times following the procedure described above.

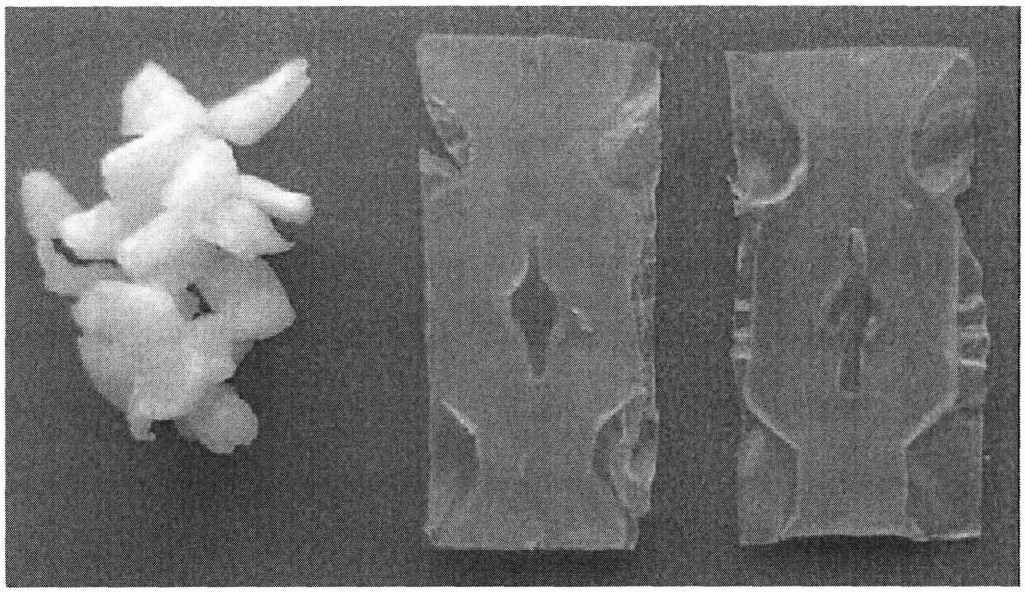

Figure 5.8. $PEHA_{53}/PS_{47}$ (ES5) core–shell as dried, processed 1 time and recycled 10 times at 25°C with a pressure of 34.5 MPa.

The processing of core-shell materials is dramatically affected by composition. Well-defined objects were generally obtained at room temperature when starting from the powdery precipitate in a PS composition range from ~45-65 wt%. For lower PS contents, the highly elastic nature of the material led to shrinkage after processing. In most cases a processing temperature of 50°C was sufficient to obtain a non-deformed sample from these systems. Similarly, processing temperatures of 40-50°C were generally required for satisfactory processing and remolding of systems with PS contents above ~65 wt%. In both cases, the improved processing at elevated temperature may be attributable to enhanced mobility of the interphase. It is also to be noted that materials of PEHA are easier to process than PBA materials. PEHA has the advantage of having a lower T_g than

PBA, which may give rise to this difference. Another reason for the ease of PEHA processing and recycling may be that it is predicted to be more miscible with PS than PBA.

A simple custom-made piston mold was constructed to study the possibility of processing baroplastics by extrusion. Materials processed by extrusion exhibited facile room temperature recycling, even for systems with higher PS content. Figure 5.9 a and b show the extrudates of $PEHA_{42}/PS_{58}$ (ES2) after 1 and 10 processing cycles under a pressure of 207 MPa (27 kN applied) at 25°C.

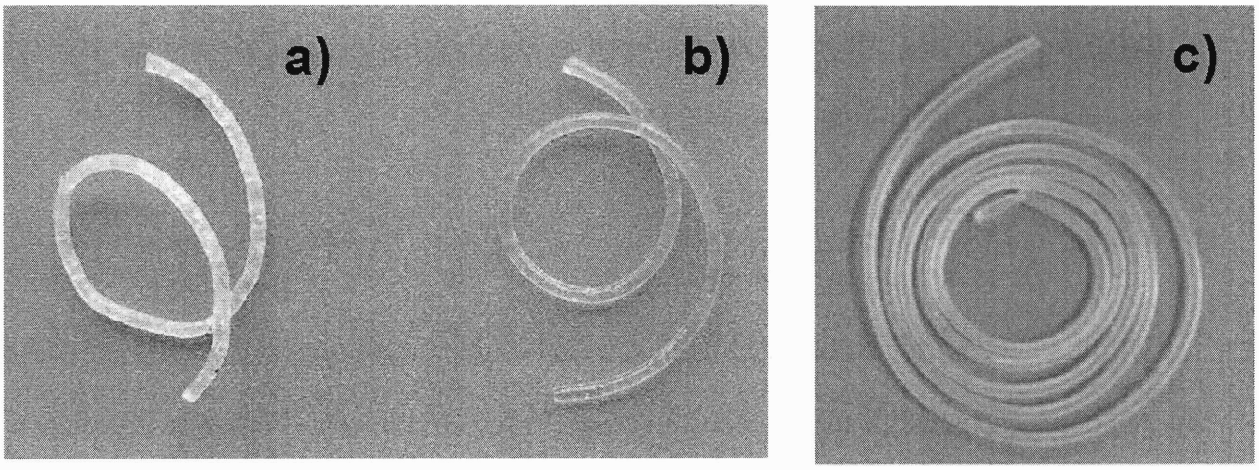

Figure 5.9. Piston-mold and extrudates of $PEHA_{42}/PS_{58}$ (ES2) processed (a) 1 time, (b) 10 times and c) 20 times at 25°C.

Figure 5.9 also shows a larger section of extruded material at the same conditions. A more uniform extrudate is obtained with increasing processing steps beginning from the powder, consistent with the higher degree of mixing shown by SANS and DSC with increased processing time, as described in more detail in the following section.

5.3 Processing mechanism

The processing mechanism was studied by SANS as in block copolymer baroplastics. SANS data for the $PEHA_{47}/PS_{53}$ nanoparticle system in the as-dried state, after one molding operation and after 10 recycles are shown in Figure 5.10a. Several important features are notable. First, each dataset exhibits a broad maximum characteristic of the interparticle spacing, suggesting that, similar to block copolymer baroplastics, the initial sample morphology is substantially preserved during low temperature processing. Upon the initial molding, the peak position shifts to slightly larger wave vector. This behavior was found for all the core-shell systems studied and reflects the material's densification under compression. With further processing, the peak position remains constant but its amplitude diminishes, suggesting enhanced mixing and a corresponding loss of contrast between PS and PEHA domains. This latter result is strong evidence that PS/PEHA indeed exhibits the predicted pressure-induced miscibility.

Figure 5.10b shows more SANS evidence of such mixing in a deuterated sample of $PBA_{34}/d8\text{-}PS_{67}$ nanoparticles (BS3) after applying 34.5 MPa of compression for different times at 25°C. The intensity of the scattering peak at $q \sim 0.085\ nm^{-1}$ (d~74 nm) decreases with increasing processing time, indicating lower contrast between PS and PBA domains consistent with increased mixing. The peak position is also observed to shift under pressure. After short processing times (1 min), a shift is seen to larger wavevector, consistent with densification of the powder. At longer times the peak shifts to lower wavevectors, suggesting an increase in the characteristic period of the nanophase

structure. This maybe due to deformation of the domains during processing, leading to larger domain sizes in the direction normal to the applied force.

SANS was measured on a PLMA/PS core-shell control sample (LS1) as a function of processing time. From Figure 5.11 it can be observed that, although there is a reduction in intensity after 5 minutes processing, the intensity increases at longer times, in contrast to PBA/PS or PEHA/PS systems where the scattering peak intensity decreases with increasing processing time (Figure 5.10b). This observed difference in pressure dependence supports the premise of mixing of baroplastic components, at least at the interphase level, when subjected to pressure during low temperature processing.

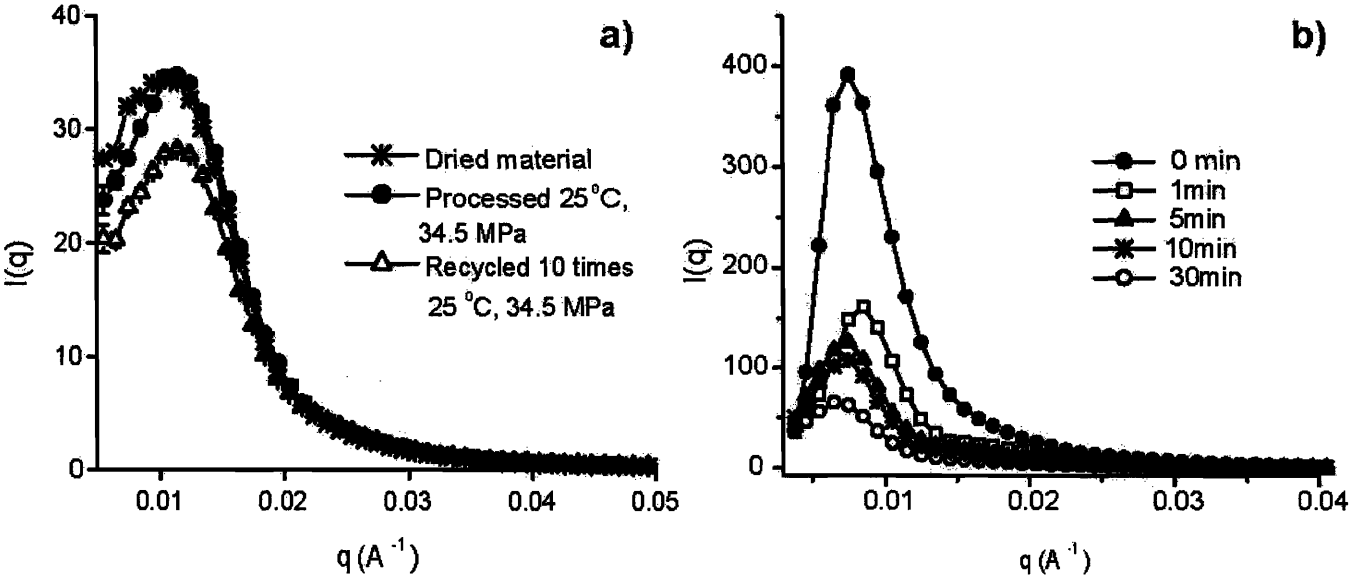

Figure 5.10. Scattering intensity profile for a) $PEHA_{53}/PS_{47}$ (ES5) core–shell with the indicated processing conditions and b) PBA_{34}/d8-PS_{67} (BS3) as a function of processing time at 25 °C under 34.5 MPa.

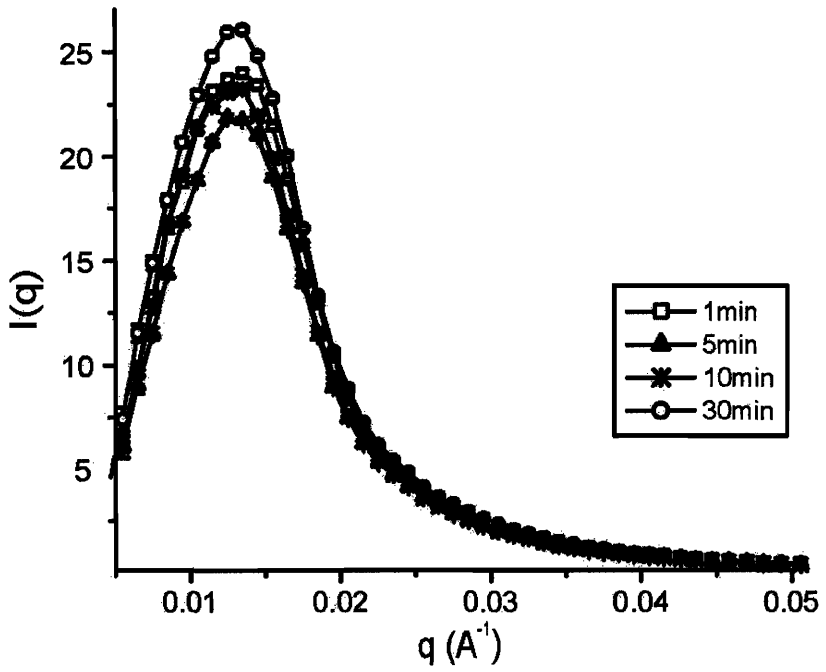

Figure 5.11. Scattering intensity profile for the $PLMA_{47}/PS_{54}$ (LS1) system as a function of processing time at 25 °C under 34.5 MPa.

A constant factor in all SANS measurements is the persistence of the intensity peak from a phase-separated structure even after several processing cycles or long processing times. The persistence of the phase separated structure after processing was also corroborated by MDSC. Figure 5.12 shows the heat flow from MDSC of (ES2) after 1, 10 and 20 processing steps with the piston-mold. It can be observed that the two distinct T_gs corresponding to the homopolymer components are present even after 20 processing cycles. In addition, it can be observed that the $T_{g,mix}$, present around 60°C, seems to increase in signal with processing cycles, probably a result of the pressure-induced mixing during processing.

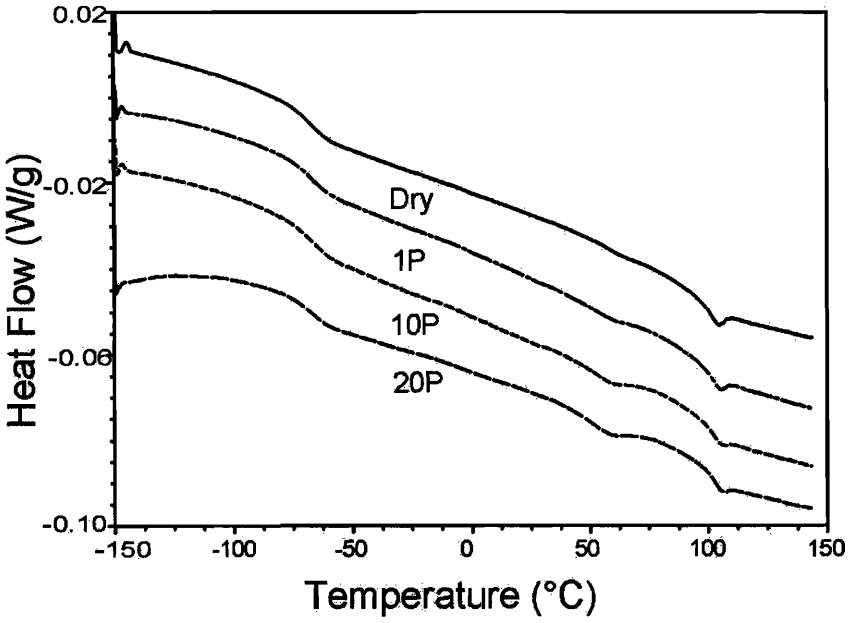

Figure 5.12. MDSC measurements of $PEHA_{42}/PS_{58}$ (ES2) as-dried, and processed 1 (1P),10 (10P) and 20 (20P) times at 25°C using the piston-mold.

Core-shell particle processing further supports the proposed semi-solid processing mechanism, where the rigid PS domains are mobilized and bound by the low T_g component. As with the block copolymer baroplastics, core-shell baroplastic nanoparticles were also able to flow and be molded at reduced temperatures, even though only partial mixing between the components was observed. In fact, total mixing between components would be undesired, since the mechanical properties of a totally mixed system would be substantially inferior to those of phase-separated systems.

The structure of $PEHA_{42}/PS_{58}$ (ES2) after 20 processing cycles in the piston mold was studied by TEM. Figure 5.13 shows TEM images of the as-dried material and the material extruded 20 times.

It can be observed that the overall core-shell structure is present even after 20 processing cycles. This result is consistent with the results from SANS and DSC where distinct domains are still present even after many processing cycles. However, it can also be observed in Figure 5.13b sections from broken particles. The breakage of a number of shells should take place in order to release the low T_g core polymer outside the particle and serve as the mobile layer and binder for other nanoparticles.

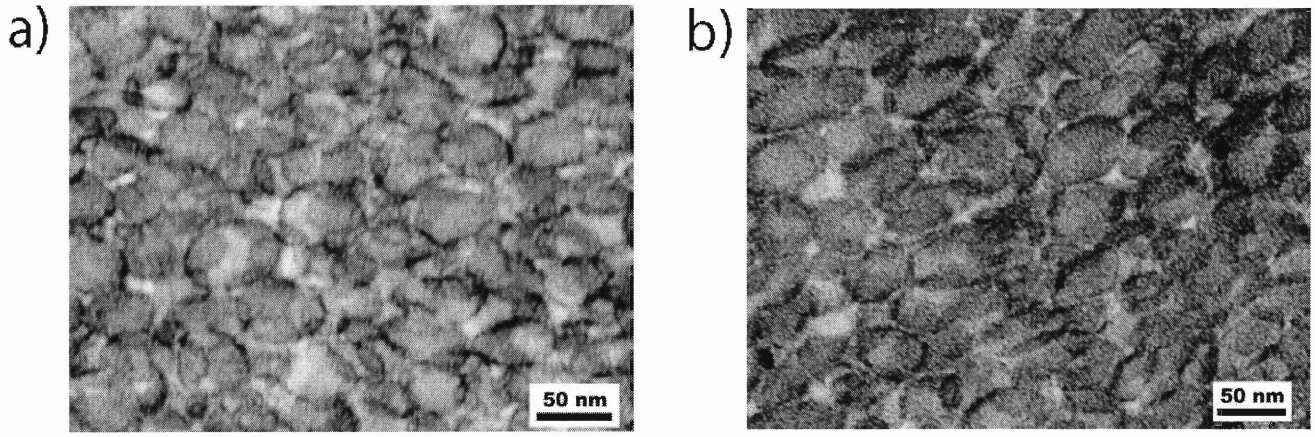

Figure 5.13. TEM image from $PEHA_{42}/PS_{58}$ (ES2) a) as-dried, and b) processed 20 times at 25°C.

The role of pressure induced miscibility on the low temperature processing of core-shell baroplastic was also studied by the use of a PLMA/PS nanoparticle control of comparable acrylate molecular weight, soft-to-hard component ratio and size to PBA_{47}/PS_{53} (BS4). The $PLMA_{46}/PS_{54}$ (LS1) core-shell could also be processed at reduced temperatures from the powdery precipitate as with the PBA/PS or PEHA/PS core-shell materials. This supports the conclusion that flow at reduced temperatures is not unique to pressure-induced miscible systems, as was observed for block copolymers, but is highly dependent on the soft-to-hard component ratio. However, differences in the

mechanical properties of the processed objects revealed the importance of pressure-enhanced mixing. Figure 5.14 shows the mechanical properties of the $PLMA_{46}/PS_{54}$ (LS1) control compared with a PBA/PS system of similar characteristics (BS4).

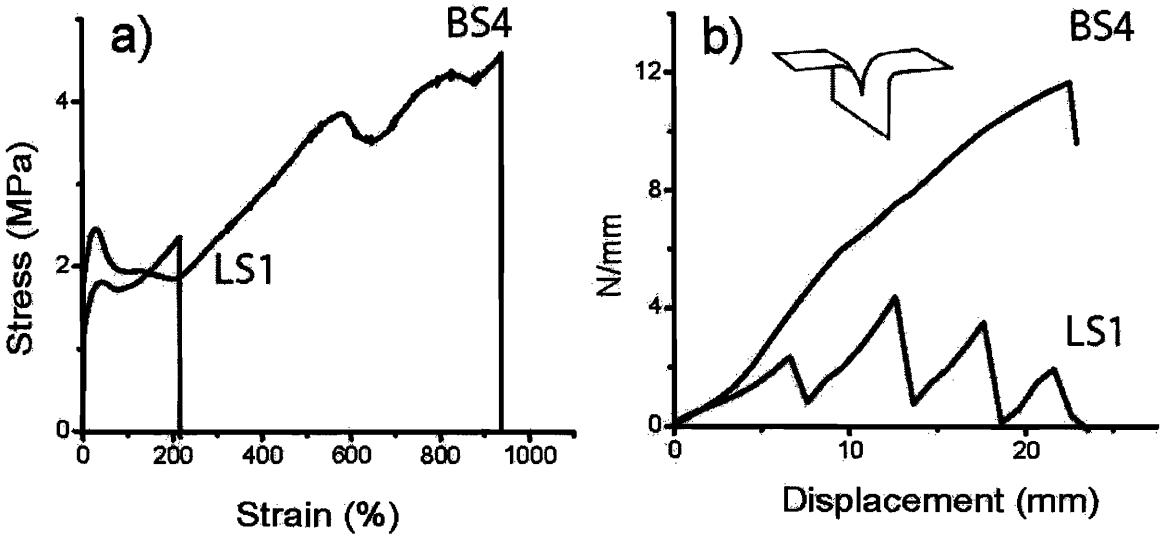

Figure 5.14. Stress vs strain and tear strength of PLMA/PS. b) Force/sample-thickness vs. displacement plot from tear strength test for a) PBA_{47}/PS_{53} (BS4) and b) $PLMA_{46}/PS_{54}$ (LS1) processed at 25°C under 34.5 MPa for 5 min.

While stress-strain measurements showed differences in performance, in particular the strain to break (Figure 6.13a and Table 6.1), the most dramatic difference was revealed by tear strength measurements, as shown in Figure 5.14b. In this measurement a trouser type sample of each system was subjected to strain at a rate of 300mm/min until it broke or reached the machine force limit. For $PLMA_{46}/PS_{54}$, the tear propagates in a series of catastrophic events after minimal stress is applied. By contrast, for PBA_{47}/PS_{53} (BS4) the tear never propagates—instead the "legs" of the specimen stretch and begin to yield. This

result highlights differences in the interphase regions of the two samples. PLMA/PS has a poor interphase between components that allows easy propagation of the tear between domains. For the PBA/PS system, enhanced intermixing due to pressure-induced miscibility provides a tougher interphase that resists tear propagation[83, 114]. These results further demonstrate the importance of pressure-induced miscibility on the mechanical properties of the molded objects.

CHAPTER 6

Mechanical Properties of Core-Shell Baroplastics

In this chapter, the mechanical properties of processed core-shell nanoparticles, with the characteristics described in the previous chapter, will be discussed. A further study of the processing by extrusion in the piston-mold and its use to estimate the viscosity is included. The effects of composition, particle size, component molecular weights and processing temperature on mechanical properties will also be discussed. In addition, the effect of further thermal treatment after processing is discussed.

6.1 Core-shell baroplastic flow through small orifices

The custom made piston-mold, as described in the experimental section, provided a simple way to test the potential extrusion of core-shell baroplastics. As shown in the previous chapter (Figure 5.9), extrudates of $PEHA_{42}/PS_{58}$ (ES2) could be obtained when processing at 25°C. In addition, the piston-mold configuration, namely length to diameter ratio (L/D), allows for characterization of the core-shell viscosity in the same fashion as in a capillary rheometer, employing the equation:[37]

$$\eta_{app} = \frac{\pi \Delta P D^4}{128 Q L} \qquad [6.1]$$

where Q is the mass flow rate and ΔP is the difference between the pressure applied and the outlet pressure (in our case atmospheric pressure). Figure 6.1 shows the obtained

apparent viscosity, η_{app}, for the $PEHA_{51}/PS_{49}$ system (ES1) as a function of the shear rate at the wall ($\dot{\gamma}$) calculated as:

$$\dot{\gamma} = \frac{32Q}{\pi D^3} \qquad [6.2]$$

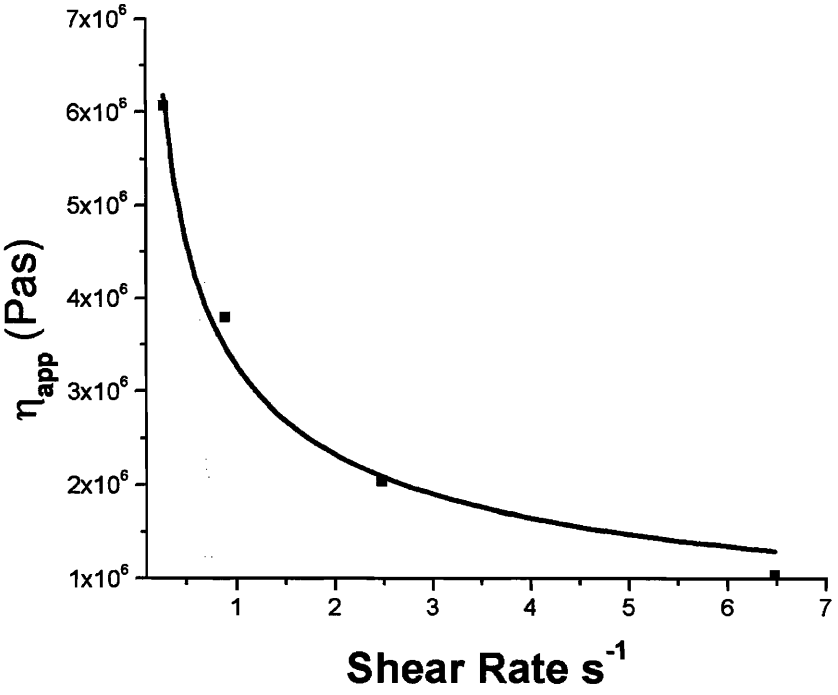

Figure 6.1. Apparent viscosity of $PEHA_{51}/PS_{49}$ (ES1) at 25°C as a function of the applied shear rate. (■) Experimental points, (–) power law fit.

The estimated viscosities through this simple calculation, η_{app} ~1-6 $\times 10^6$ Pa·s are in the neighborhood of that of working glass, on the higher range of polymer processing and on the same order as those for chocolate cold extrusion[41, 42, 37]. From the dependence of viscosity on shear rate, the extruded material behaves as a pseudoplastic fluid, exhibiting a power law dependence on $\dot{\gamma}$ of the form: [37]

$$\eta = \eta_0 \cdot \dot{\gamma}^{n-1} \qquad [6.3]$$

where η_0 has a value of 3.27×10^6 Pa·s and n is equal to 0.503.

Changes in the rheological behavior could also occur by chain scission during processing. To examine this possibility, GPC measurements were performed on $PEHA_{42}/PS_{58}$ as-dried, and after 10 and 20 extrusion cycles. As shown in Figure 6.2, the PEHA distribution shifts towards lower molecular weights as a function of the number of processing cycles. The raw material PEHA has a M_w of about 1.28×10^6 g/mol, compared with 595 kg/mol after 10 extrusion cycles, and 465 kg/mol after 20 cycles. This change is not surprising, since shear scission of very large chains (> 1M g/mol) during flow through small channels has been reported previously[110]. It is also typical that such chain scission occurs near the middle of the chain, [111, 112] as observed in the present system.

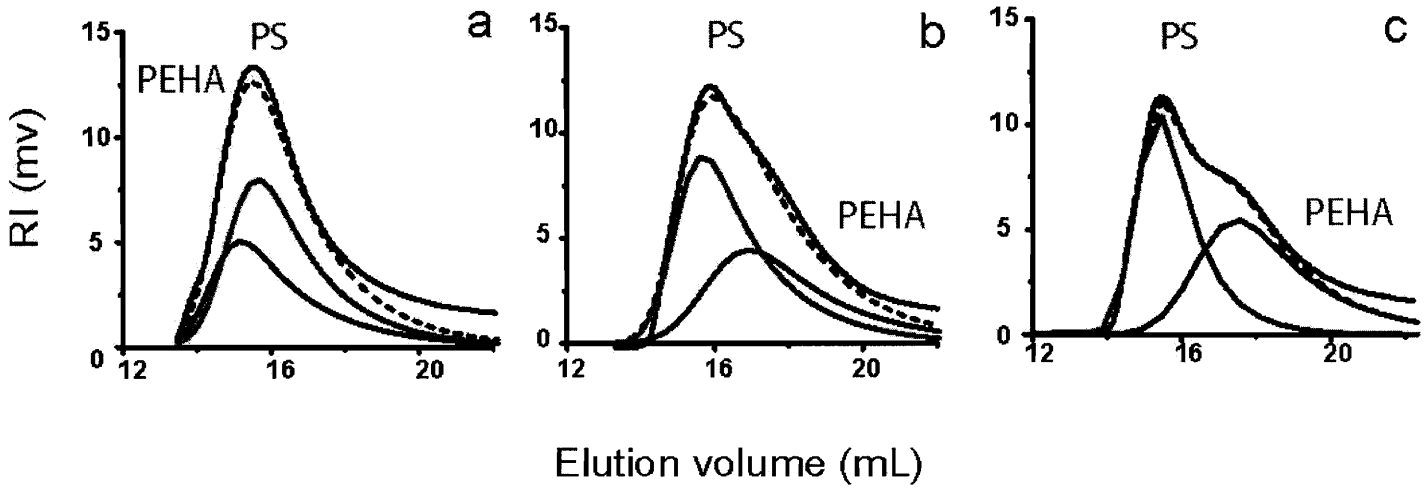

Figure 6.2 GPC traces for $PEHA_{42}/PS_{58}$ (ES2). a) as-dried, and processed b) 10 times and c) 20 times at 25°C with piston-mold. Fitted molecular weight distributions for PEHA (blue) and PS (red) shown.

The PS chains, by contrast, retain a M_w of 1.1×10^6 kg/mol. The same experiment was performed on a lower core molecular weight sample, PBA_{56}/PS_{44} (BS5). In this case no evidence of chain scission for either component was observed after processing.

These results support the proposed processing mechanism, where the acrylate component serves as a "binder" between the core-shell particles and provides a mobile matrix for the rigid PS domains. The mobile low T_g component would be the one subjected to shear, carrying the largely intact PS domains during processing. This would explain why the PS molecular weight distribution is mostly conserved after multiple recycles.

6. 2 Mechanical properties

The mechanical properties of the core-shell particles were obtained by tensile testing, as described in the experimental methods chapter. The measured modulus, yield strength strain to break, and ultimate strength are shown in Table 6.1.

A diverse range of mechanical properties can be achieved depending on the low T_g to high T_g component ratio. Figure 6.3 shows stress-strain curves for three PBA/PS nanoparticle systems of different compositions that were processed by compression molding at 50°C with an applied pressure of 34.5 MPa for 5 min (curves a, b, c). The mechanical properties are found to be highly sensitive to composition, with moduli and strains to break ranging from 209 MPa and 400% for a material with 58 wt% PS (curve a), to 13 MPa and 1200% for a system with 41 wt% PS (curve c).

Table 6.1. Mechanical properties of core-shell nanoparticles

Core/Shell[a]	# of Samples	Young Modulus (MPa)	Yield Strength (MPa)	Strain to Break (%)	Strength at break (MPa)
BS1 PBA_{43}/PS_{57}	3	26 ± 14	---	202 ± 31	2.6 ± 0.6
BS4 PBA_{47}/PS_{53}	2	110 ± 1.84	2.3 ± 0.21	945 ± 10.61	4.66 ± 0.11
BS5 PBA_{56}/PS_{44}	7	12.40 ± 1.9	0.40 ± 0.02	182 ± 68	0.14 ± 0.04
BS6 (50°C) PBA_{59}/PS_{41}	3	13 ± 4	0.6 ± 0.1	Outside range (>1100 %)	@1000% 1.2 ± 0.33
BS7 PBA_{42}/PS_{58}	3	180 ± 39	4.28 ± 0.07	134 ± 26	3.2 ± 0.2
BS7 (50°C) PBA_{42}/PS_{58}	4	215 ± 15	4.92 ± 0.22	146 ± 124	4.3 ± 0.8
BS8 PBA_{37}/PS_{63}	3	199 ± 14	4.85 ± 0.4	210 ± 31	5.2 ± 1.1
BS9 PBA_{36}/PS_{64}	4	64 ± 6.8	2.8 ± 0.1	81 ± 6	1.5 ± 0.3
BS10 PBA_{49}/PS_{51}	3	96 ± 8.6	2.1 ± 0.1	664 ± 36.6	3.5 ± 0.2
BS11 PBA_{51}/PS_{49}	3	50 ± 5	1.2 ± 0.1	911 ± 92	1.9 ± 0.1
BS11 (50°C) PBA_{51}/PS_{49}	3	78 ± 24	1.9 ± 0.2	1132 ± 14	2.7 ± 0.4
ES1 (50°C) $PEHA_{51}/PS_{49}$	2	180 ± 39	0.5 ± 0.05	914 ± 93	1.5 ± 0.1
ES2 (50°C) $PEHA_{42}/PS_{58}$	2	77 ± 7.8	1.9 ± 0.1	678 ± 34	2.9 ± 0.2
ES3 (50°C) $PEHA_{62}/PS_{38}$	11	3.8 ± 1.8	---	486 ± 140	0.64 ± 0.5
ES4 (50°C) $PEHA_{61}/PS_{39}$	3	3.5 ± 1	---	218 ± 48	0.1 ± 0.02
LS1 PLMA/PS	3	59.87 ± 8.39	1.82 ± 0.06	239 ± 33.87	2.23 ± 0.36
PS-*b*-PB (130°C)	2	13 ± 3	0.8 ± 0.04	Outside range (>1100 %)	@1000% 1.2 ± 0.1
PS-*b*-PI-*b*-PS (130°C)	3	1 ± 0.4	---	Outside range (>1100 %)	@1000% 4.5 ± 0.3

a. Samples processed at 25°C unless noted.

Curves d and e of Figure 6.3 show for comparison the stress-strain curves of SIS (curve d) and SB (curve e) commercial block copolymers processed by compression molding at 130°C. The core-shell systems exhibit higher yield stresses and moduli than the styrenic block copolymer TPEs, but somewhat lower strain to break.

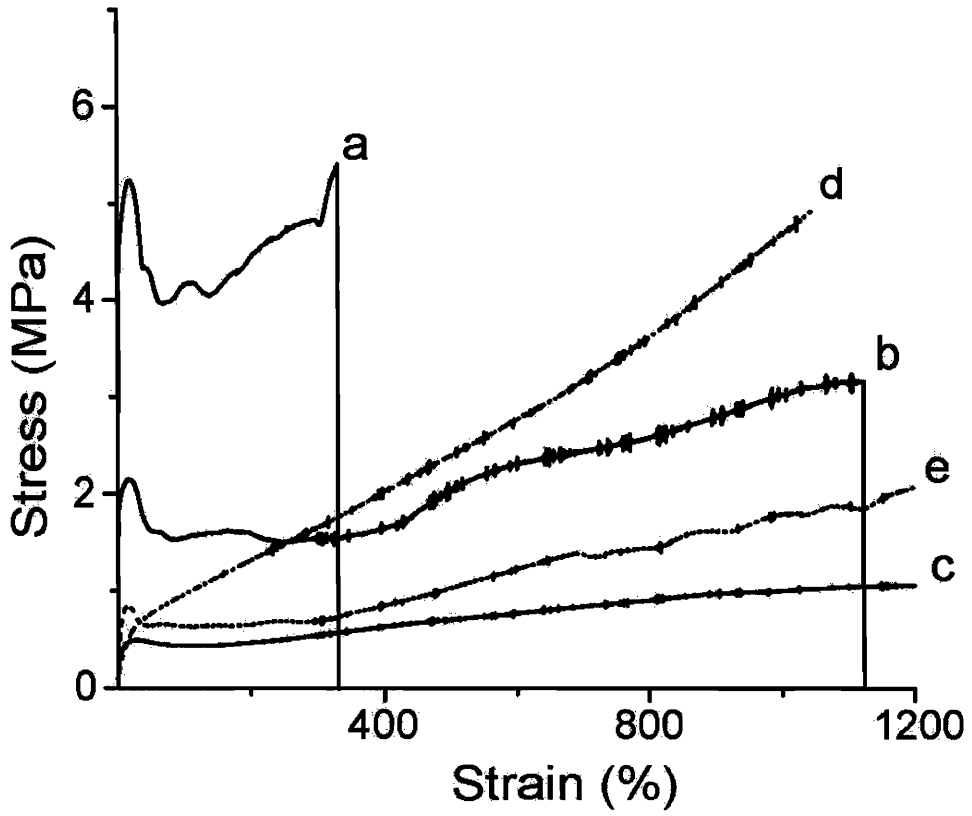

Figure 6.3. Stress vs strain curve for the core-shell baroplastics a) PBA_{42}/PS_{58} (BS7), b) PBA_{51}/PS_{49} (BS10), c) PBA_{59}/PS_{41} (BS6) and commercial TPEs d) SIS and e) SB.

Tensile set was additionally measured for lower PS content core-shell materials PBA_{59}/PS_{41} (BS6) and $PEHA_{62}/PS_{38}$ (ES3) to compare with the block copolymer TPEs. Tensile set is a measure of the recovery capability of the material after a 100% strain for a specified time (10 min). The reported number is the percentage of permanent

deformation after the test. For PBA_{59}/PS_{41} (BS6) and $PEHA_{62}/PS_{38}$ (ES3), the tensile set values are 23% and 10%, respectively, similar to the SB diblock value (9%), but substantially higher than the SIS triblock (3%)[82].

Processing method was found to have a significant effect on the mechanical properties of a tested specimen[114]. Curve (a) in Figure 6.4 shows a representative tensile test from a PBA_{51}/PS_{49} sample (BS11) that was processed by compression molding at 25°C. Curve (b) in Figure 6.4 shows the same material extruded at 25°C using a piston-mold with a square opening that forms a flat ribbon instead of a cylinder. This ribbon was cut to a dog bone similar to films obtained by compression molding. Although the modulus and the tensile strength are similar, there is a significant difference in the strain to break, - 900% for the compression molded sample vs. 200% for the extruded film. Multiple processing through the piston-mold was performed at a pressure of 175 MPa (an applied force of 22 kN) at room temperature. Curve (c) in Figure 6.4 shows the mechanical behavior for the same PBA_{51}/PS_{49} system (BS11) processed 10 times by extrusion. A substantial change in properties is seen compared with the original processed specimen. There is an increase in the modulus, from 37 MPa to 78 MPa, and in the tensile strength, from 1.8 MPa to 2.64 MPa, with a decrease in strain to break of about 100%. As described above, multiple extrusions through the piston-mold resulted in chain scission of the large polyacrylate chains to roughly half their original molecular weight. The change in mechanical properties might be ascribed to a decrease in PBA molecular weight and an increase in interphase between PS and PBA domains.

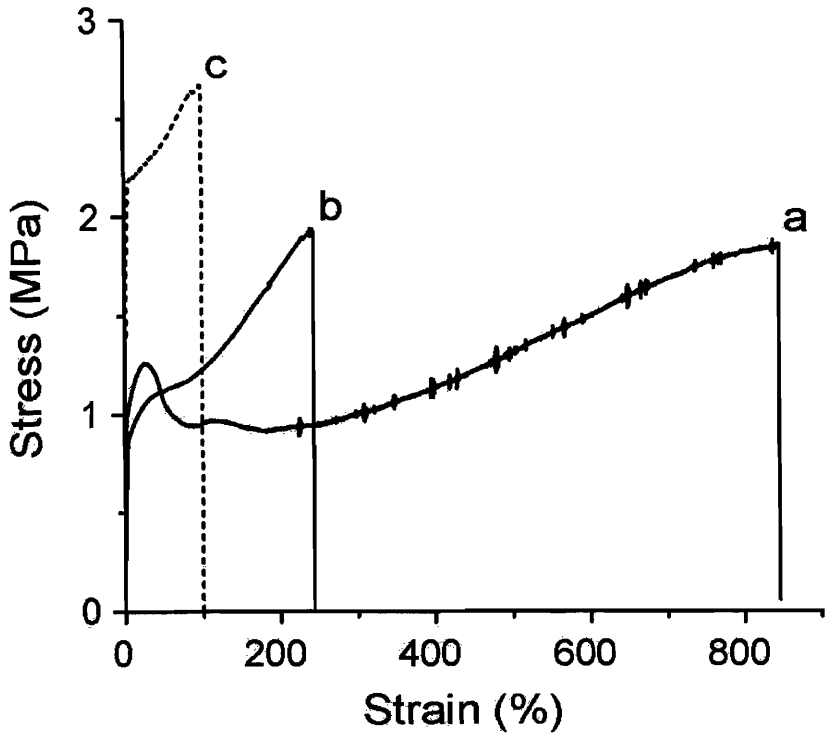

Figure 6.4. Stress vs strain curves for PBA_{51}/PS_{49} (BS10), a) processed by compression molding at 25°C under 34.5 MPa for 5min, and processed with the piston mold b) 1 time, c) 10 times at 25°C.

The effect of particle size on the mechanical behavior of core-shell materials was also studied. Figure 6.5 compares the stress-strain curves for PBA_{42}/PS_{58} (BS7), having an average diameter of 53 nm, and PBA_{43}/PS_{57} (BS1), with 201 nm average diameter. Interestingly, the larger particles do not exhibit the yielding peak notable for the smaller diameter sample. In addition, a substantial reduction in modulus occurs, from 180 MPa for the smaller nanoparticles (a) to 26 MPa for the larger ones (b). For higher PS contents, a similar size effect was observed comparing the PBA_{37}/PS_{63} (BS8) system having an average diameter of 78 nm with the larger PBA_{36}/PS_{64} (BS9) system having 154 nm diameter particles. In this case, the change in Young's modulus, from 199 to 64

MPa, is coupled to a substantial decrease in strain to break, as can be observed from curves (c) and (d) in Figure 6.5.

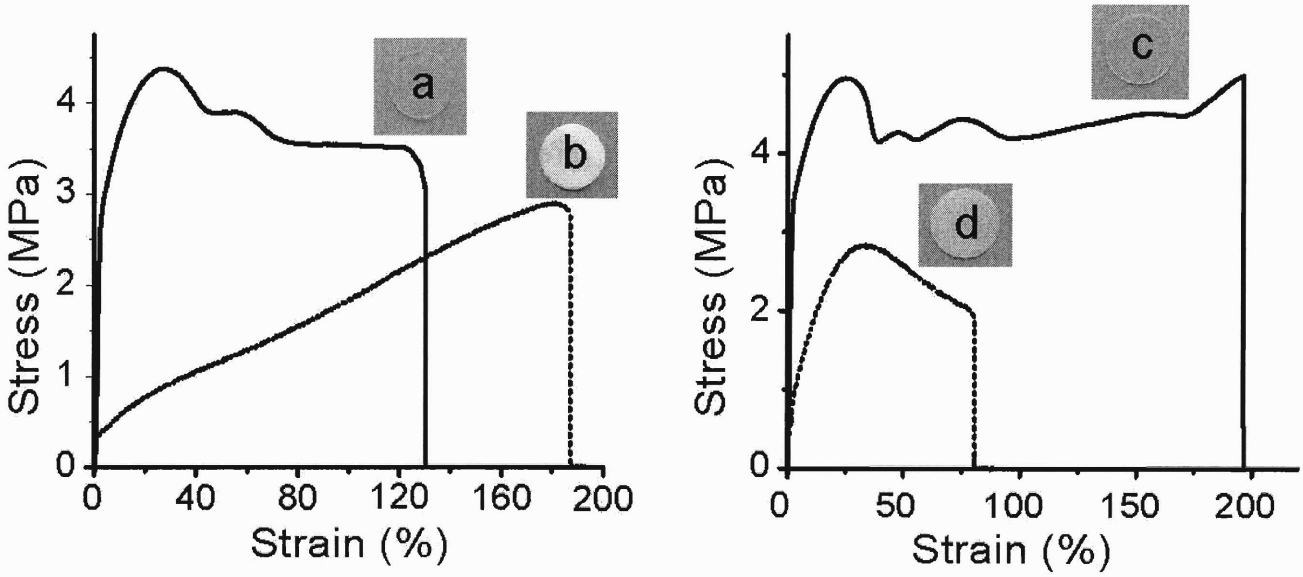

Figure 6.5. Stress vs strain curves and processed films for a) PBA_{42}/PS_{58} (BS7) and b) PBA_{43}/PS_{57} (BS1) molded at 25°C under 34.5 MPa for 5 min, c) PBA_{37}/PS_{63} (BS8) and d) PBA_{36}/PS_{64} (BS9) molded at 35°C under 34.5 MPa for 5 min.

For core-shell baroplastics, the nanoparticle diameter establishes the domain size of each component and, perhaps more importantly, the amount of surface area between them. As the domain size becomes larger, the soft component becomes less efficient as a toughener. For example, melt mixed blends of PS and PB, in a comparable composition range to our materials, form domain sizes of ~2 microns, which lead to low Young's modulus (below 25 MPa), and elongations at break below 80%[14]. Because core-shell baroplastic components intermix under pressure to achieve cohesion, the larger the surface area per volume between the two domains, the better the mechanical properties of

the processed form. For larger particles, the retention of distinct hard and soft domains after processing is further manifested in their translucent or opaque optical properties after molding (Figure 6.5 insets).

Core and shell molecular weights also have an effect on the mechanical properties of the processed baroplastics. As shown in Figure 6.6, the lower acrylate molecular weight BS5 and ES4 systems exhibit a lower strain to break and correspondingly a lower strength at break than the higher molecular weight BS6 and ES3. However, as observed from Table 6.1, the modulus and yield strength are similar, even though the PS molecular weight is lower in the higher molecular weight acrylate samples.

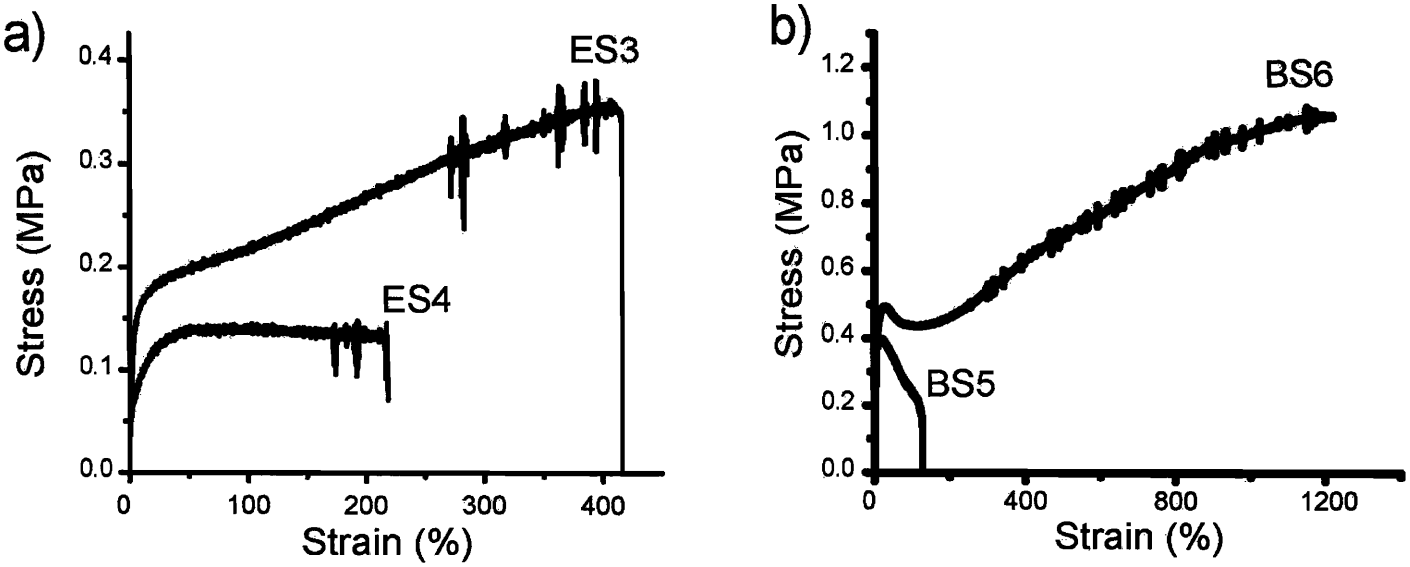

Figure 6.6. Stress vs strain curves for a) $PEHA_{62}/PS_{38}$ (ES3) and $PEHA_{61}/PS_{39}$ (ES4) and b) PBA_{56}/PS_{44} (BS5) and PBA_{59}/PS_{41} (BS6).

This suggests that the modulus and yield strength depend more on the PS content than on its molecular weight for these core-shell materials. It also points out that the strain to break and ultimate strength might depend heavily on the molecular weight of the acrylate, which works as a carrier and binder for the PS domains. In addition, a difference in mechanical properties between the low and high molecular weight samples (ES3 vs. ES4 and BS5 vs. BS6) was readily observed, as the lower molecular weight systems were very soft to touch and difficult to process and handle due to stickiness. Such tackiness also suggests incomplete PS coverage of the PBA for these samples.

6.3 Temperature effect on processing

Processing temperature also affects the final mechanical properties of the core-shell materials. Figure 6.7 shows stress-strain plots for $PEHA_{51}/PS_{49}$ (ES1) processed at 25°C and 50°C by compression molding under an applied pressure of 34.5 MPa for 5 min.

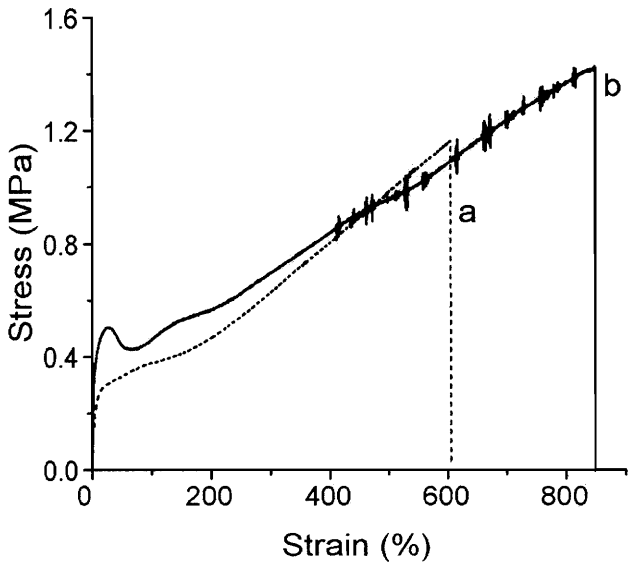

Figure 6.7. Stress vs strain curve for $PEHA_{51}/PS_{49}$ (ES1) processed at 34.5 MPa for 5 min at a) 25°C and b) 50°C.

Processing 25 degrees above room temperature increases the modulus from 10 to 180 MPa and the strain to break from 550 to 900%. The improved mechanical properties for higher processing temperatures may reflect better cohesion between particles due to higher chain mobility providing increased interdiffusion.

The effect on processability by small changes in temperature can clearly been observed in Figure 6.8. Although all the temperatures used are still far below the T_g of PS, it can be seen that a better shape is obtained from compression molding at 50°C. For lower PS contents, less than ~50 wt% PS, the highly elastic nature of the material usually led to shrinkage after processing, as can be observed in the 25°C sample in Figure 6.8. Shrinkage is greatly reduced when processing above 50°C

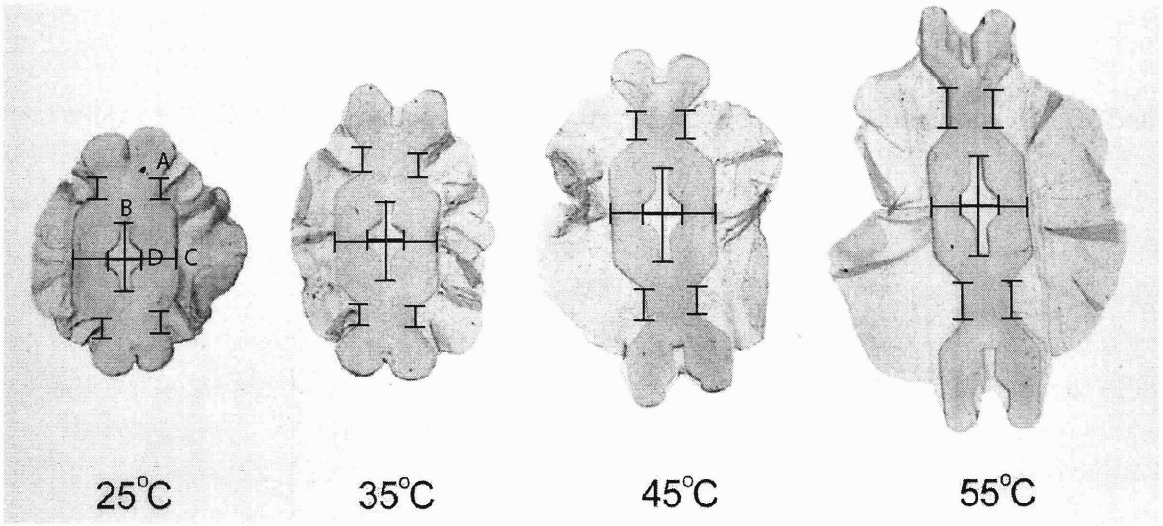

Figure 6.8. Processed samples of PBA_{53}/PS_{47} (ES5) under 34.5 MPa for 5 min at the indicated temperatures.

It can be also be observed that there is more deformation after processing in the vertical direction (dimensions A and B on Figure 6.8) than in the horizontal direction (dimensions D and C on Figure 6.8). This indicates that the application of pressure to the sample was not uniform, and that the chains more likely to shrink once the object is released from the mold are those in the direction where the mold is open during processing (vertical direction).

Also, as expected from the time-temperature superposition principle, samples processed at higher temperatures had similar processability to samples processed for longer times at low temperatures. A $PEHA_{51}/PS_{49}$ (ES1) sample processed at 50°C for 5 min under 5000 psi show the same degree of shrinkage than a sample processed at 30°C under the same pressure overnight.

At higher temperatures, close to or above the T_g of PS, the core and shell components can macrophase separate. Since there is no chemical bond between components, the core and the shell homopolymers are free to phase separate once the PS gains enough mobility. Mechanical properties, in particular the elastic modulus, changed dramatically when the processed samples were thermally treated. The specimens became harder and more rigid. Figure 6.9 shows the evolution of the modulus for a PBA_{51}/PS_{49} sample with temperature and time. It should be noted that even thermal treatment at temperatures below the PS T_g have an effect on the modulus, becoming more substantial at temperatures above the T_g of PS.

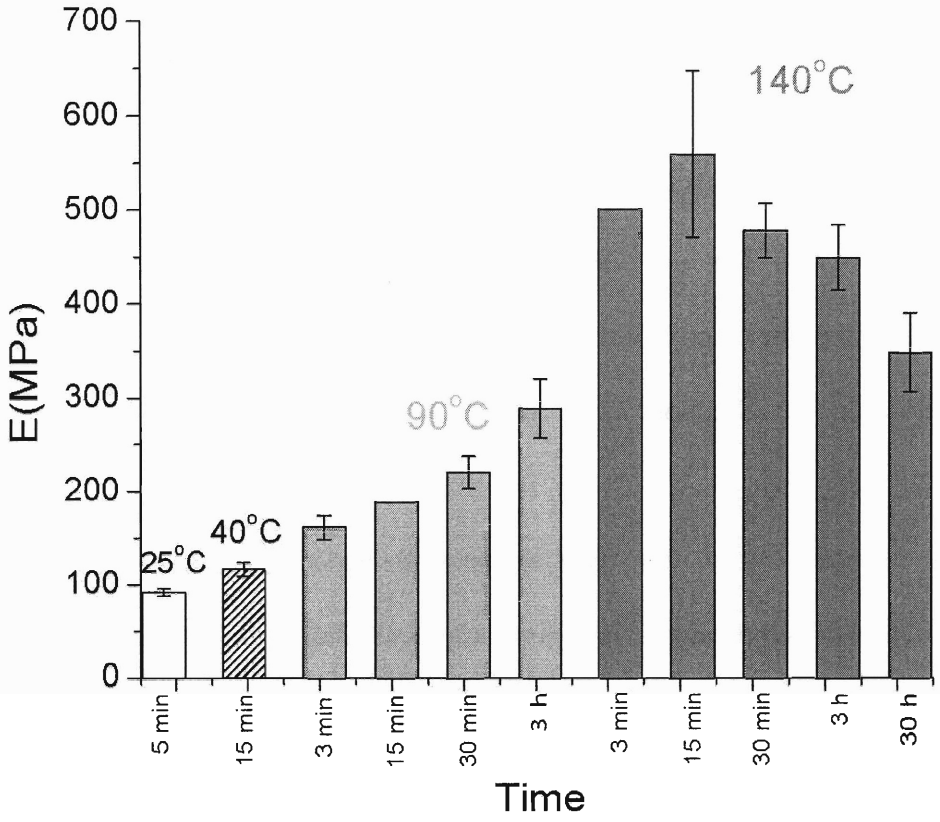

Figure 6.9. Elastic modulus for PBA_{51}/PS_{49} specimens processed at 25°C under 34.5 MPa for 5 min and thermally treated at the indicated temperatures for different time periods.

The observed change in mechanical properties was traced by dynamical rheological measurements as a function of temperature. The storage (G') and loss (G") modulus as function of temperature of a PBA_{47}/PS_{53} (BS4) sample are shown in Figure 6.10. It can be observed that up to 60°C there is a small decrease in the G' and an increase in G", most likely as a result of increased mobility of the polymer chains, as discussed above. After 60°C, there is a dramatic increase in both moduli, reaching to a maximum at 90°C. This increase is due to the enhanced phase separation between components as the temperature approaches the PS T_g. Once the temperature is above 100°C, the rigid PS phase softens and the modulus decreases with time, as shown for samples annealed at 140°C for

extended periods. This is most likely due to the formation of large homopolymer domains resulting in inferior mechanical properties.

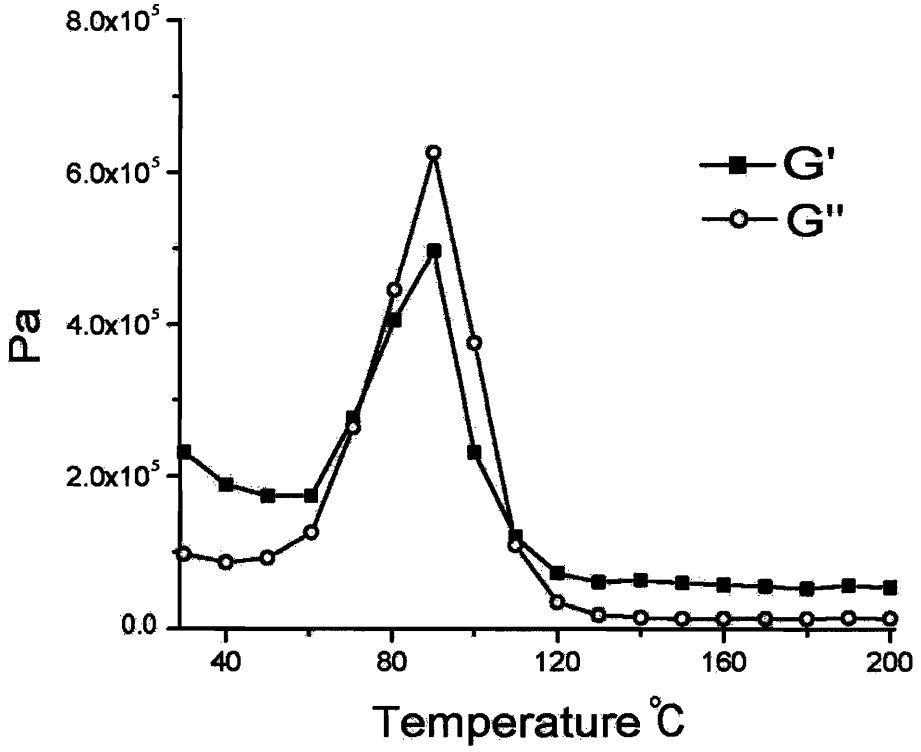

Figure 6.10. Dynamical rheological measurements of a PBA_{47}/PS_{53} (BS4) sample as a function of increasing temperature.

The change in mechanical properties is due to the formation of large PS domains. The structure of the sample treated at 140°C for 3 hours was observed through TEM. Figure 6.11 shows the micrograph of a cryomicrotomed section of the thermally treated sample. It can be observed that large domains of PS are present (darker sections, selectively stained by RuO_4) surrounded by a PBA matrix. It is particularly interesting that the PS domains, although ~10x larger that the original core-shell particles, appear largely

disconnected even after 3 hours of thermal treatment. Macrophase separation was also confirmed during the second heating cycle of the DSC, as the mixed state T_g totally disappeared.

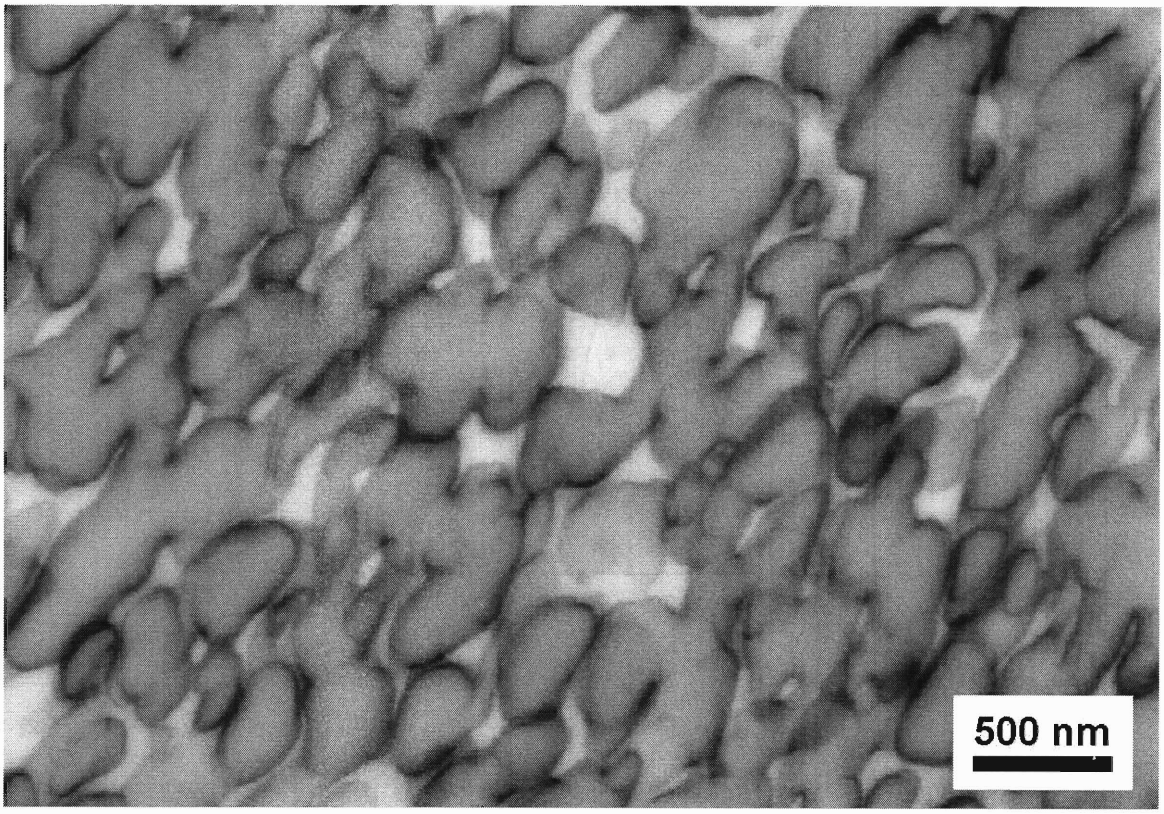

Figure 6.11. TEM micrograph of a PBA_{51}/PS_{49} specimen processed at 25°C under 34.5 MPa for 5 min and treated at 140°C for 3 hours.

Macrophase separation was also readily identified visually as processed specimens become opaque after thermal treatment. Figure 6.12 shows a processed sample at 25°C next to another sample that was further annealed at 140°C for 5 min.

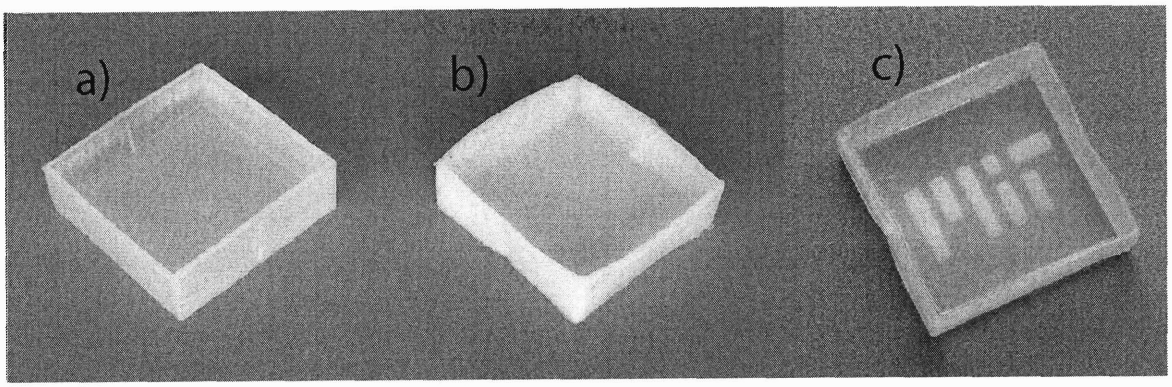

Figure 6.12. Processed samples of PBA_{37}/PS_{63} (BS2) at a) before and b) after a thermal treatment at 140°C for 5 min. c) Sample of $PEHA_{41}/PS_{59}$ (ES6) processed 25°C under 34.5 MPa for 5 min and locally heated with hot aluminum mold to create pattern.

In addition, Figure 6.12c shows a sample where heat was applied in specific regions for approximately 5 seconds by a heated metal stamp with the MIT logo, demonstrating even further the optical contrast between the processed core-shell and macrophase separated states.

CHAPTER 7

Conclusions and Future Work

The proposed low temperature processing of baroplastics has been demonstrated. Simple compression molding of block copolymers and core-shell nanoparticles is possible at temperatures as low as room temperature by the application of pressure. Core-shell baroplastics molding further demonstrated that low temperature processing is not particular to block copolymers but is a more general phenomenon.

7.1 Block copolymer baroplastics

Although ATRP provides a simple method of block copolymer synthesis, precise control over the resulting polymer could not be achieved. However, the obtained PS-*b*-PBA and PS-*b*-PEHA materials demonstrated that low temperature processing is possible and provided enough information to understand the underlying mechanism. Characterization of the processed materials revealed that incomplete mixing is taking place during processing and that distinct domains are still present after the pressurization. These results suggest that the rigid PS domains are mobilized by the soft component, which would explain the dramatic effect of composition on the mechanical properties and processability. At low PS contents, where the rigid domains are dispersed by the mobile phase, the materials will flow easily but poor mechanical properties are achieved, since they depend mostly on the soft component's intrinsic characteristics. In contrast, at high

PS contents the PS domains lack of enough mobility to flow and process, yielding brittle materials. Intermediate compositions (close to 50 wt% PS) seemed ideal for the low temperature processing of block copolymers with good mechanical properties. The triblock copolymer of PS-*b*-PBA-*b*-PS further confirmed that complete mixing doesn't occur during processing. However, it can be processed at conditions where a pressure demixing control sample, PS-*b*-PB-*b*-PS did not even form a cohesive object.

The experiments carried out with the control sample, PLMA-*b*-PS, indicate that pressure induced mixing is not the only factor controlling low temperature processing. However, pressure induced miscibility improves dramatically the processing and the mechanical properties of the processed product.

Although block copolymer baroplastics can be successfully processed, their mechanical properties might not be sufficient for direct commercial application (compared with commodity TPEs for example). Nevertheless, they open new horizons for other materials where the low temperature-processing phenomenon could be exploited. Lovell and Taniguchi were able to design, synthesize and process biodegradable polyester baroplastics, which could potentially benefit from low processing temperature since such materials are susceptible to degradation at higher temperatures (usually required for processing) [115].

New systems such as the ones proposed in Chapter 3, in particular those with higher T_gs, might improve the mechanical properties of baroplastic block copolymers. Crystalline components could also potentially improve the mechanical properties. Low temperature

processability has been already been demonstrated with biodegradable baroplastics having crystalline components[115]. Recently it is has been published that certain crystal forms of syndiotatic polystyrene and isotactic poly(4-methylpentene-1) can melt by the application of pressure[116, 117]. This could provide a new route to improve mechanical properties while retaining the low temperature-processing feature.

In this work only diblock and triblock copolymers have been investigated, but there are other block copolymer structures such as graft copolymers that would be worth studying for their pressure-induced phase behavior and low temperature processability. This architecture presents smaller domain sizes than block copolymers, which could bring an advantage to pressure inducing mixing during processing, facilitating flow and perhaps improving the resulting mechanical behavior.

7.2 Core-shell baroplastics

Emulsion polymerization proved a simple and robust route to form blend materials with phase separated domains comparable in size to block copolymers. An important feature of the core-shell particles is the high molecular weights obtained, which affects their processing and mechanical properties. However, particles with core molecular weights on the order of $1x10^6$ g/mol, are able to form well-defined and transparent objects at low temperatures. Core-shell baroplastic processed particles have mechanical properties comparable to commercial thermoplastic elastomers that can be tuned by composition, size and processing conditions.

Their structural characterization confirmed several of the observations in block copolymers, such as the incomplete mixing and domain retention after several processing cycles. Core-shell particle studies also demonstrated the importance of pressure-induced miscibility. As observed for polystyrene-*b*-poly(lauryl methacrylate), a core-shell sample of the same system can be processed at low temperature. PS/PLMA core-shell nanoparticles processed, forming well-defined and transparent objects. However, the PLMA/PS system has inferior mechanical properties to a comparable PBA/PS core-shell, suggesting that pressure-induced mixing improves the cohesion of the processed object by creating better interphases between components.

Ibrahim conducted a simple economic viability study for the core-shell particles, which indicates that their commercial implementation may be possible[118]. In addition, large-scale batches of core-shell particles (~500g) could be synthesized with relatively little change in reaction procedure. Other industrially relevant studies about core-shell baroplastics that need to be addressed are the possibility of controlling the mechanical properties by mixtures of particles of different compositions in the emulsion state to obtained intermediate properties. The same approach could be tried to add other non-polymeric additives such as pigments or fillers[119, 120]. The charge of the surfactant during the emulsion state can be used to form self –assembled structures that could be afterwards processed without thermal disruption.

To examine the addition of non-polymeric components, a simple experiment was carried out where charged silica particles (20 wt% SiO_2) were mixed with a PBA/PS core-shell

while in the emulsion state. The precipitated product was able to process at the same conditions as the core-shell by itself. This demonstrated that a substantial amount of non-polymeric material can be incorporated into the core-shell systems and mobilized by the low temperature processing mechanism. The obtained sample became stronger, with a modulus increase from 70 to 160 MPa, retaining a good strain to break of about 270%.

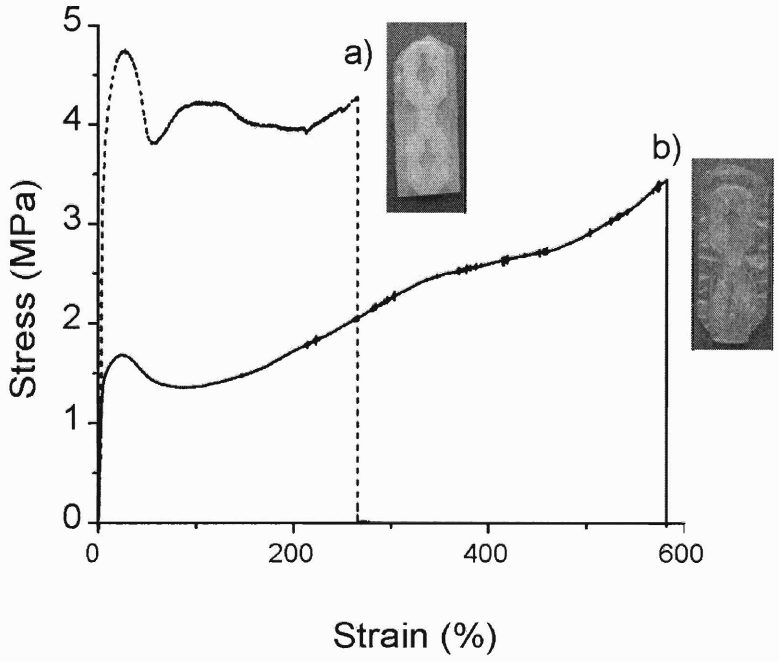

Figure 7.1 Stress vs. strain plot for a PBA/PS processed for 5 min under 34.5 MPa for 5 min a) as obtained from polymerization b) with 20% SiO_2 added.

However, the obtained product was opaque, indicating that the silica particles aggregate and macrophase separate. This situation might be improved if an individual particle is enclosed inside of a core-shell particle[121]. This approach might prevent macrophase separation between the inorganic and the polymer matrix, achieving higher dispersion and better mechanical properties[122].

Particles with other functionalities might also be enclosed in core-shell particles. For example, particles with optical or magnetic properties might also benefit from the forced separation between particles and the virtual conservation of the core-shell structure after processing[122-125].

As shown in Chapter 6, the microstructure of the core-shell particles can be selectively modified by the application of heat. As the two components macrophase separate, the materials became opaque and more rigid. The ability to selectively modify the mechanical properties of a processed object, reinforcing specific regions by the application of heat instead of using two different materials, could be industrially advantageous. In addition, the change in opacity, as shown in Figure 6.12c, could be used to permanently mark or write on a processed object, solving certain regular printing issues on plastics such as ink compatibility and fading by wear.

Appendix A

A.1 Block copolymers synthesis

Block copolymers were prepared by atom transfer radical polymerization (ATRP) either in one step (1 pot) or 2 sequential steps (2 pots). A typical recipe for a one-pot synthesis of polystyrene-*b*-poly (2-ethyl hexyl acrylate) is shown in Table A.1

Table A.1 Recipe for the ATRP of diblock copolymers

First Block	
Styrene	27.5 ml (0.20 mol)
Toluene	20 ml
2-Methyl bromo propionate (MBP)	0.089 ml ($1.2 * 10^{-3}$ mol)
CuCl	0.119 g ($8 * 10^{-4}$ mol)
N,N,N′,N′,N"-pentamethyldiethylene triamine (PMDETA)	0.5 ml ($2.4 * 10^{-3}$ mol)
Second Block	
2-ethyl hexyll acrylate	41.65 ml (0.2 mol)
Toluene	20 ml

Monomers were passed through an activated (basic) alumina column to remove the inhibitor prior to usage. All other chemicals were used as received. The metal co-catalyst CuCl was also used as received and stored under vacuum.

CuCl can easily oxidize into Cu^{2+} overtime. The oxidation to Cu^{2+} is identifiable by a change in color from white to green. The presence of large quantities of Cu^{2+} in ATRP reaction mixtures can severely affect the formation of free radicals, substantially

slowing down the polymerization rate. CuCl reactant with visible signs of Cu^{2+} present can be purified by stirring in glacial acetic acid overnight, filtering and washing with ethanol and drying under vacuum at 80°C for several days. [71]

A custom made reactor by Chemglass was used for the synthesis. It consisted of a round bottom flask (of 100, 250 or 500 mL) with a side opening with a Teflon valve and a Teflon screw cap on the top, as shown in Figure A.1. The purpose of the side valve is to have access to the reactor during the polymerization and reduce the chance of any infiltration of oxygen during the addition of reactants or during sample extraction.

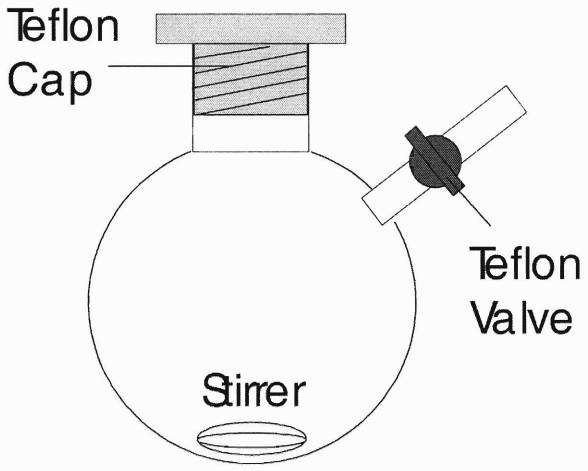

Figure A.1. Chemglass reactor with side Teflon valve.

A typical procedure is as follows: The required amount of CuCl is added to the reactor and the vessel tightly closed, that subjected to 3 pump-purge cycles of vacuum followed by N_2. Toluene, PMDETA and styrene, which had been previously bubbled for 30

minutes with N_2, are added through the reactor's side valve. After the addition of PMDETA, the color of the reaction solution turns light green, due to the formation of the catalyst complex. Finally, the initiator is added and the reactor is placed into a preheated oil bath at 110°C. The reaction is followed by GPC and takes about 24 hours. After the GPC trace shows that the first monomer has reacted near completion (close to the target molecular weight), the second monomer, 2-ethyl acrylate, and additional toluene, which were previously bubbled with N_2, are injected into the reactor.

After the second monomer reacts to completion, the reaction solution is diluted with toluene and passed though a neutral alumina column to remove the Cu catalyst. The purified solution is then precipitated into methanol. The obtained polymer is filtered and redissolved in dichloromethane for further precipitation. The final powder is obtained after drying in the vacuum oven at room temperature for 3 days.

For the two-step synthesis (2 pots) the reaction for the first monomer is carried out as describe above, with the difference that once the first polymerization has reach the target molecular weight the reaction is stopped and the reactor is opened. The macroinitiator is passed through a neutral alumina column and precipitated in methanol. Two more precipitations are carried out before drying the product overnight at 25°C under vacuum.

The product of the first reaction is weighed and dissolved in toluene before adding to a clean reactor. The required CuCl and ligand, the second monomer and additional toluene are then added and the mixture is stirred and bubbled with N_2 for 30

minutes before placing it into an oil bath at 110°C. The reaction is carried out to near completion and purified as described above.

For the triblock copolymer, a bifunctional initiator, 2,6–dibromoheptanedioate, is used and the reaction is carried in the same manner as for diblock copolymers.

A.2 Core-shell nanoparticle synthesis

The core-shell nanoparticles were prepared by emulsion polymerization in de-ionized water. A typical recipe for PBA/PS core-shell nanoparticles is shown in Table A.2.

Table A.2. Recipe for the emulsion synthesis of core-shell nanoparticles

Core monomer	
De-ionized water (DI water)	150ml
trimethyl(tetra-decyl) ammonium bromide (TTAB)	3.75g (15 wt% of monomer)
Butyl acrylate	28 ml (~25g)
Acetone	4 g
2,2' azobis (2 methyl propion-amide) dihydrochloride (V50)	0.2 g
Shell monomer	
De-ionized water (DI water)	150ml
trimethyl(tetra-decyl) ammonium bromide (TTAB)	3.75g (15 wt% of monomer)
Styrene	28 ml (~25g)
2-Dodecanethiol (transfer agent)	0.1 ml

Monomers were purified in the same manner as described for the block copolymer synthesis and the reaction was carried out in a 500 ml reactor with a side Teflon valve as pictured in Figure A.1.

The procedure for the formation of the core particles is as follows: DI water and TTAB are added to the reactor and stirred vigorously for 15 min. All of the TTAB should be dissolved before the addition of acetone and the butyl acrylate. The reactor is placed inside an oil bath at 60°C, and the reaction mixture is bubbled and stirred for 1 hour, to obtain a uniform white emulsion. The initiator is dissolved in DI water (4 ml) before its addition to the reactor. The polymerization is carried out for 24h before the addition of the second monomer.

In another flask, the DI water, the surfactant (TTAB), the styrene monomer and the transfer agent are mixed and stirred vigorously while bubbled with N_2 for 1 hour. The emulsified monomer is then added drop wise to the core polymerization reactor using a transfer needle. The addition is controlled by the flow of N_2 into the system and is set to approximately 2 drops/second. After all the emulsified styrene is added, the reactor is closed and the shell polymerization is carried out for another 24 hours. The product is then precipitated in methanol, and washed in a mixture of methanol and water (50/50) before drying for 3 days in the presence of phosphorous pentoxide (for complete removal of water).

To obtain larger particles, the amount of TTAB was significantly reduced (about 0.01 wt% relative to monomer for ~200nm particles) and stirred for longer periods of time to

achieve a homogeneous emulsion. The variations in molecular weight for the core were obtained by adding transfer agent (~0.1 ml) at the first step of the polymerization.

Large quantity batches (~450g) of core-shell particles were also possible to perform by simple scaling the amounts from the method described above. The reaction was carried out in a 5L vessel and stirred with a motor powered external agitator. Figure A.2 shows the experimental setup for the large-scale batch, the precipitation step and the obtained product.

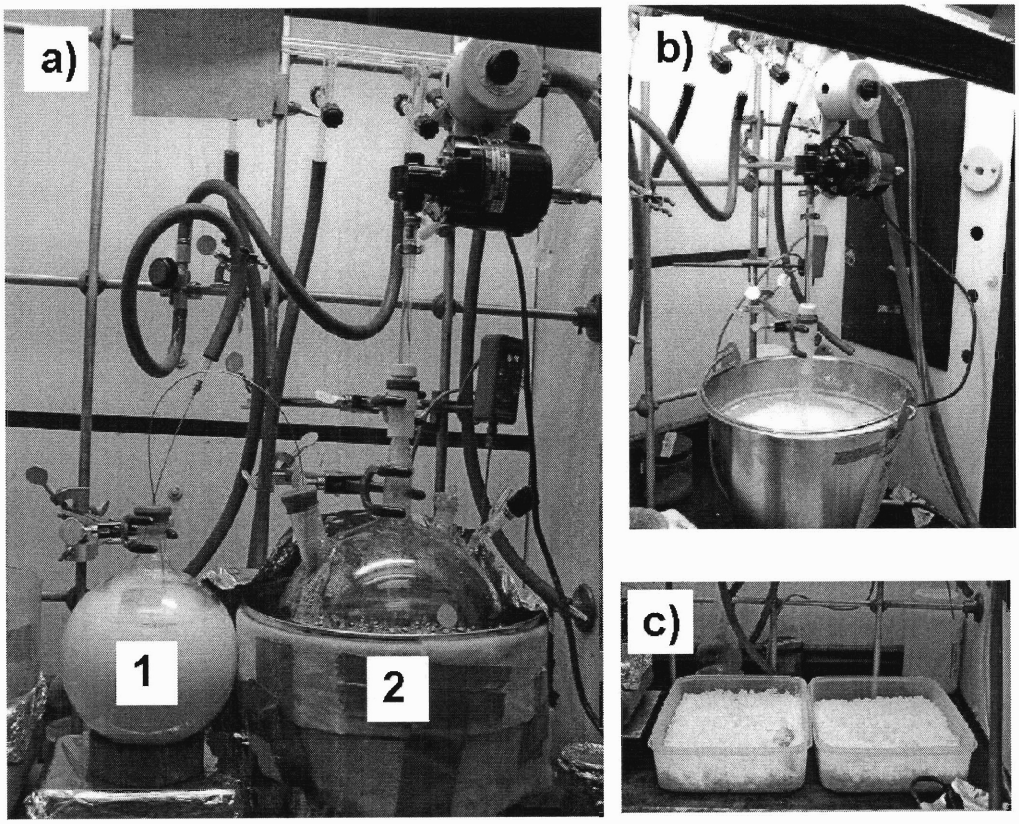

Figure A.2. Large-scale batch of core-shell particles. a) Transfer set up, where the emulsified styrene (1) is being transfered to the main reactor (2) by using a transfer needle. b) Precipitation and washing setup. c) Obtained core-shell particles.

References

1. Utracki, L.A. in "Polymer Blends Handbook Vol. 1 & 2" (Utracki, L.A. ed.) Kluwer Academic Publishers, Norwell, MA. **2002**, chap. 1, 5, 15.
2. Paul, D.R.; Bucknall, C. B. "Polymer Blends, Volume 1: Formulation" John Wiley & Sons, Inc; New York, **2000**.
3. Flory, P.J. "Principles of Polymer Chemistry" Cornell University Press: Ithaca, NY, **1953**, chap. 10.
4. Sanchez, I.C.; Panayiotou, C. G. in "Models for Thermodynamic and phase equilibria calculations" (Sandler S. I. ed.) Marcel Decker, NY, **1993**, pg. 222-227.
5. Van Dijk, M.A.; Wakker, A. "Concepts of Polymer Thermodynamics" Technomic Publishig Co., Inc. PA, **1997**.
6. Koningsveld, R.; Stockmayer, W.H.; Nies, E. "Polymer Phase Diagrams. A textbook" Oxford University Press, **2001**, pg. 135, 170.
7. Dormidontova, E." Role of competitive PEO-water and water-water hydrogen bonding in aqueous solution PEO behavior" *Macromolecules* **2002**, *35*, 987.
8. Han, C.C. et al. "Temperature, composition and molecular-weight dependence of the binary interaction parameter of polystyrene poly(vinyl methyl-ether) blends" *Polymer* **1988**, *29*, 2002.
9. Jager, H.; Vorenkamp, E.J.; Challa, G. " LCST behavior in blends of PMMA with PVC" *Polym. Commun.* **1983**, *24*, 290.
10. Di Lorenzo, M.L.; Frigione, M. "Compatibilization criteria and procedures for binary blends: A review". *J. Polym. Eng.* **1997**, *17*, 429.

11. Ziegler, M.J.; Matyjaszewski, K. "Atom transfer radical copolymerization of methyl methacrylate and n-butyl acrylate". *Macromolecules* **2001**, *34*, 415.

12. Verbeek, C.J.R. "The influence of interfacial adhesion, particle size and size distribution on the predicted mechanical properties of particulate thermoplastic composites". *Mat. Lett.* **2003,** *57*, 1919.

13. Joseph, S.; Thomas, S. "Morphology development and mechanical properties of polystyrene/polybutadiene blends". *Eu. Polym. J.* **2003**, *39*, 115.

14. Kulasekere R. et al. "Homopolymer interfaces reinforced with random copolymers" *Macromolecules* **1996**, 29, 5493.

15. Hadjuk, D.M. et al. "The Gyroid: A new equilibrium morphology in weakly segregated diblock copolymers" *Macromolecules* **1994**, *27*, 4063.

16. World wide web http://btp8x8.phy.uni-bayreuth.de/haarer/research/pap.html downloaded 6-20-2005.

17. Fischer, H.; Weidisch, R.; Stamm, M.; Budde, H.; Horing, S. "The phase diagram of the system poly(styrene-*block*-*n*-butyl methacrylate)". *Colloid Polym. Sci.* **2000**, 278, 1019.

18. Holden, G.; Legge, N.R. in "Thermoplastic elastomers 2nd Ed" (Holden, G. et al. ed.) **1996**, pg. 47-54.

19. Harper, C.A. in "Handbook of plastics, elastomers and composites 3rd Edition". McGraw-Hill, **1996**, Chap 5.

20. Lodge, T. P. " Block copolymers: Past successes and future challenges" *Macromol. Chem. Phys.* **2003**, *204*, 265.

21. Ruzette, A.V.; Leibler, L.; "Block copolymers in tomorrow's plastics" *Nature Materials* **2005**, *4*, 19.

22. Lopes, W.A.; Jaeger, H.M. "Hierarchical self-assembly of metal nanostructures on diblock copolymer scaffolds" *Nature* **2001**, *414*, 735.

23. Thurn-Albrecht, T. et al. "Ultrahigh-density nanowire arrays grown in self-assembled diblock copolymer templates" *Nature* **2000**, *290*, 2126.

24. Freedonia Group Report "Thermoplastic Elastomers to 2007", Dec **2003**.

25. Fahrlander, M.; Bruch, M.; Menke, T.; Friedich, C. "Rheological behavior of PS-melts containing surface modified PMMA-particle" *Rheol. Acta* **2001**, *40*, 1.

26. Nelliappan, V. et al. "Effect of the core/shell latex particle interphase on the mechanical behavior of rubber-toughened poly (methyl methacrylate)" *J. Appl. Polym Sci.* **1997**, *65*, 581.

27. Echte, A. "Rubber-toughened styrene polymers. A review" *ACS symposium series* 222. ACS Washington **1989**, pg. 15.

28. Dos Santos, F. D.; Fabre, P.; Drujon, X.; Meunier, G.; Leibler, L. "Films from soft-core/hard-shell hydrophobic latexes: structure and thermomechanical properties" *J. Polym. Sci. Part B Polym. Phys.* **2000**, *38*, 2989.

29. Dos Santos, F. D.; Leibler, L. "Large deformation of films from soft-core/hard-shell hydrophobic lattices". *J. Polym. Sci. Part B Polym. Phys.* **2003**, *41*, 224.

30. Feng, J.; Winnik, M.A.; Shivers, R.R.; Clubb, B. "Polymer blend latex films: Morphology and transparency". *Macromolecules* **1995**, *28*, 7671.

31. Ha, J.W.; Park, I. J.; Lee, S.B.; Kim, D. K. "Preparation and characterization of core-shell particles containing perfluoroalkyl acrylate in the shell". *Macromolecules* **2002**, *35*, 6811.

32. Lee, C.F.; Chen, Y.H.; Chiu, W.Y. "Morphology, thermal property, and mechanical property of core-shell latex polymers. I. Effect of heating and pressuring on PBA/PS linear composite polymer" *J. Applied. Polym. Sci.* **1998**, *69*, 13.

33. Kalinina, O.; Kumacheva, E. "Nanostructured polymer films with liquid inclusions. 1.Structural blocks" *Macromolecules* **2001**, *34*, 6380.

34. Caruso, F. "Nanoengineering of particle surfaces" *Adv. Mater.* **2001**, *13*, 11.

35. Pham, H. H.; Kumacheva, E. "Core-shell particles: Building blocks for advanced polymer materials" *Macromol. Symp.* **2003**, *192*, 191.

36. Morton-Jones, D.H. "Polymer Processing" Chapman & Hall, **1993**, chap. 5, 8 and 9

37. Silverstein, M.S.; Narkis, M. "Elastomeric latex domain-interpenetrating polymer networks: Physical and rheological properties" *Polym. Eng. Sci.* **1989**, *29*, 824.

38. Silverstein, M.S.; Narkis, M. "Capillary extrusion of elastic emulsion crosslinked interpenetrating networks" *Polym. Eng. Sci.* **1985**, *25*, 257..

39. Ward, I.M.; Taraiya, A.K.; Coates, P.D. in "Solid phase processing of polymers" (Ward, I.M.; Coates, P.D. and Dumoulin, M.M. ed.) Hanser, Munich, **2000**, chap. 9.

40. Penwell, R.C.; Porter, R.S.; Middleman, S. " Determination of the pressure coefficient and pressure effects in capillary flow". *J. Polym Sci. Part A-2*, **1971**, *9*, 731.

41. Denn, M.M. "Temperature drop-flow rate equation for adiabatic capillary flow with a pressure and temperature- dependent viscosity" *Polym. Eng. & Sci.* **1981**, *21*, 65.

42. Huang, J-C.; Leong, K-S. "Shear viscosity, extensional viscosity, and die swell of polypropylene in capillary flow with pressure dependence" *J. Appl. Polym. Sci.* **2002**, *84*, 1269.

43. Laun, H.M. "Capillary rheometry for polymer melts revisited" *Rheol. Acta* **2004**, *43*, 509.

44. Hasegawa, H. et al. "Small-angle neutron scattering studies on phase behavior of block copolymers". *J. Phys. Chem. Solids.* **1999**, *60*, 1307.

45. Steinhoff, B. et al. "Pressure Dependence of the Order-to-Disorder transition in polystyrene/polyisoprene and polstyrene/poly(methylphenylsiloxane) diblock copolymers" *Macromolecules* **1998**, *31*, 36.

46. Frielinghaus, H.; Schwahn, D.; Mortensen, K.; Almdal, K.; Springer, T. " Composition fluctuations and coil conformation in a poly (ethylene-propylene)-poly(ethylethylene) diblock copolymer as a function of temperature and pressure". *Macromolecules* **1996**, *29*, 3263.

47. Shwahn, D.; Frielinghaus, H.; Mortensen, K.; Almdal, K. "Temperature and pressure dependence of the order parameter fluctuations, conformational compressibility, and the phase diagram of the PEP-PDMS diblock copolymer" *Phys. Rev. Lett.* **1996**, *77*, 3153.

48. Rabeony, M. et al. "Effect of pressure on polymer blend miscibility: A temperature-pressure superposition" *Macromolecules* **1998**, *31*, 6511.

49. Hadjuk, D.A.; Gruner, S.M.; Erramilli, S.; Register, R.A.; Fetter, L.J. "High pressure effects on the order-disorder transition in block copolymer melts". *Macromolecules* **1996**, *29*, 1473.

50. Imre, A.R.; Kraska, T.; Yelash, L.V.; "The effect of pressure on the liquid-liquid phase equilibrium of two polydisperse polyalkylsiloxane blends" *Phys. Chem. Chem. Phys.* **2002**, *4*, 992.

51. Hammouda, B.; Balsara, N.P.; Lefebvre, A.A.; "Small angle neutron scattering from pressurized polyethylbutylene/polymethylbutylene blends". *Macromolecules* **1997**, 30, 5572.

52. Jiang, S.; Jiang, W.; Wolf, B.; An, L.; Jiang, B. "Pressure-induced compatibility in PEO/(PEO-*b*-DMS) polymer mixtures". *Macromolecules* **2002**, *35*, 5727.

53. Pollard, M.; Russell, T.P.; Ruzette, A.V.; Mayes, A.M.; Gallot, Y. "The effect of hydrostatic pressure on the lower critical ordering transition in diblock copolymers". *Macromolecules* **1998**, 31, 6493.

54. Ruzette, A.V.G.; Mayes, A.M.; Pollard, M.; Russell, T.P.; Hammouda, B. "Pressure effects on the phase behavior of styrene/n-alkyl methacrylate block copolymers". *Macromolecules* **2003**, *36*, 3351.

55. Ruzette, A.V.G. et al. "Phase behavior of diblock copolymers between styrene and n alkyl methacrylates" *Macromolecules* **1998**, 31, 8509.

56. Ryu, D.Y.; Lee, D.H.; Jang, J.; Kim, J.K. "Complex Phase behavior of a weakly interaction binary polymer blend". *Macromolecules* **2004**, *37*, 5851.

57. Ruzette, A.V.G.; Banerjee, P.; Mayes, A.M.; Rusell, T.P. "A simple model for baroplastic behavior in block copolymer melts" *J. Chem. Phys.* **2001**, *114*, 8205.

58. Ruzette, A.V. "Molecular design of ordering transitions in block copolymers" PhD. Thesis June **2000**, MIT.

59. Goodship, V. in "Introduction to Plastic Recycling" Rapra Technology LTD. **2001**, UK. Chap. 3.

60. Odian, G. "Principles of Polymerization, 3rd Edition" John Wiley & Sons, **1991**, pg. 463.

61. Gumbs, R.; Penczek, S.; Jagur-Grodzinski, J.; Szwarc, M. "Simultaneous cationinc homopolymerizations of vinylcarbazole and oxetane" *Macromolecules* **1969**, *2*, 77.

62. Feldthisen, J.; Ivan, B.; Müller, H.E. "Synthesis of linear and star-shaped block copolymers of isobutylene and methacrylates by combination of living cationic and anionic polymerizations" *Macromolecules* **1998**, *31*, 578.

63. Patten, T.E.; Matyjaszewski, K. "Atom transfer radical polymerization and the synthesis of polymeric materials" *Adv. Mat.* **1998,** *10*, 901.

64. Matyjaszewski, K.; Xia, J.; "Atom transfer radical polymerization" *Chem. Rev.* **2001**, *101*, 2921.

65. Matyjaszewski, K.; Shipp, D. A; Mcmurtry, G.P.; Gaynor, S.G.; Pakula, T. "Simple and effective one-pot synthesis of (meth)acrylic block copolymers through atom transfer radical polymerization" *J. Polym Sci Part A: Polym Chem.* **2000**, *38*, 2023.

66. Cassebras, M.; Pascual, S.; Polton. A.; Tardi M.; Vairon, J-P. "Synthesis of di- and triblock copolymers of styrene and butyl acrylate by controlled atom transfer radical polymerization" *Macromol. Rapid. Commun.* **1999**, *20*, 261.

67. Martin-Gomis, L.; Fernandez-Garcia, M.; de la Fuente, J.L.; Lopez Madruga, E.; Cerrada, M. L. "Physical properties of PBMA-b-PBA-b-PBMA triblock copolymers synthesized by atom transfer radical polymerization". *Macromol. Chem. Phys.* **2003**, *204*, 2007.

68. Moineau, G.; Minet, M.; Teyssie, P.; Jerome, R. " Synthesis of fully acrylic thermoplastic elastomers by atom transfer radical polymerization (ATRP) 2. Effect of the catalyst on the molecular control and the rheological properties of the triblock copolymers" *Macromol. Chem. Phys.* **2000**, *201*, 1108.

69. Kumar, D.; Butler, G.B. "Methods of formation of organic particles of controlled sizes". J.M.S. Rev. *Macromol. Chem. Phys.* **1997**, *C37*, 303.

70. Sundberg, D.C.; Durant, Y. G. "Latex particle morphology, fundamental aspects: a review" *Polym Reac. Eng.* **2003**, *11*, 379.

71. Stubbs, J.M.; Sundberg, D.C. "A round robin study for the characterization of latex particle morphology-multiple analytical techniques to probe specific structural features" *Polymer* **2005**, *46*, 1125.

72. Landfester, K.; Spiess, H.W. "Characterization of interphases in core-shell latexes by solid-state NMR." *Acta. Polym.* **1998**, *49*, 451.

73. Sibayama, M.; Jinnai, H.; Hashimoto, T. in "Experimental methods in polymer science. Modern methods in polymer research and technology" (Tanaka, T. ed.) Academic press, San Diego CA, **2000**. Chap.2. pg. 105-114, 124-139.

74. Gallagher, P.K. in "Thermal Characterization of polymeric materials 2nd Ed." (Turi. E. A. ed.), **1997**, Academic Press, San Diego, CA. pg. 6,7.

75. Song, M.; Hammiche, A.; Pollock, H.M.; Hourston, D.J.; Reading, M. "Modulated differential scanning calorimetry: 1. A study of the glass transition behavior of blends of poly(methylmethacrylate) and poly(styrene-co-acrilonitrile)". *Polymer* **1995**, *36*, 3313.

76. Hourston, D.J.; Song, M; Hammiche, A.; Pollock, H.M.; Reading, M. "Modulated differential scanning calorimetry: 6. Thermal characterization of multicomponent polymers and interfaces" *Polymer*, **1997**, *38*, 1.

77. Chescoe, D.; Goodhew. P.J. "The operation of transmission and scanning electron microscopes" Oxford University press, NY **1990**.

78. ASTM "Standard test methods for vulcanized rubber and thermoplastic elastomers-tension" Designation D412-98a.

79. Gagnon, K.D.; Lenz, R.W.; Farris, R.J. "The mechanical properties of a thermoplastic elastomer produced by the bacterium *Pseudomonas oleovorans*" *Rubb. Chem. & Tech.* **1992**, 65, 761.

80. Ward, I.M.; Hadley, D.W. in "An introduction to the mechanical properties of solid polymers". John Wiley & Sons, West Sussex, England 1993, pg.284-286.

81. ASTM "Standard test method for tear strength of conventional vulcanized rubber and thermoplastic elastomers- tension" Designation D624-00.

82. Rodgers, P.A. "Pressure volume temperature relationships for polymeric liquids- A review of equations of state and their characteristic parameters for 56 polymers" *J. of App. Polym. Sci.* **1993**, *48*,1061.

83. Sanchez, I.C.; Lacombe, R. H. "Elementary molecular theory of classical fluids-Pure fluids" *J. Phys. Chem.* **1976**, *80*, 2352.

84. Lacombe, R. H.; Sanchez, I.C. "Statistical thermodynamics of fluis mixtures" *J. Phys. Chem.* **1976**, *80*, 2569.

85. Simha, R.; Somcynsky, T. "On the statistical thermodynamics of spherical and chain molecule fluids" *Macromolecules* **1969**, *2*, 342.

86. Stroeks, A.; Nies, E. "Liquid-liquid phase behavior of mixture according to the Simha-Somcynsky theory" *Polym. Eng. Sci.* **1988**, *28*, 1347.

87. Freed, K. F.; Dudowicz, J. "Lattice cluster theory for pedestrians: Models for random copolymer blends" *Macromol. Symp.* **2000**, *149*, 11.

88. Dudowicz, J.; Freed, K. F. "Pressure dependence of polymer fluids: Application of the lattice cluster theory" *Macromolecules* **1995**, *28*, 6625.

89. Gross, J.; Sadowski G. "Modeling polymer systems using the perturbed-chain statistical associating fluid theory equation of state" *Ind. Eng. Chem. Res.* **2002**, *41*, 1084.

90. Favari, F.; Bertucco, A.; Elvassore, N.; Fermeglia, M. "Multiphase multicomponent equilibria for mixtures containing polymers by the pertubation theory" *Chem. Eng. Sci.* **2000**, *55*, 2379.

91. Cho, J. "Analysis of phase separation in compressible polymer blends and block copolymers" *Macromolecules* **2000**, *33*, 2241.

92. Cho, J. "Analysis of compressible diblock copolymer melts that microphase separate upon cooling" *Macromolecules* **2001**, *34*, 6097.

93. Ruzette, A.-V. G.; Mayes, A. M. "A simple free energy model for weakly interacting polymer blends" *Macromolecules* **2001** *34*, 1894.

94. Gonzalez-Leon, J.A.; Mayes, A.M. "Phase behavior prediction of ternary polymer mixtures" *Macromolecules* **2003** *36*, 2508.

95. Zoller, P., Walsh, D. "Standard Pressure-Volume-Temperature data for polymers" Technomic Publishing Co. Lancaster PE. **1995**.

96. Boudouris, D.; Constantinou, L.; Panayiotou, C. "A group contribution estimation of the thermodynamic properties of polymers" *Ind. Eng. Chem. Res.* **1997**, *36*, 3968.

97. Bicerano, J. "Prediction of Polymer Properties 3rd edition" Marcel Dekker Inc. N.Y. **2002**.

98. Van Krevelen, D. W.; Hoftyzer, P.J. "Properties of Polymers. Correlation with Chemical Structure" Elsevier: NY, **1972**.

99. Gonzalez-Leon J. A.; Acar, M. H., Ryu, S.-W. ; Ruzette, A.-V. G. ; Mayes, A. M. "Low temperature processing of 'baroplastics' by pressure-induced flow" *Nature* **2003**, *426*, 424.

100. Ryu, D.Y.; Lee, D.J. ;Kim, J.K.; Lavery, K.A.; Russell, T.P. Effect of hydrostatic pressure on closed-loop phase behavior of block copolymers. *Phys. Rev. Lett.* **2003,** *90*, 235501-1.

101. Hajduk, D. A.; Urayama, P.; Gruner, S. M.; Erramilli, S. "High-pressure effects on the disordered phase of block copolymer melts" *Macromolecules* **1995**, *28*, 7148.

102. Fox, T.G. "Influence of diluent and of copolymer composition on the glass temperature of a polymer system" *Bull. Am. Phys. Soc.* **1956**, *1*, 123.

103. Fasolka, M.J.; Banerjee, P.; Mayes, A.M.; Pickett, G.; Balazs, A. C. "Morphology or ultrathin supported diblock copolymer films: Theory and experiment" *Macromolecules* **2000**, *33*, 5702.

104. Beckett, S.T. et al. "The cold extrusion of chocolate" *Trans. IchemE* **1994**, *72*,47.

105. Flemings, M.C. "Behavior of metal alloys in the semisolid state". *Metall. Trans. B* **1991** *22B,* 269.

106. Ehrenstein, G.W. "Polymeric Materials Structure-Properties-Applications" Hanser publishers, Munich, **2000**.

107. Britton, D. J.; Lovell, P.A.; Heatley, F.; Venkatesh, R. "Chain transfer to polymer in emulsion copolymerizations" *Macromol. Symp.* **2001**, *175*, 95.

108. Aguiar, A.; Gonzalez-Villegas, S.; Rabelero, M.; Medizabal, E.; Puig, J.E.; Dominguez, J.M.; Katime, I. "Core-shell polymers with improved mechanical properties prepared by microemulsion polymerization" *Macromolecules* **1999**, *32*, 6767.

109. Gonzalez-Leon, J.A.; Ryu, SW.; Hewlett, S.A.; Ibrahim, S.H.; Mayes, A.M. "Core-shell polymer nanoparticles for baroplastic processing" *Macromolecules* **2005**, *38*, 8036.

110. Dumoulin, M.M. in "Polymer Blends Handbook Vol.2" (Utracki, L.A. ed.) Kluwer, Dordrecht, **2002**. Sec. 10.11

111. Buchholz, B.A.; Zahn, J.M.; Kenward, M.; Slater, G.W.; Barron, A. E. "Flow-induced chain scission as a physical route to narrowly distributed, high molar mass polymers" *Polymer* **2004**, *45*, 1223.

112. Ballauf, M.; Wolf, B.A. "Degradation of chain molecules .1. Exact solution of the kinetic-equations" *Macromolecules* **1981**, *14*, 654.

113. Metzner, A.B.; Metzner, A.P. "Stress levels in rapid extensional flows of polymeric fluids" *Rheol. Acta* **1970**, *9*, 174.

114. Ajji, A. in "Polymer Blends Handbook Vol.1" (Utracki, L.A. ed.) Kluwer, Dordrecht, **2002.** Sec. 4.1, 4.6.

115. Lovell, N. G. "The Design, Synthesis and Properties of Pressure-Processable Biodegradable Block Copolymers." MS Thesis, September **2005**, MIT.

116. van Hooy-Corstjens, C. S. J.,; Höhne, W.H.; Rastogi, S. "Inverse melting in syndiotactic polystyrene" *Macromolecules* **2005**, *38*, 1814.

117. Rastogi, S; Newman, M.; Keller, A. "Pressure-induced amorphization and disordering on cooling in a crystalline polymer" *Nature*, **1991**, *353*, 55.

118. Ibrahim, S.H. "Evaluation of the economic feasibility of core-shell baroplastic polymers and a comparison to traditional thermoplastic elastomers" MS Thesis, September **2005**, MIT.

119. Tiarks, F.; Landfester, K.; Antonietti, M. "Silica nanoparticles as surfactants and fillers for latexes made by miniemulsion polymerization" *Langmuir* **2001**, *17*, 5775.

120. Mori, H.; Müller, A.H.E.; Klee, J.E. "Intelligent colloidal hybrids via reversible pH-induced complexation of polyelectrolyte and silica nanoparticles" *J. Am. Chem. Soc.* **2003**, *125*, 3712.

121. Ramirez, L.P.; Landfester, K. "Magnetic polystyrene nanoparticles with high magnetite content obtained by miniemulsion process" *Macromol. Chem. Phys.* **2003**, *204*, 22.

122. Morais, P.C.; Lima, E.C.D.; Rabelo, D.; Reis, A.C.; Pelegrini, F. "Magnetic resonance of magnetite nanoparticles dispersed in mesoporous copolymer matrix" *IEEE Trans. Magnetics* **2000**, *36*, 3038.

123. Chatterjee, J.; Haik, Y.; Chen, C. "Polyethylene magnetic nanoparticle: a new magnetic materials for biomedical applications" *J. Magnetism. & Magnetic Mat.* **2002**, *246*, 382.

124. Garcia-Santamaria, F.; Salgueirino-Maceira, V.; Lopez,; Liz-Marzan, L.M. "Syntehtic oplas based on silica-coated gold nanoparticles" *Langmuir* **2002**, *18*, 4519.

125. Quaroni, L.; Chumanov, G. "Preparation of polymer-coated functionalized silver nanoparticles" *J. Am. Chem. Soc.* **1999**, *121*, 10642.